

THE CYSTIC FIBROSIS TRANSMEMBRANE  
CONDUCTANCE REGULATOR AND ACID-BASE  
TRANSPORTERS OF THE MURINE DUODENUM

---

A Dissertation  
presented to  
the Faculty of the Graduate School  
University of Missouri-Columbia

---

In Partial Fulfillment  
of the Requirements for the Degree

Doctor of Philosophy

---

by  
JANET ELIZABETH SIMPSON

Dr. Lane L. Clarke, Dissertation Supervisor

AUGUST 2006

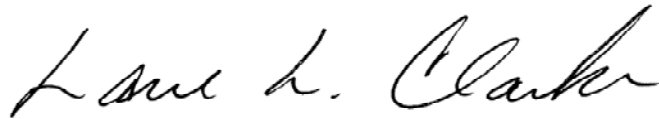
The undersigned, appointed by the Dean of the Graduate School, have examined the Dissertation entitled

THE CYSTIC FIBROSIS TRANSMEMBRANE CONDUCTANCE REGULATOR  
AND ACID-BASE TRANSPORTERS OF THE MURINE DUODENUM

Presented by Janet Elizabeth Simpson

A candidate for the degree of Doctor of Philosophy

And hereby certify that in their opinion is worthy of acceptance.



---

Lane Clarke, DVM, PhD, Dissertation Supervisor  
Associate Professor, Department of Biomedical Sciences



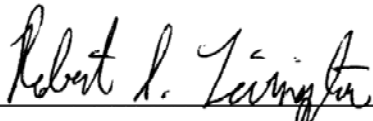
---

Douglas Bowles, PhD  
Associate Professor, Department of Biomedical Sciences



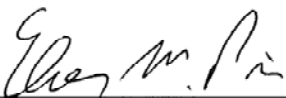
---

Craig Franklin, DVM, PhD  
Associate Professor, Department of Veterinary Pathobiology



---

Robert Livingston, DVM, PhD  
Associate Professor, Department of Veterinary Pathobiology



---

Elmer Price, PhD  
Associate Professor, Department of Biomedical Sciences

## ACKNOWLEDGEMENTS

I would like to express my deep gratitude to my advisor, Dr. Lane Clarke. I have thoroughly enjoyed my research experience in his laboratory and appreciate all his support and encouragement. He provided me with an excellent foundation in biomedical research and continually challenged me throughout my research project to help me grow as a scientist. I would also like to acknowledge my committee: Drs. Douglas Bowles, Craig Franklin, Bob Livingston, and Elmer Price. They have been extremely supportive and were not hesitant to offer advice that would improve my work.

In addition, I am indebted to the members of the Clarke lab both past and present, including Nancy Walker, Lara Gawenis, KT Boyle, and Emily Bradford, for their constant help and advice. Each person contributed to the work in this dissertation, and I thank them.

I would also like to recognize the faculty members of the Comparative Medicine Department, especially Drs. Lon Dixon, Craig Franklin, Cindy Besch-Williford, and Bob Livingston, for the invaluable training and mentoring they provided to me during my residency program. I want to especially thank Dr. Craig Franklin. He was an excellent advisor who encouraged me throughout to pursue all my goals both as a researcher and as a laboratory animal veterinarian. I would also like to thank all the OAR and RADIL staff who contributed to both my residency and research activities. Finally, I would like to acknowledge the support of my fellow Comparative Medicine Program trainees for their professional support and especially their friendship.

Most importantly, I would like to thank my husband, Dr. Sam Simpson, who has been there with me every step along the way. He is the one person who always believes in me and pushes me to achieve my goals. Without him, this would not have been possible.

I would also like to acknowledge the grant awards that supported this work, including the National Institutes of Health Grants T32-RR07004 and DK-48816, and Cystic Fibrosis Foundation Grant CLARKE05G0.

## TABLE OF CONTENTS

ACKNOWLEDGEMENTS.....	ii
LIST OF FIGURES.....	vii
LIST OF ABBREVIATIONS.....	xi
ABSTRACT.....	xiii
Chapter	
1. INTRODUCTION AND BACKGROUND.....	1
Gastrointestinal Physiology and Morphology	
Cystic Fibrosis	
Duodenal HCO <sub>3</sub> <sup>-</sup> Secretion	
Apical Membrane Cl <sup>-</sup> /HCO <sub>3</sub> <sup>-</sup> Exchangers	
Carbonic Anhydrase	
Intestinal Transport of Peptides and Peptidomimetics	
Regulation of Intracellular pH (pH <sub>i</sub> ) during PEPT1 Transport	
Dissertation Overview	
2. CHLORIDE CONDUCTANCE OF CFTR FACILITATES BASAL Cl <sup>-</sup> /HCO <sub>3</sub> <sup>-</sup> EXCHANGE IN VILLOUS EPITHELIUM OF INTACT MURINE DUODENUM.....	18
Introduction	
Materials and Methods	
Results	
Discussion	

3.	PAT-1 IS THE PREDOMINANT APICAL MEMBRANE $\text{Cl}^-/\text{HCO}_3^-$ EXCHANGER IN THE UPPER VILLOUS EPITHELIUM OF MURINE DUODENUM.....	51
----	---	----

Introduction

Materials and Methods

Results

Discussion

4.	INHIBITION OF PAT-1 IMPAIRS THE ABILITY OF UPPER VILLOUS EPITHELIAL CELLS OF THE MURINE DUODENUM TO REGULATE $\text{pH}_i$ DURING $\text{H}^+$ -DIPEPTIDE TRANSPORT.....	79
----	--	----

Introduction

Materials and Methods

Results

Discussion

5.	CONCLUSIONS AND FUTURE STUDIES.....	107
----	-------------------------------------	-----

CFTR Facilitation of Basal  $\text{Cl}^-/\text{HCO}_3^-$  Exchange in the Villous Epithelium of Intact Murine Duodenum

Identification of the Apical Membrane Anion Exchanger(s) Responsible for Basal Bicarbonate Secretion

The Role of PAT-1 in Intestinal Peptide Absorption

## APPENDIX

1.	$\text{pH}_i$ MEASUREMENT IN INTACT INTESTINAL TISSUE.....	125
----	--	-----

Setup of Perfusion Lines for Microfluorimetry Studies

Setting up for a BCECF Microfluorimetry Study

Starting a BCECF Microfluorimetry Experiment

Image Acquisition and Analysis

	Cleaning up following Experiment	
2.	CALIBRATION OF FLUORESCENT RATIO IN TERMS OF $pH_i$ .....	139
	Setting up for a $pH_i$ Calibration Experiment	
	Calibration of 495/440 Ratio in Terms of $pH_i$	
3.	DETERMINATION OF BUFFERING CAPACITY AND BASE FLUX.....	144
	Setting up for an Intrinsic Buffering Capacity Experiment	
	Method for Measuring Intrinsic Buffering Capacity via $NH_4Cl$ Prepulse	
	General Principles and Calculations for Determining Intrinsic Buffering Capacity	
	Calculating $HCO_3^-$ Buffering Capacity, Total Buffering Capacity and Flux Rates	
	BIBLIOGRAPHY.....	151
	VITA.....	164

## LIST OF FIGURES

Figure	Page
1.1 Photomicrograph showing a cross-section of a crypt and villus.....	2
1.2 Photograph showing the murine gastrointestinal tract and its major anatomical structures .....	2
1.3 Generic model of an intestinal villous epithelial cell.....	4
1.4 Photomicrograph of the small intestine from a human CF patient with meconium ileus and a CF mouse .....	6
1.5 Two proposed models for cAMP-stimulated HCO <sub>3</sub> <sup>-</sup> secretion.....	9
1.6 Cellular localization of CFTR, AE4, DRA, PAT-1, and PEPT1 in the duodenum.....	10
1.7 Current model for intestinal peptide transport through PEPT1 .....	16
2.1 Images of BCECF-loaded villi from murine duodenum.....	24
2.2 Anion exchange in duodenal villous epithelium exhibits Cl <sup>-</sup> and HCO <sub>3</sub> <sup>-</sup> dependence.....	30
2.3 Comparison of pH <sub>i</sub> and Cl <sup>-</sup> /HCO <sub>3</sub> <sup>-</sup> exchange in duodenal villous epithelium of WT and CF mice .....	32
2.4 Effect of anion exchange inhibitors on Cl <sup>-</sup> /HCO <sub>3</sub> <sup>-</sup> exchange rates in WT and CF villous epithelium.....	34
2.5 Effect of cell depolarization on Cl <sup>-</sup> /HCO <sub>3</sub> <sup>-</sup> exchange rates in WT and CF villous epithelia.....	35
2.6 Effects of anion substitution or glybenclamide on HCO <sub>3</sub> <sup>-</sup> efflux in WT and CF duodenal villous epithelia.....	38
2.7 Effect of a preceding period of SO <sub>4</sub> <sup>2-</sup> uptake on Cl <sup>-</sup> /HCO <sub>3</sub> <sup>-</sup> exchange in WT duodenal villous epithelium.....	41



2.8	mRNA expression of mDRA and mPAT-1 in the small intestine of gender-matched littermate WT and CF mouse pairs .....	42
3.1	mRNA expression of DRA, PAT-1, and AE4 in microdissected murine duodenal villi .....	60
3.2	Anion exchange activity in the duodenal villous epithelium of WT and AE4 (-) mice .....	62
3.3	Anion exchange activity in the duodenal villous epithelium of WT and DRA (-) mice .....	64
3.4	Comparison of $\text{Cl}^-/\text{HCO}_3^-$ exchange activity and baseline $\text{pH}_i$ and in duodenal villous epithelium of WT and PAT-1 (-) mice.....	66
3.5	Comparison of $\text{SO}_4^{2-}/\text{HCO}_3^-$ exchange in the duodenal villous epithelium of WT and PAT-1 (-) mice .....	68
3.6	Comparison of NHE3 expression and apical membrane $\text{Na}^+/\text{H}^+$ exchange activity in WT and PAT-1 (-) small intestine .....	70
3.7	Baseline $\text{pH}_i$ studies in the duodenal villous epithelium of WT and PAT-1 (-) mice.....	72
4.1	Measurement of $\text{H}^+$ /peptide absorption and $\text{H}^+$ /peptide-induced acidification in murine duodena during inhibition of apical $\text{Na}^+/\text{H}^+$ exchange .....	89
4.2	Regulation of $\text{pH}_i$ during Gly-Sar uptake during inhibition of carbonic anhydrases.....	91
4.3	Regulation of $\text{pH}_i$ during Gly-Sar uptake and $\text{H}^+$ /peptide absorption in murine duodena during inhibition of apical $\text{Cl}^-/\text{HCO}_3^-$ exchange .....	94
4.4	Comparison of baseline $\text{pH}_i$ and $\text{pH}_i$ regulation in duodenal villous epithelium of WT and PAT-1 (-) mice during Gly-Sar absorption .....	97

4.5	Comparison of $\text{Cl}^-/\text{HCO}_3^-$ exchange activity in duodenal villous epithelium of WT and PAT-1 (-) mice during luminal Gly-Sar absorption.....	100
4.6	Cell model depicting the proposed activity of PAT-1 and CA II in the presence of peptide absorption.....	105
5.1	Two proposed models for reduced $\text{Cl}^-/\text{HCO}_3^-$ exchange in the CFTR (-) upper duodenal villus .....	108
5.2	The effect of glybenclamide on DRA $\text{Cl}^-/\text{HCO}_3^-$ exchange activity .....	110
5.3	Isolation of DRA activity in the presence and absence of CFTR.....	111
5.4	Transepithelial $\text{HCO}_3^-$ secretion across duodena from PAT-1 (-) and DRA (-) and WT mice as measured by pH stat.....	113
5.5	Rates of $\text{HCO}_3^-$ influx and efflux in upper and lower villous epithelia of WT duodenum .....	115
5.6	$\text{HCO}_3^-$ influx and efflux of PAT-1 (-) and WT and AE4 (-) and WT lower villous epithelium .....	116
5.7	Rates of $\text{Cl}^-/\text{HCO}_3^-$ exchange in WT, DRA (-), and DRA (-)/CFTR (-) duodenal lower villous epithelia .....	117
5.8	Changes in $\text{pH}_i$ during luminal $\text{Cl}^-$ removal and replacement in WT, DRA (-), and DRA (-)/CFTR (-) lower villous epithelia.....	118
5.9	Summary of baseline $\text{pH}_i$ , $\text{HCO}_3^-$ influx, and $\text{HCO}_3^-$ efflux rates in lower villous epithelial cells from WT and CF mice.....	120
A1.1	Schematic of horizontal Ussing chamber .....	130
A1.2	Schematic of duodenal preparation to visualize lower villous epithelium .....	131
A1.3	Experimental setup for measurement of $\text{pH}_i$ in epithelial cells of intact duodenal villi.....	133

A1.4	High power photograph of a setup for measurement of $\text{pH}_i$ in epithelial cells of intact duodenal villi.....	134
A1.5	Locale in the mid-region of a single villus for the measurement of epithelial cell $\text{pH}_i$ .....	136
A2.1	Time course of 495/440 fluorescence-excitation ratio during exposure to high $\text{K}^+$ -nigericin solutions of different pHs epithelium .....	142
A2.2	Dependence of normalized fluorescence-excitation ratio on $\text{pH}_i$ .....	143
A3.1	Plot of intrinsic buffering and $\text{HCO}_3^-$ buffering capacity vs. $\text{pH}_i$ .....	149

## LIST OF ABBREVIATIONS

$[\text{NH}_4^+]_i$  – Intracellular ammonium

AE – Anion exchanger

BCECF-AM – 2',7'-bis-(2-carboxyethyl)-5-(and-6)-carboxyfluorescein acetoxymethyl

CA – Carbonic anhydrase

CF – Cystic fibrosis

CFTR – Cystic fibrosis transmembrane conductance regulator

$\text{Cl}^-$  – Chloride

CLD – Congenital chloride-losing diarrhea

DIDS – 4,4'-diisothiocyanatostilbene-2,2'-disulfonate

DRA – Down-regulated in adenoma

EIPA – 5-(N-ethyl-n-isopropyl)-amiloride ester

Gly-Sar – Glycyl-sarcosine

$\text{HCO}_3^-$  – Bicarbonate

IBR – Isethionate-bicarbonate Ringer

$I_{sc}$  – Short-circuit current

J – Flux

KBR – Kreb's bicarbonate Ringer

$\text{Na}^+$  – Sodium

NBC – Na<sup>+</sup>/HCO<sub>3</sub><sup>-</sup> cotransporter

NFA – Niflumic acid

NHE – Na<sup>+</sup>/H<sup>+</sup> exchanger

NKCC1 – Na<sup>+</sup>/K<sup>+</sup>/2Cl<sup>-</sup> cotransporter

NMDG – N-methyl-D-glucamine

PAT-1 – Putative anion transporter 1

PEPT1 – H<sup>+</sup>/peptide cotransporter

pH<sub>i</sub> – Intracellular pH

SO<sub>4</sub><sup>2-</sup> – Sulfate

TBR – TES buffered Ringer

TES – N-tris methyl-2-aminoethanesulfonic acid

TTX – Tetrodotoxin

β<sub>HCO<sub>3</sub><sup>-</sup></sub> – Bicarbonate buffering capacity

β<sub>i</sub> – Intrinsic buffering capacity

β<sub>total</sub> – Total buffering capacity

# THE CYSTIC FIBROSIS TRANSMEMBRANE CONDUCTANCE REGULATOR AND ACID-BASE TRANSPORTERS OF THE MURINE DUODENUM

Janet Elizabeth Simpson

Dr. Lane Clarke, Dissertation Supervisor

## ABSTRACT

The alkaline mucus barrier of the duodenum plays an important role in protecting the epithelium from acidic chyme entering from the stomach. Active  $\text{HCO}_3^-$  secretion involves the apical membrane activities of the cystic fibrosis transmembrane conductance regulator (CFTR)  $\text{Cl}^-$  channel, the protein that is defective in cystic fibrosis, and  $\text{Cl}^-/\text{HCO}_3^-$  exchangers. Under basal, non-stimulated conditions, studies of CF patients and mouse models indicate that bicarbonate secretion by anion exchange predominates. In addition, basal bicarbonate secretion is reduced in the CF duodenum, but the specific pathophysiology of the deficiency has yet to be elucidated. Therefore, the goal of this research is to investigate basal bicarbonate secretion in the upper duodenal villous epithelium of the CF mouse and to determine the identity of the anion exchanger(s) that participates in this process. Under basal conditions, our studies reveal that  $\text{Cl}^-$  channel activity by CFTR facilitates apical membrane  $\text{Cl}^-_{\text{in}}/\text{HCO}_3^-_{\text{out}}$  exchange by providing a  $\text{Cl}^-$  ‘leak’ and is responsible for the reduced rate of  $\text{Cl}^-/\text{HCO}_3^-$  exchange in the murine CF intestine. Using mice with gene-targeted deletions of the apical membrane  $\text{Cl}^-/\text{HCO}_3^-$  exchangers PAT-1, DRA, and AE4, PAT-1 was found to be the major  $\text{Cl}^-/\text{HCO}_3^-$  exchanger of the upper villus of the duodenum. These studies also revealed a propensity

for PAT-1 to act as a base-importer (i.e.,  $\text{Cl}^-_{\text{out}}/\text{HCO}_3^-_{\text{in}}$ ) in native villous epithelium. The ability of PAT-1 to function as a base-importer may be physiologically relevant as the upper villous epithelium of the duodenum is exposed to acid challenge not only from gastric effluent, but also from  $\text{H}^+$  influx during nutrient absorption, e.g., PEPT1-mediated absorption. Furthermore, PAT-1 has been shown to interact with carbonic anhydrase II (CAII), the most widely expressed isozyme of the small intestine. Examination of CAII and PAT-1 (-) mice indicated that both PAT-1 and CAII contribute to  $\text{pH}_i$  regulation during peptide absorption. PAT-1 was found to principally function in  $\text{Cl}^-_{\text{out}}/\text{HCO}_3^-_{\text{in}}$  exchange during the dipeptide absorption, thus allowing for transmembrane movement of membrane-impermeant  $\text{HCO}_3^-$ . Taken together, these data indicate the existence of a  $\text{HCO}_3^-$  metabolon whereby PAT-1 and CAII mediate  $\text{HCO}_3^-$  uptake during  $\text{H}^+$ /peptide transport to minimize intracellular acidification and sustain peptide absorption.

## **Chapter 1**

### **INTRODUCTION AND BACKGROUND**

#### **Gastrointestinal Physiology and Morphology**

The gastrointestinal tract is responsible for the digestion and absorption of nutrients, absorption/secretion of electrolytes and water to help regulate fluid volume, sequestration of feces, and defecation. The intestine can be divided into two main portions, the small and large intestine. The functional unit of the small intestine is the crypt-villus axis (Figure 1.1), which consists of crypts, a maturation zone, and villi. The epithelial cells of the crypt are undifferentiated and mature as they migrate from villus to the tips (66). Within the crypt-villus axis, there is a gradient for secretion and absorption where secretion chiefly occurs in the crypts and absorption in the villi (31;39;76). The small intestine can be divided further into the duodenum, jejunum, and ileum (Figure 1.2), and it principally functions in luminal digestion and absorption of carbohydrates, proteins, and fats and also in water and electrolyte transport (31). In addition, the duodenum, which is located just distal to the stomach, provides an alkaline mucus barrier to help protect the intestinal epithelium from the acidic chyme exiting the stomach (36). The large intestine, which is devoid of villi, is composed of surface epithelia and numerous crypts which extend deep into the mucosa containing epithelial, mucous, and endocrine cells. Migration of epithelial cells is similar in the large intestine with undifferentiated cells migrating from the lower half of the crypts towards the surface. Anatomically, the large intestine is divided into the cecum, colon, and rectum, and is



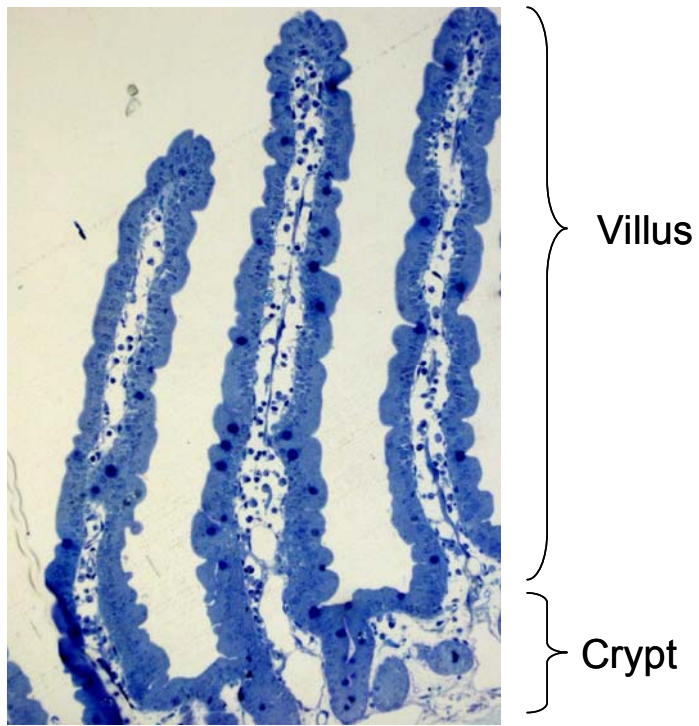


**Figure 1.1.** Photomicrograph showing a cross-section of a crypt and villus (20X magnification stained with toluidine blue).

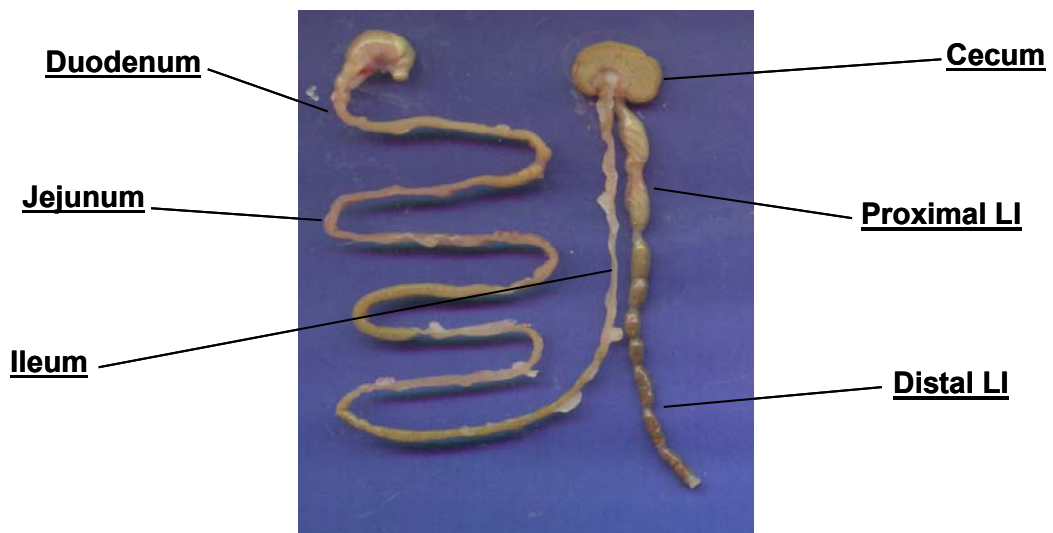


**Figure 1.2.** Photograph showing the murine gastrointestinal tract and its major anatomical structures.

primarily responsible for the extraction of water and electrolytes from the lumen, microbial fermentation, storage of feces, and defecation (11).

Enterocytes are simple columnar epithelial cells that cover the surface of the intestine in a single layer that is periodically interrupted by mucus-secreting goblet cells (66). The enterocytes are connected by tight junctions and serve as a barrier to the macromolecular contents of the intestinal lumen. Through the tight junctions, the intestinal epithelium allows for the passage of water and some electrolytes and nutrients paracellularly (66). The enterocytes themselves are polarized with distinct apical (a.k.a., luminal, mucosal) and basolateral (a.k.a., blood, serosal) membranes that permit transcellular ion transport processes. A cell model of a small intestinal villous enterocyte is depicted in Figure 1.3. Ion transporters localized to the apical membrane include  $\text{Cl}^-/\text{HCO}_3^-$  exchangers (e.g., *slc26a3*, down-regulated in adenoma, DRA; *slc26a6*, putative anion transporter 1, PAT-1; and *slc4a9*, anion exchanger isoform 4, AE4),  $\text{Na}^+/\text{H}^+$  exchangers (e.g., NHE2 and NHE3), nutrient transporters (e.g., the  $\text{H}^+$ /peptide cotransporter PEPT1 and  $\text{Na}^+$  coupled nutrient transporters), and anion channels such as the cystic fibrosis transmembrane conductance regulator (CFTR) (31). The transporters of the apical membrane primarily allow for vectorial movement of electrolytes and nutrients from the intestinal lumen (31;88). Carbonic anhydrases (CAs) are expressed both extra- and intracellularly and reversibly catalyze the conversion of  $\text{CO}_2$  and  $\text{H}_2\text{O}$  to  $\text{H}^+$  and  $\text{HCO}_3^-$  (95). The basolateral transporters include the  $\text{Na}^+/\text{K}^+$  ATPase,  $\text{K}^+$  channels,  $\text{Na}^+/\text{K}^+/\text{2Cl}^-$  cotransporter (NKCC1),  $\text{Na}^+-\text{HCO}_3^-$  cotransporters (NBCs),  $\text{Na}^+/\text{H}^+$  exchanger isoform 1 (NHE1), and the  $\text{Cl}^-/\text{HCO}_3^-$  exchanger AE2 (31). The

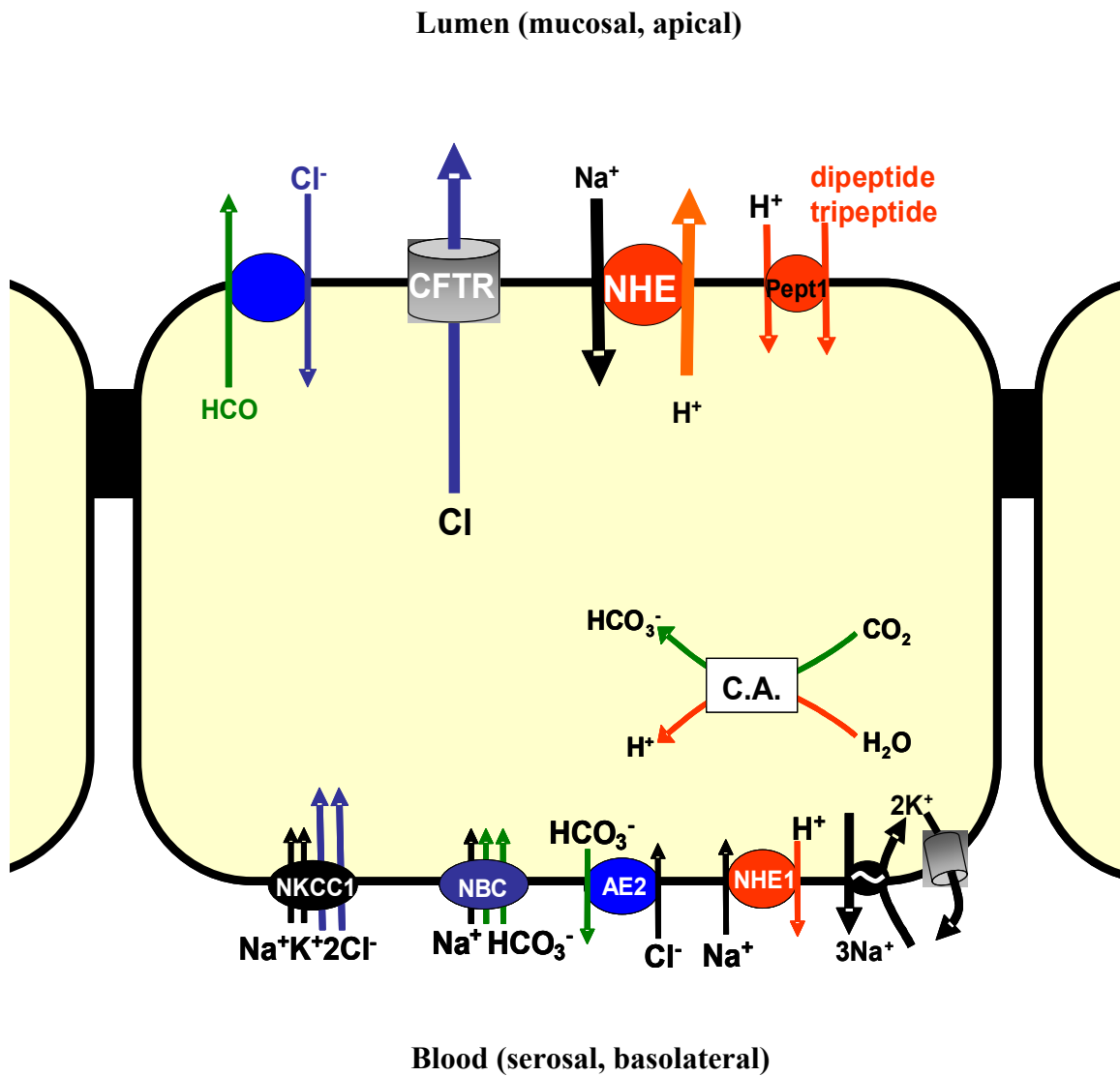
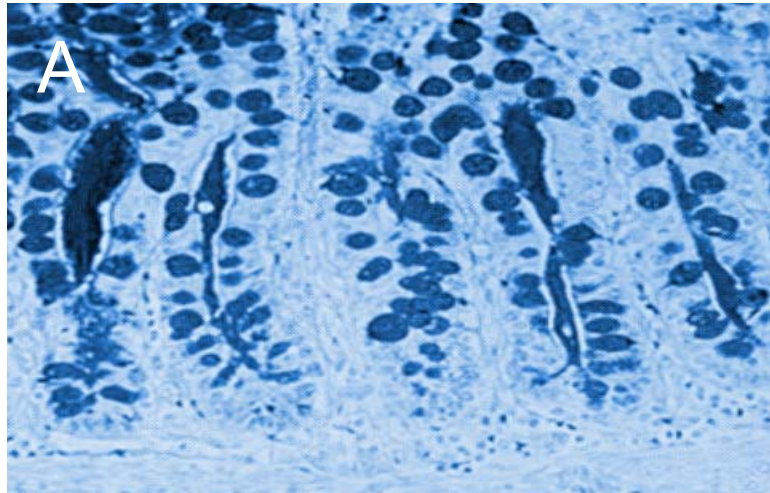


**Figure 1.3.** Generic model of an intestinal villous epithelial cell. Relevant ion transporters are labeled.

principal functions of the basolateral transporters are to regulate cell volume and pH regulation, establish membrane potential, and take up ions for transcellular secretion.

## **Cystic Fibrosis**

Cystic fibrosis (CF) is an autosomal recessive disease that is the most common lethal genetic disorder in the Caucasian population (27). CF affects approximately 30,000 children and adults in the United States with the median age of survival being 36.8 years according to a recent survey by the Cystic Fibrosis Foundation, and it is estimated that approximately 5% of the population are clinically silent heterozygous carriers (2). CF is caused by a mutation in CFTR, a cyclic nucleotide-activated anion channel that is expressed in the apical membrane of epithelial cells in the airways, pancreatic ducts, intestine, salivary and sweat ducts, and gallbladder (7;86). As result, there is a loss of anion secretion principally  $\text{Cl}^-$  through CFTR as well as the loss of direct and indirect regulatory influence over many transepithelial electrolyte transport processes including  $\text{HCO}_3^-$  secretion (25;43;45;46;96) and NaCl absorption (6). In CF patients, over 1400 mutations of CFTR have been identified (3); however, the most common is the  $\Delta\text{F508}$  mutation (~70% of all cases), which occurs due to a deletion of the phenylalanine residue at position 508 of CFTR (52;86). Abnormalities in CFTR lead to disruption of anion secretion and excessive salt and water absorption in ion transport in various epithelial lined organs resulting in the plugging of ducts with tenacious secretions. As a result, CF presents as a multi-organ disease whose manifestations include meconium ileus (Figure 1.4), distal intestinal obstructive disease, duodenal acidity, airway mucociliary clearance failure and exocrine pancreatic insufficiency (122). A CF mouse



Arey, J.B. and Valdes-Dapena, M., *Pathology of the Gastrointestinal Tract*, 1992

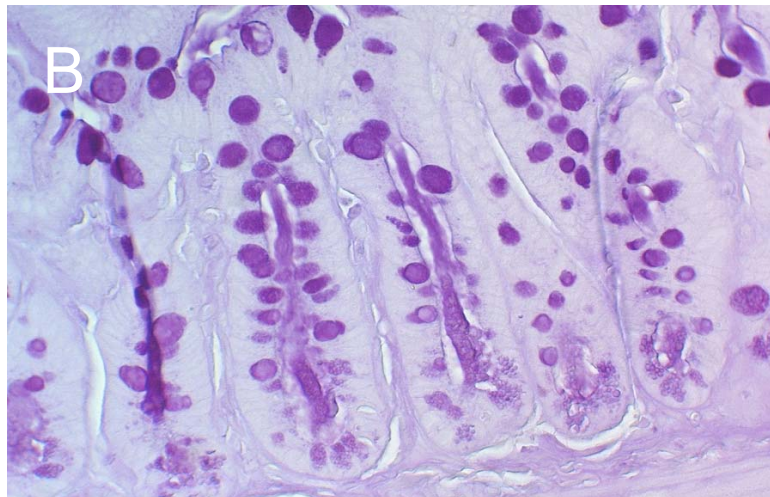


**Figure 1.4.** Photomicrograph of the small intestine (high magnification 400X) from **A.** a human CF patient with meconium ileus and **B.** a CF mouse. Histopathologically, the CF intestine is characterized by goblet cell hyperplasia and mucoid casts within the crypts. The obstructive syndrome and histopathologic appearance are accurately reproduced in CF mouse models.

model was initially developed in 1992 due to targeted disruption of the murine homolog of the *cftr* gene (97). Subsequently, additional mouse models have been generated that carry CFTR specific mutations corresponding to both mild (R117H) and severe (DF508, G551D) forms of human CF (29;115;126). CF mouse models have been shown to lack cAMP-stimulated apical membrane anion secretion through CFTR in epithelial tissues (23); however, they do differ from human CF patients with regard to organ level pathology. The mouse model accurately recapitulates the intestinal phenotype of cystic fibrosis exhibiting poor growth rates, duodenal acidity due to deficient  $\text{HCO}_3^-$  secretion, and a severe intestinal obstructive syndrome (97) (Figure 1.4) that can be lethal if not treated orally with an osmotic laxative (22). In contrast to human CF patients, CF mice normally do not present with overt airway or pancreatic disease, which is proposed to be due to the presence of an alternate  $\text{Cl}^-$  conductance pathway in these organs (23).

### **Duodenal $\text{HCO}_3^-$ Secretion**

The alkaline mucus barrier of the duodenum plays an important role in protecting the epithelium from acidic chyme entering from the stomach (36). Active  $\text{HCO}_3^-$  secretion involves the apical membrane activities of the CFTR and  $\text{Cl}^-/\text{HCO}_3^-$  exchangers. Under basal, non-stimulated conditions, pH stat studies of CF patients and CF mouse models indicate that bicarbonate secretion by anion exchange predominates in the duodenum (84). In addition, most studies show that basal bicarbonate secretion is reduced in the CF duodenum, but the specific pathophysiology of the deficiency has yet to be elucidated (84). In contrast to basal secretion, during cAMP stimulation (a result of paracrine and neural action under physiological conditions), electrogenic  $\text{HCO}_3^-$

secretion predominates, and this response is essentially absent in the CFTR(-) duodenum (25;87). Two models for cAMP-stimulated  $\text{HCO}_3^-$  secretion have been proposed as depicted in Figure 1.5 (75). One model supports activation of an apical membrane  $\text{HCO}_3^-$  conductance. It is known that CFTR conducts  $\text{HCO}_3^-$  in addition to  $\text{Cl}^-$ , but its permeability is significantly less ( $P_{\text{HCO}_3^-} : P_{\text{Cl}^-} \approx 0.25$ ) (41;80), and the permeability may be reduced further due to anomalous mole fraction behavior of the channel (105). A second model proposed for cAMP-stimulated secretion involves the interaction of CFTR with anion exchange proteins. Studies of pancreatic duct epithelium first postulated that a cAMP-stimulated  $\text{Cl}^-$  channel (CFTR) indirectly facilitates  $\text{Cl}^-/\text{HCO}_3^-$  exchange by recycling  $\text{Cl}^-$ , thus, maintaining a favorable outside:inside concentration gradient for  $\text{Cl}^-$  (75). Other studies of recombinant proteins indicate the possibility of direct intermolecular associations between anion exchange proteins and CFTR. During cAMP stimulation, the STAS domain of Slc26a transporters, a major class of apical membrane  $\text{Cl}^-/\text{HCO}_3^-$  exchangers, has been shown to enhance CFTR channel activity (56), whereas the regulatory domain of CFTR has been shown to increase  $\text{Cl}^-/\text{base}$  exchange by these anion exchanger proteins (60).

Expression studies of villous epithelium show the presence of CFTR (104) and apical membrane  $\text{Cl}^-/\text{HCO}_3^-$  exchanger proteins including at least two members of the sulfate permease family, i.e., Slc26a3 (DRA) and Slc26a6 (PAT-1), and one member of the anion exchanger family, Slc4a9 (AE4) (48) (Figure 1.6). Although reduced relative to crypt epithelium, functional CFTR is present on the intestinal villi in both human and mouse (39;76). Villi and epithelial microvilli increase the intestinal surface area by

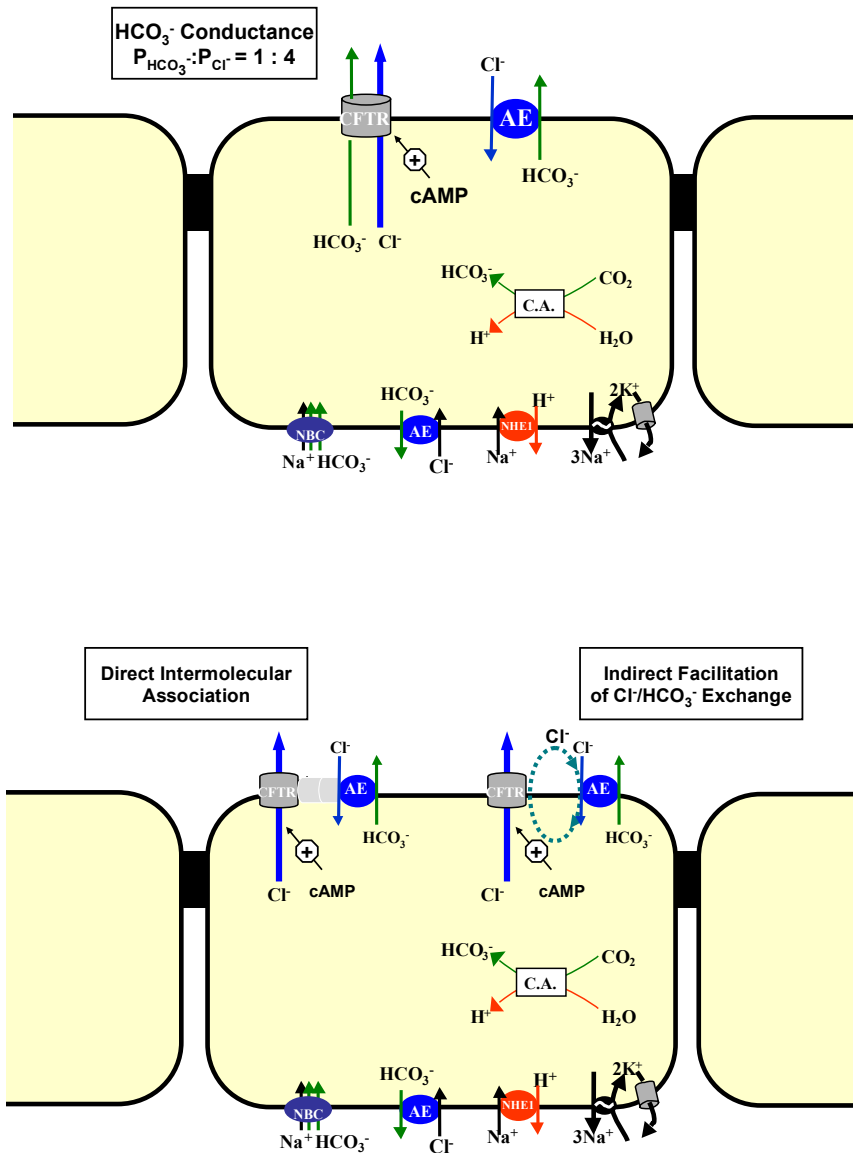


**Figure 1.5.** Two proposed models for cAMP-stimulated  $\text{HCO}_3^-$  secretion. One model (upper) supports CFTR  $\text{HCO}_3^-$  conductance. The second model (lower) involves the interaction of CFTR with anion exchange proteins either by direct intermolecular association or by indirect facilitation of  $\text{Cl}^-/\text{HCO}_3^-$  exchange.



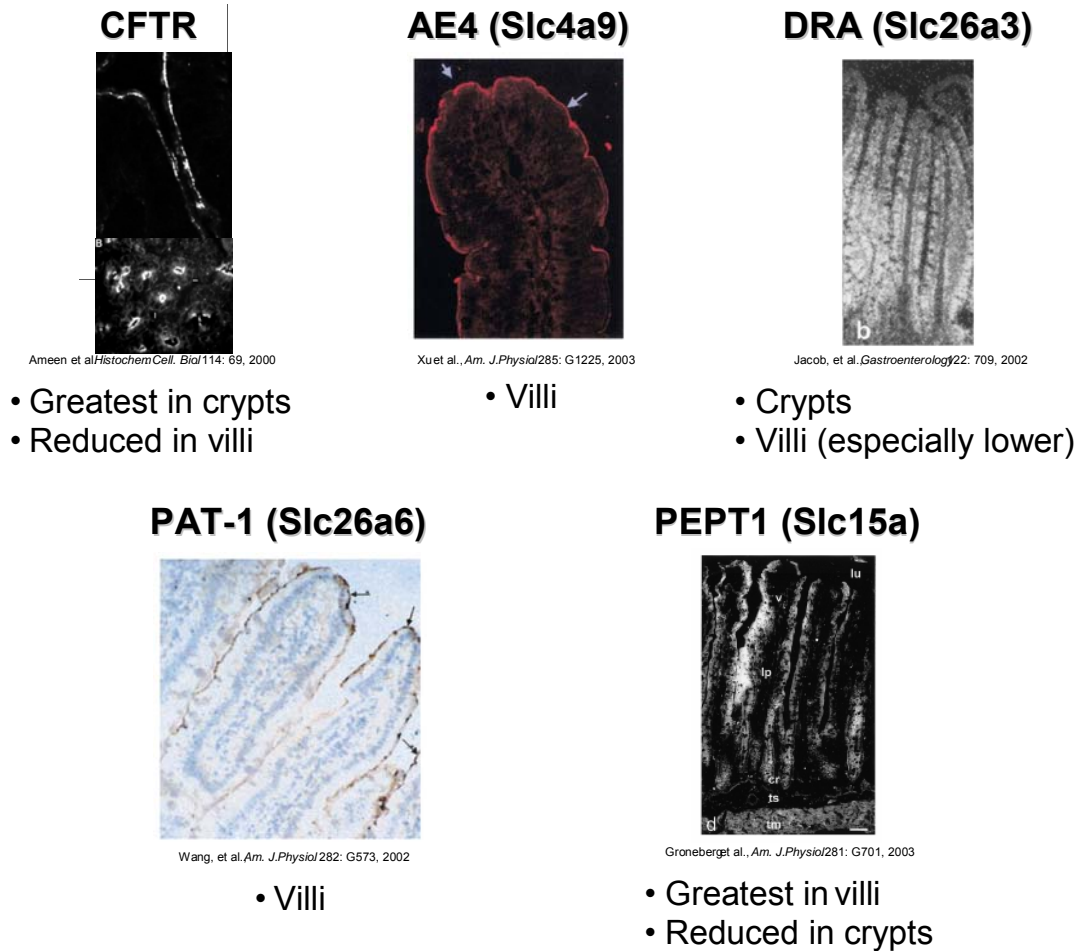


**Figure 1.6.** Cellular localization of CFTR, AE4, DRA, PAT-1, and PEPT1 in the duodenum.

~200-fold; thus, the contribution of  $\text{HCO}_3^-$  secretion from these structures is likely considerable. However, little is known about the processes of  $\text{HCO}_3^-$  transport and their role in protecting these epithelial projections from the acidic luminal effluent.

### **Apical Membrane $\text{Cl}^-/\text{HCO}_3^-$ Exchangers**

#### *Anion Exchanger 4*

One member of the SLC4 bicarbonate transporter family, Slc4a9 (AE4) (125) has been localized to the apical membrane of duodenal villous and gastric epithelium (54). Functional expression studies in *Xenopus* oocytes indicate that AE4 has  $\text{Cl}^-/\text{HCO}_3^-$  exchange activity (125).

#### *Slc26a $\text{Cl}^-/\text{HCO}_3^-$ Exchangers*

The ten members of the multifunctional anion exchanger gene family (Slc26a) are responsible for transporting a wide variety of monovalent and divalent anions including  $\text{SO}_4^{2-}$ ,  $\text{Cl}^-$ ,  $\text{I}^-$ , formate, oxalate, hydroxyl and  $\text{HCO}_3^-$  (72). These transporters are involved in a number of physiological processes including bicarbonate secretion by the distal nephron and pancreas, transepithelial NaCl transport, skeletal development, and thyroid hormone synthesis, and mutations in at least 4 family members result in genetic disease (72). Two family members, Slc26a3 (DRA) and Slc26a6 (PAT-1), have been conclusively shown to function as  $\text{Cl}^-/\text{HCO}_3^-$  exchangers and are localized to the apical membrane of epithelial tissues, including the villous epithelium (48).

#### *a. DRA*

DRA was initially identified as a potential tumor suppressor that was down-regulated in adenomas and induced growth suppression when over-expressed in

cultured cells (18). DRA is predominantly expressed in the gastrointestinal tract with highest levels in the colon and duodenum (48). Studies utilizing recombinant proteins have shown that DRA transports  $\text{HCO}_3^-$  in exchange for luminal  $\text{Cl}^-$ ,  $\text{SO}_4^{2-}$ , or oxalate (72). Conflicting reports exist regarding the sensitivity of DRA to the distillbene DIDS, but niflumic acid and tenidap have been shown to be effective inhibitors (20;72). Studies of recombinant DRA expressed in HEK 293 cells indicate that removal of extracellular  $\text{Cl}^-$  causes depolarization, which has led to the proposal that DRA is electrogenic, exchanging  $\geq 2\text{Cl}^-$  per  $\text{HCO}_3^-$  (55). However, these results are at odds with studies showing that membrane depolarization with high external  $\text{K}^+$  concentration does not affect activity (73), and investigations of DRA expressed in *Xenopus* oocytes that have not found alterations in membrane potential during  $\text{Cl}^-_{\text{in}}/\text{HCO}_3^-_{\text{out}}$  exchange (69;72). Loss-of-function mutation in human DRA (SLC26A3) is the causal factor in the inherited disease congenital chloride-losing diarrhea (CLD), which results from defective intestinal  $\text{Cl}^-/\text{HCO}_3^-$  exchange and is characterized by a diarrhea with high  $\text{Cl}^-$  content and systemic alkalization (51;71). Initial reports of clinical disease in the DRA knockout mouse model (i.e., diarrhea, chloride stool concentration, and growth retardation) closely resemble that of human CLD (17). The severe intestinal manifestations of CLD may reflect a functional coupling between DRA and the major apical membrane  $\text{Na}^+/\text{H}^+$  exchangers (NHE2 and NHE3) responsible for electroneutral  $\text{NaCl}$  absorption, as based on evidence of functional coupling of these exchangers in recombinant cell systems and changes in DRA expression in the NHE3 knockout intestine (73).

b. *PAT-1*

PAT-1 was first identified as the apical Cl<sup>-</sup>/formate exchanger in renal tubules, i.e., CFEX (53). PAT-1 demonstrates abundant expression in the apical membrane of the kidney, pancreas, and intestine (53). This exchanger is the most versatile member of the Slc26a family transporting Cl<sup>-</sup>, HCO<sub>3</sub><sup>-</sup>, SO<sub>4</sub><sup>2-</sup>, oxalate, formate, and hydroxyl (72). Previous transport studies indicate that PAT-1 is electrogenic but, in contrast to DRA, removal of extracellular Cl<sup>-</sup> results in cell hyperpolarization, suggesting a stoichiometry of 1Cl<sup>-</sup>:≥2 HCO<sub>3</sub><sup>-</sup> (55). However, recent studies of mPAT-1 expressed in *Xenopus* oocytes indicate that Cl<sup>-</sup>/HCO<sub>3</sub><sup>-</sup> exchange is electroneutral whereas Cl<sup>-</sup>/oxalate exchange is electrogenic (19). Preliminary studies in the knockout mouse model reveal that PAT-1 is important in apical membrane Cl<sup>-</sup>/base exchange of the proximal renal tubule and contributes to HCO<sub>3</sub><sup>-</sup> secretion in the duodenum; although investigations of PAT-1 (-) mice have revealed no overt disease and normal growth rates (114;119).

### **Carbonic Anhydrase**

Carbonic anhydrases, which efficiently catalyze the reversible hydration of CO<sub>2</sub> to HCO<sub>3</sub><sup>-</sup> and H<sup>+</sup>, play a critical role in driving the transport of HCO<sub>3</sub><sup>-</sup> across cells and epithelial layers. They are categorized based upon their cellular localization: 1) cytosolic, 2) mitochondrial, 3) membrane-associated, and 4) secreted with cytosolic CAII being the most widely expressed isozyme in the small intestine. CAs are found in virtually every cell type and play critical roles in CO<sub>2</sub> transport, intracellular buffering, and the regulation of intracellular and extracellular pH (95). In addition, several lines of

evidence have demonstrated both functional and physical relationships between CAs and  $\text{Cl}^-/\text{HCO}_3^-$  exchange proteins (4;102) allowing the formation of a bicarbonate transport metabolon that accelerates transmembrane  $\text{HCO}_3^-$  flux.

### **Intestinal Transport of Peptides and Peptidomimetics**

The intestinal brush border possesses several transport systems that allow for the absorption of peptides and amino acids produced during luminal protein digestion. Evidence indicates that most amino acids are absorbed more efficiently when presented to the lumen in the form of small peptides, which are transported by the apical  $\text{H}^+$  peptide cotransporter SLC15A1 (PEPT1) (28). The PEPT1 protein has the ability to transport all the 400 different dipeptides and 8000 different tripeptides derived from luminal protein digestion regardless of net charge, molecular size, and solubility (57). In addition, many orally delivered drugs which have dipeptide and tripeptide structures, including  $\beta$ -lactam antibiotics and ACE inhibitors, and bacterial products, such as f-MLP and muramyl dipeptide, cross the absorption barrier by means of transport through PEPT1 (15;38;70;116).

PEPT1 is expressed along the longitudinal axis of the small intestine with greatest levels in the duodenum and jejunum. Expression is not detectable in the crypts but increases from the villous base to its highest levels in the villous tips with protein expression almost exclusively restricted to the brush border membrane of the intestinal mucosa (Figure 1.6) (38). In response to certain substrates, fasting, and starvation, PEPT1 expression is upregulated by means of increased PEPT1 transcription (74;106;117). In addition, insulin, leptin, and clonidine may increase PEPT1-mediated

transport as a result of increased trafficking of PEPT1 to the apical membrane from a preformed cytoplasmic pool (10;14;107).

### **Regulation of Intracellular pH (pH<sub>i</sub>) during PEPT1 Transport**

Transport via PEPT1 is electrogenic and is coupled to an inwardly directed proton gradient that allows for transport of peptides against a concentration gradient (65).

H<sup>+</sup>/peptide influx exhibits a stoichiometry of 1:1, which occurs irrespective of the net charge associated with the peptide, but there is a clear preference for non-charged species (57). Studies of intestinal cell lines have shown that proton di-/tripeptide uptake results in intracellular acidification, and this decrease in pH<sub>i</sub> will diminish the driving force for PEPT1-mediated transport unless the proton load is reduced by means of intracellular buffering or proton efflux (110;111). Therefore, optimal peptide absorption must rely upon the cooperation of a number of transport proteins present in intestinal epithelial cells. The current model for the regulation of pH<sub>i</sub> during PEPT1 transport (Figure 1.7) is based upon studies conducted in intestinal cell lines endogenously expressing PEPT1 and Na<sup>+</sup>/H<sup>+</sup> exchanger proteins (50). In the absence of CO<sub>2</sub>/HCO<sub>3</sub><sup>-</sup> in the bathing medium, these investigations revealed that PEPT1-mediated transport activates the apical membrane NHE3 (112;113). As a result, H<sup>+</sup> can be exported across the apical membrane maintaining pH<sub>i</sub> and the driving force for peptide absorption. Sodium influx via NHE3 exits the cell by means of the basolateral Na<sup>+</sup>/K<sup>+</sup> ATPase, and the resulting increase in intracellular K<sup>+</sup> is dissipated by basolateral K<sup>+</sup> channels. This model, however, may be incomplete because it does not consider the contributions of acid-base transport proteins that are functional in the presence of CO<sub>2</sub>/HCO<sub>3</sub><sup>-</sup> (i.e., under physiologic conditions).

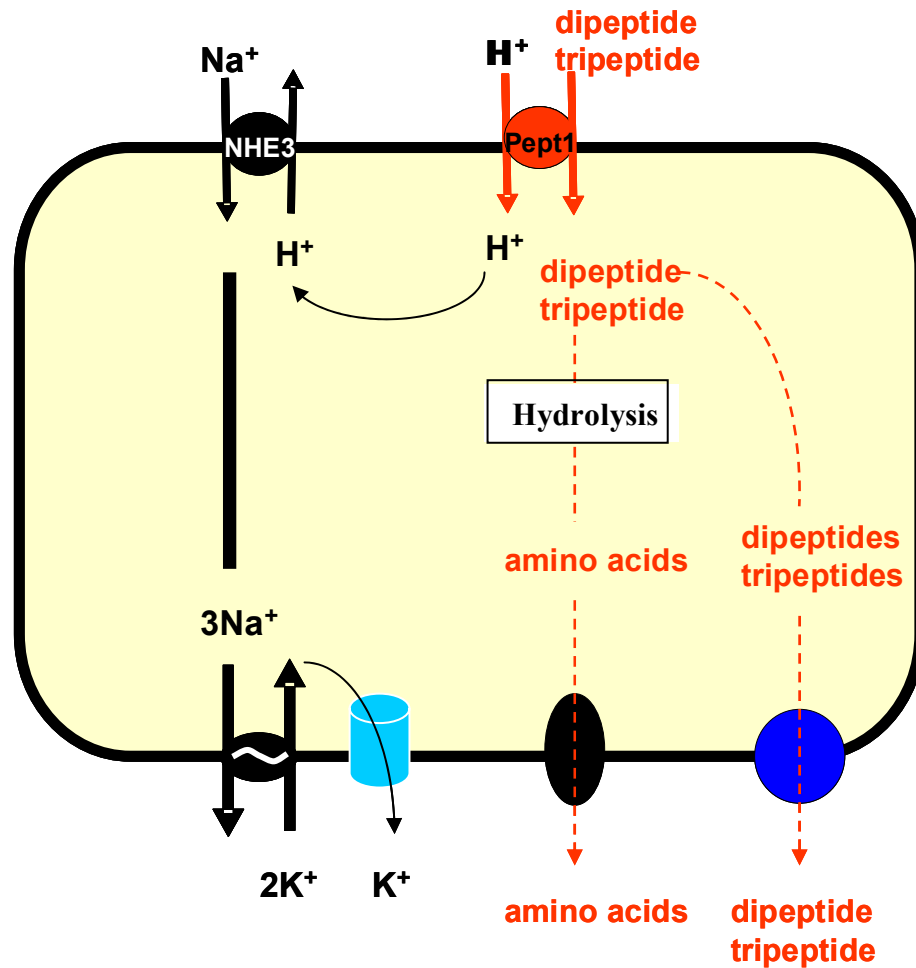


**Figure 1.7.** Current model for intestinal peptide transport through PEPT1 and the resulting cooperative action of various membrane transport proteins based on recombinant protein studies and performed in the absence of CO<sub>2</sub>/HCO<sub>3</sub><sup>-</sup> in the media.

One study performed in the presence of  $\text{CO}_2/\text{HCO}_3^-$  has demonstrated that intracellular carbonic anhydrase activity can facilitate diffusive  $\text{H}^+$  movement thereby maintaining a transmembrane ion gradient that allows for maximal absorption via PEPT1 in murine small intestinal villous epithelia (103). Additional studies are required under physiologic conditions to gain a complete understanding of the various acid-base transport proteins involved in sustaining PEPT1-mediated absorption through across native epithelium.

### **Dissertation Overview**

This chapter gives the reader an overview of gastrointestinal ion transport physiology, cystic fibrosis, and peptide transport. The following chapters summarize the physiology research performed by the author over the last four years. Chapter 2 summarizes the role of CFTR and  $\text{Cl}^-/\text{HCO}_3^-$  exchange in the process of basal bicarbonate secretion in the murine duodenal villous epithelium. In chapter 3, the predominant apical  $\text{Cl}^-/\text{HCO}_3^-$  exchanger of the murine duodenal upper villus is identified through the use of knockout mouse models for AE4, DRA, and PAT-1. Finally, chapter 4 discusses a potential role for PAT-1 in the regulation of  $\text{pH}_i$  during PEPT1 transport. Together, these chapters document an investigation of the physiologic roles of PAT-1, DRA, and AE4 in the murine duodenal villus and their interactions with CFTR and PEPT1. Chapter 5 contains summary and conclusions from the preceding chapters and a discussion of potential future experiments based on this work.



## Chapter 2

# CHLORIDE CONDUCTANCE OF CFTR FACILITATES BASAL $\text{Cl}^-/\text{HCO}_3^-$ EXCHANGE IN VILLOUS EPITHELIUM OF INTACT MURINE DUODENUM

### Introduction

The alkaline mucus barrier of the duodenum plays an important role in protecting the epithelium from damage by acid chyme entering from the stomach (36). Alkalinity of the surface mucus is sustained by transcellular processes of  $\text{HCO}_3^-$  secretion that involve coordination of the activities of the cystic fibrosis transmembrane conductance regulator (CFTR) and anion exchanger proteins (25;84;99). Under basal, non-stimulated conditions, pH stat studies of cystic fibrosis (CF) patients and CF mouse models indicate that bicarbonate secretion by anion exchange predominates in the duodenum (25;26;84;87). Most studies further show that basal  $\text{HCO}_3^-$  secretion is reduced in CF duodenum, but the pathophysiology of this deficiency has not been elucidated (26;84;87). In contrast to basal secretion, it is known that CFTR is essential to cAMP stimulation of  $\text{HCO}_3^-$  secretion, a consequence of increased prostanoid and neural activity induced by exposure of the duodenum to the gastric effluent (36). The mechanism of this process has been an area of intense investigation in recent years. Most controversy surrounds the question of whether CFTR, a cAMP-stimulated anion channel (6), provides a conductive pathway for  $\text{HCO}_3^-$  ions across the apical membrane of the epithelium. CFTR is permeable to  $\text{HCO}_3^-$  but at a reduced level relative to  $\text{Cl}^-$  ( $P_{\text{HCO}_3^-} : P_{\text{Cl}^-} \approx 0.25$ ) (41;80), and the permeability may be reduced further due to anomalous mole fraction behavior of the

channel (105). However, studies of intact intestine from animal models are consistent with dominance of a  $\text{HCO}_3^-$  conductance in that 75 - 80% of cAMP-stimulated  $\text{HCO}_3^-$  secretion is preserved in the absence of luminal (apical)  $\text{Cl}^-$ , a condition that inhibits the activity of the apical membrane  $\text{Cl}^-/\text{HCO}_3^-$  exchange proteins (25;99). Interpretation of these data must accommodate recent evidence that CFTR permeability to  $\text{HCO}_3^-$  is dynamically regulated both by intracellular factors (85) and, important to this discussion, by extracellular  $\text{Cl}^-$  concentration, i.e.,  $\text{HCO}_3^-$  permeability increases in the absence of extracellular  $\text{Cl}^-$  (89).

A second model proposed for cAMP-stimulated secretion involves the interaction of CFTR with anion exchange proteins. Studies of pancreatic duct epithelium first postulated that a cAMP-stimulated  $\text{Cl}^-$  channel (CFTR) indirectly facilitates  $\text{Cl}^-/\text{HCO}_3^-$  exchange by recycling  $\text{Cl}^-$ , thus, maintaining a favorable outside:inside concentration gradient for  $\text{Cl}^-$  (75). Subsequent investigations of other epithelia and heterologous expression systems demonstrated that CFTR activation stimulates  $\text{Cl}^-/\text{HCO}_3^-$  exchange activity (60;61). In the duodenum, studies of brush border membrane vesicles have shown that  $\text{Cl}^-/\text{HCO}_3^-$  exchange is increased by cAMP stimulation (33) and evidence of CFTR facilitation of  $\text{Cl}^-/\text{HCO}_3^-$  exchange in intestinal mucosa was provided by investigations of cAMP-stimulated murine duodenum during isolation of carbonic anhydrase activity (25) and inhibition of the NKCC1  $\text{Na}^+/\text{K}^+/2\text{Cl}^-$  cotransporter (118). Recent studies have immunolocalized several anion exchange proteins to the apical membrane of intestinal epithelium including at least two members of the sulfate permease family, i.e., Slc26a3 (known as the down-regulated in adenoma gene DRA) and Slc26a6 (known as the putative anion transporter-1 PAT-1 or chloride-formate exchanger CFEX),

and one member of the anion exchanger family, Slc4a4 (i.e., AE4) (64;79;125). The Slc26a anion exchangers and CFTR possess PSD-25/Disc-large/zonula occludens-1 (PDZ) domains that enable co-localization of these proteins on the binding sites of scaffolding proteins such as the Na<sup>+</sup>/H<sup>+</sup> exchanger regulatory factor (NHERF) (59;63;91). Further, studies of recombinant proteins indicate the possibility of direct intermolecular associations between the anion exchange proteins and CFTR. During cAMP stimulation, the STAS domain of Slc26a transporters has been shown to enhance CFTR channel activity whereas the regulatory R domain of CFTR increases Cl<sup>-</sup>/base exchange by the anion exchangers (56). Thus, our model of the interactions between CFTR and the apical membrane anion exchangers during cAMP-stimulation must be modified to include molecular associations between proteins.

Situated for direct exposure to gastric acid effluent, the villi of the duodenal mucosa are presented with a unique challenge in maintaining a protective alkaline mucus barrier. Although it is well-documented that CFTR expression is greatest in the crypts, CFTR mRNA and protein expression extend to the villous tips and greatest levels of expression occur in the duodenum (5;104). Evidence of CFTR channel activity in the villous epithelium includes X-ray microanalysis of intestinal cryosections from normal and CF jejuna indicating CFTR-dependent Cl<sup>-</sup> secretion (76), and BCECF studies of intact duodenum from normal and CF mice demonstrating the presence of a CFTR-dependent HCO<sub>3</sub><sup>-</sup> conductance (39). In addition to the presence of a functional CFTR, all three of the known apical membrane anion exchangers (DRA, PAT-1 and AE4) in the duodenum have been immunolocalized to the villous epithelial cells (64;79;125). Thus, the basic components for HCO<sub>3</sub><sup>-</sup> transport are present, but little is known about the

physiology of  $\text{HCO}_3^-$  secretion across the abundant mucosal surface area of the villous epithelium.

In the present study, we investigate basal activity of anion exchange across the apical membrane of epithelial cells in the mid-region of villi of intact duodenal mucosa from wild-type (WT) and CFTR-null (CF) mice using BCECF microspectrofluorimetry of intracellular pH ( $\text{pH}_i$ ). The duodenal mucosa was mounted in a horizontal Ussing-type chamber that allowed independent superfusion of the luminal and basolateral surfaces of the epithelium. Using this system, the characteristics of anion exchange were investigated in the presence or absence of CFTR activity in the villous epithelium.

## **Materials and Methods**

### *Animals*

The experiments in this study used mice 8 - 12 wks old that were either homozygous for the S489X mutation of the murine homolog of CFTR ( $\text{cfr}^{\text{tm1UNC}}$ ) or homozygous for the mCFTR  $\Delta\text{F508}$  mutation ( $\text{cfr}^{\text{tm1Kth}}$ ) and maintained on a C57BL/6J background (>6 generations) (97;126). The mutant mice were identified by using a PCR based analysis of tail snip DNA, as previously described (24). No significant differences in experimental parameters were noted between the two CF mouse models which were compared with WT littermate mice. All mice were maintained *ad libitum* on standard laboratory chow (Formulab 5008 Rodent Chow; Ralston Purina) and drinking water containing an oral osmotic laxative (Schwartz Pharma, Seymour, IN) with the following composition (in g/L): 60.00 polyethylene glycol 3350 (PEG), 1.46 NaCl, 0.75 KCl, 1.68  $\text{NaHCO}_3$ , and 5.68  $\text{Na}_2\text{SO}_4$ . The mice were housed singly in a temperature (22-26°C) and

light (12:12-h light-dark cycle)-controlled room in the Association for Assessment and Accreditation of Laboratory Animal Care (AAALAC) accredited animal facility at the Dalton Cardiovascular Research Center. Intestinal tissues for experiments were obtained from mice 2-4 months of age. The mice were fasted overnight prior to experimentation but were provided with water *ad libitum*. All experiments involving animals were approved by the University of Missouri Animal and Use Committee

#### *Fluorescence Measurement of Intracellular pH and Image Analysis*

The method used for imaging intact intestinal epithelium was based on techniques for imaging murine isolated duodenal villi, as previously described (39). Animals were sacrificed by asphyxiation in a 100% CO<sub>2</sub> atmosphere followed by bilateral pneumothorax. The duodenum was removed via an abdominal incision and was immediately placed in an ice-cold, oxygenated Ringer's solution. The duodenal segment was opened along the mesenteric border using sharp dissection and pinned flat with mucosal side down in a Sylgard-filled Petri dish. After scoring along one end of the preparation with a scalpel blade, the serosa and muscularis externa were removed along the longitudinal axis by blunt dissection using fine forceps. Dissection was confirmed by histological examination. The muscle-stripped intestinal preparations were mounted luminal (apical) side up on a horizontal bilateral perfusion chamber in which mucosal and serosal surfaces were independently bathed. Throughout the experimental period, all duodenal preparations were treated with indomethacin (1 μM) and tetrodotoxin (TTX, 0.1 μM) to minimize the effect of endogenous prostaglandins and neural tone, respectively (13;90). To immobilize villi for imaging, the tips of a small percentage (< 1%) of the villi were trapped under strands of a loose nylon mesh that was placed over the mucosal

surface of the preparation. The duodenal preparation was washed with a solution containing 100  $\mu\text{M}$  DL-dithiothreitol and then incubated with 16  $\mu\text{mol/L}$  of 2',7'-bis-(2-carboxyethyl)-5-(and-6)-carboxyfluorescein acetoxymethyl ester (BCECF-AM) for 10 minutes on the luminal side in a isethionate-bicarbonate Ringer solution (IBR) containing (in mM): 140.0  $\text{Na}^+$ , 55.0  $\text{Cl}^-$ , 55.0 isethionate $^-$ , 25.0  $\text{HCO}_3^-$ , 5.2  $\text{K}^+$ , 5.0 N-tris methyl-2-aminoethanesulfonic acid (TES), 4.8 gluconate $^-$ , 2.8  $\text{PO}_4^{2-}$ , 1.2  $\text{Ca}^{2+}$ , 1.2  $\text{Mg}^{2+}$ , 10.0 glucose, and 6.8 mannitol that was gassed with 95%  $\text{O}_2$ : 5%  $\text{CO}_2$  at 37°C (pH 7.4). As described previously (39;44), the duodenal villous epithelium was loaded with BCECF-AM (Figure 2.1A) and an area in the mid to upper region of a single, immobilized villus (~ 1 mm from the villous tip) was visualized using a 10X water-immersion objective (Figure 2.1B). Approximately 10 epithelial cells were selected for ratiometric analysis using a 40X water immersion objective (Figure 2.1C). Viability of the cells after preparation was evaluated using trypan blue exclusion. Changes in intracellular pH ( $\text{pH}_i$ ) were measured by the dual excitation wavelength technique (440 and 495 nm) and the villi were imaged at a 535 nm emission wavelength. Autofluorescence (in the absence of BCECF) was measured in villous epithelia from 6 mice and the average emission at each wavelength was subtracted for background correction. Ratiometric images were acquired at 20 second intervals with a Sensi-Cam digital camera (Cooke, Auburn Heights, MI) and images were processed using Axon Imaging Workbench 2.2 (Axon Instruments, Union City, CA). The 495: 440 nm ratios were converted to  $\text{pH}_i$  using a standard curve generated by the  $\text{K}^+$ /nigericin technique (12;108).

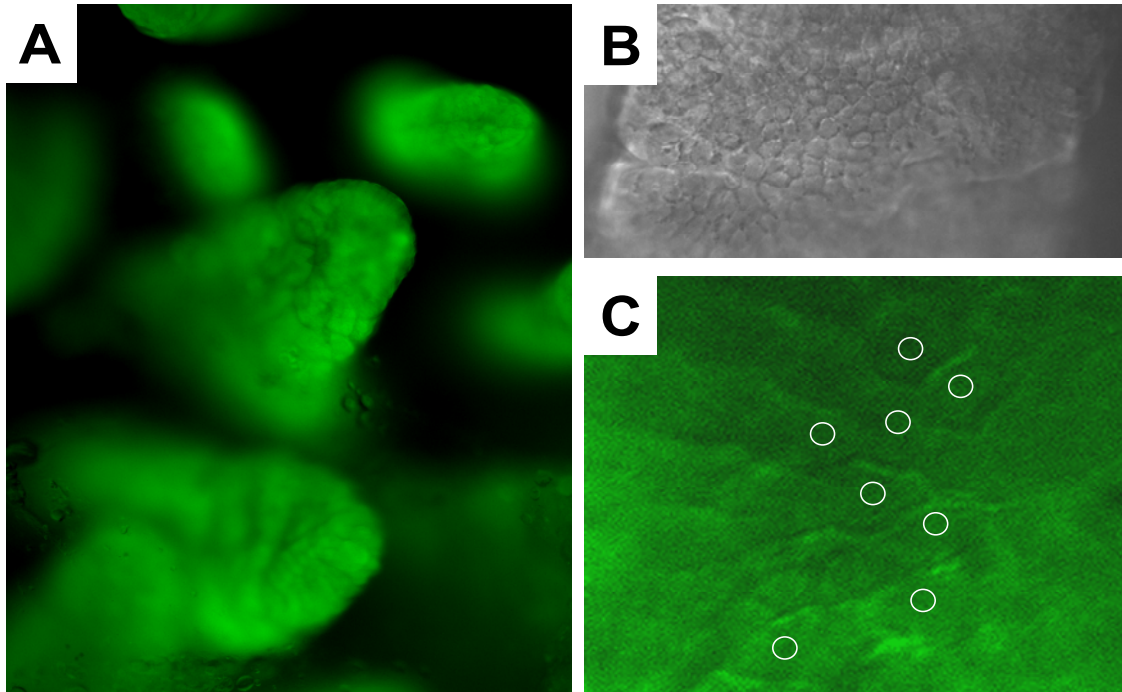


**Figure 2.1.** Images of BCECF-loaded villi from murine duodenum. **A.** Low power image of BCECF-loaded duodenal villi visualized by conventional fluorescent microscopy using an upright, water-immersion objective (100X,  $\lambda$  535 nm). **B.** High power *en face* image of the upper mid-region of a single, immobilized duodenal villus visualized by light microscopy using an upright, water-immersion objective (400X). **C.** Enhanced high power *en face* image of BCECF-loaded duodenal epithelium in the mid-region of a single villus (400 X,  $\lambda$  535 nm). White circles denote regions of interest within individual epithelial cells used for data acquisition.

### *Determination of Buffering Capacity and Base Flux*

Intracellular buffering capacity ( $\beta_i$ ) of WT and CF duodenal villous cells was estimated by the ammonium alkalization technique (121). Briefly, intact duodenal tissue was mounted in a horizontal bilateral perfusion chamber and loaded with BCECF-AM as described above. The tissue was superfused with a  $\text{Na}^+$  and  $\text{HCO}_3^-$ -free ringer containing varying concentrations of  $\text{NH}_4\text{Cl}$ .  $[\text{NH}_4^+]_i$  was calculated from the Henderson-Hasselbalch equation, and  $\beta_i$  was determined as  $\Delta[\text{NH}_4^+]_i/\Delta\text{pH}_i$ . Consistent with previous observations (8;82), no differences in  $\text{pH}_i$  between WT and CF murine intestinal epithelial cells were apparent. Interestingly, the  $\text{pH}_i$  of the villous epithelial cells in the intact mucosa (31.8 mM at pH 7.6) exceeded previous estimates of  $\text{pH}_i$  in isolated murine colonic crypts (26.7 at pH 7.6) and isolated murine duodenocytes (6.4 mM at pH 7.6) (8;82). The total buffering capacity ( $\beta_{\text{total}}$ ) was calculated from the equation  $\beta_{\text{total}} = \beta_i + \beta_{\text{HCO}_3^-} = \beta_i + 2.3 \times [\text{HCO}_3^-]_i$ , where  $\beta_{\text{HCO}_3^-}$  is the buffering capacity of the  $\text{HCO}_3^-/\text{CO}_2$  system and  $[\text{HCO}_3^-]_i$  is the intracellular concentration of  $\text{HCO}_3^-$ . The rates of  $\text{pH}_i$  change measured in these experiments were converted to transmembrane net base flux ( $J(\text{B}^-)$ ) using the equation  $J(\text{B}^-) = \Delta\text{pH}/\Delta t \times \beta_{\text{total}}$ . The  $\beta_{\text{total}}$  values used in the determination of net base flux were calculated from the above equation using the average  $\text{pH}_i$  during the 90-s period of linear  $\Delta\text{pH}/\Delta t$  changes (see below).

### *Measurement of apical membrane anion exchange*

Duodenal preparations were typically perfused with IBR on the luminal side. The basolateral superfusate consisted of a  $\text{Cl}^-$ -free IBR ( $\text{Cl}^-$  replaced with isethionate $^-$ ) gassed with 95%  $\text{O}_2$ : 5%  $\text{CO}_2$  at 37°C (pH 7.4) and contained 1  $\mu\text{M}$  5-(N-ethyl-n-isopropyl)-amiloride (EIPA) to block the activity of  $\text{Na}^+/\text{H}^+$  exchanger isoform 1 (NHE1). For



nominally  $\text{HCO}_3^-$ -free solutions,  $\text{NaHCO}_3$  was replaced equimolar with NaTES and gassed with 100 %  $\text{O}_2$ . For solutions with high  $[\text{K}^+]$ , 75 mM NaCl and  $\text{Na}^+$ -isethionate were replaced equimolar with KCl and  $\text{K}^+$ -isethionate, respectively, in both luminal and basolateral superfusates. Experiments to measure anion exchange consisted of  $\text{pH}_i$  alkalization induced by replacement of luminal  $\text{Cl}^-$  with isethionate $^-$  on an equimolar basis. After a stable  $\text{pH}_i$  was obtained (approximately 2 min),  $\text{pH}_i$  recovery was initiated by replacing isethionate $^-$  with  $\text{Cl}^-$ . In some experiments,  $\text{SO}_4^{2-}$  and  $\text{NO}_3^-$  were used to replace  $\text{Cl}^-$  on an equimolar basis during  $\text{pH}_i$  recovery. Rates of anion exchange during alkalization and recovery ( $\Delta\text{pH}/\Delta t$ ) were calculated from a linear regression of the values from the first 90 sec of the initial  $\text{pH}_i$  changes during  $\text{Cl}^-$  removal and replacement, respectively. For inhibitor studies, 1 mM 4,4'-diisothiocyanatostilbene-2,2'-disulfonate (DIDS) was added to the luminal superfusate from a 10 mM stock solution in IBR or 100  $\mu\text{M}$  niflumic acid (NFA) was added to the luminal superfusate from a 100 mM stock in DMSO. For glybenclamide studies, 100  $\mu\text{M}$  glybenclamide was added to the luminal superfusate from a 250 mM stock in DMSO.

#### *Northern blot analysis*

Northern blot analysis of total mRNA was performed as previously described (21). Total RNA from murine duodenum was extracted using TRI-Reagent (Molecular Research Center, Inc.), according to manufacturer's instructions. RNA was mixed with Glyoxal sample buffer (BioWhittaker Molecular Applications, Rockland, ME), separated by 1% agarose gel electrophoresis and transferred to a Hybond-N+ nylon membrane (Amersham Biosciences, Piscataway, NJ). The blot was probed using  $\alpha$ -dCTP  $^{32}\text{P}$ -labeled cDNA PCR product for murine DRA (mDRA), murine PAT-1

(mPAT-1) and the L32 ribosomal protein. For the mDRA probe, the RT-PCR product was obtained using the sense and antisense oligonucleotide primers with the following sequences: 5'-GGTTTAGCATTTGCTCTGCTGG and 5'-TTACAGTCATGATGAGTTCGATG. For the mPAT-1 probe, the RT-PCR product was obtained using the sense and antisense oligonucleotide primers with the following sequences: 5'-GCGACTCTCTGAAAGAGAAGTG and 5'-TCAGAGTTTGGTGGCCAAAACA. Radiographic density of bands was measured using a Kodak Imaging Station 2000R and expression levels of mDRA and mPAT-1 were normalized to L32.

### *Materials*

The fluorescent dye BCECF acetoxymethyl ester was obtained from Molecular Probes (Eugene, OR). Tetrodotoxin was obtained from Biomol International L.P. (Plymouth Meeting, PA). All other materials were obtained from either Sigma Aldrich (St. Louis, MO) or Fisher Scientific (Springfield, NJ).

### *Statistics*

All values are reported as mean  $\pm$  SEM. Data between two treatment groups were compared using a 2-tailed unpaired Student *t*-test assuming equal variances between groups. Data from multiple treatment groups were compared using a one-way analysis of variance with a *post hoc* Tukey's *t*-test. A probability value of  $p < 0.05$  was considered statistically significant.

## Results

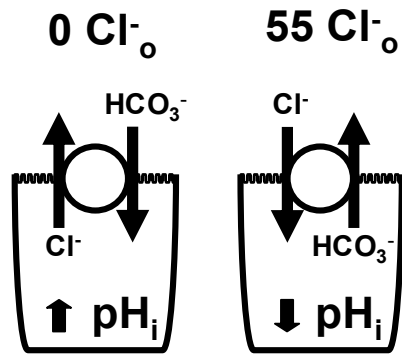
### *Cl<sup>-</sup>/HCO<sub>3</sub><sup>-</sup> exchange in villous epithelium of murine duodenum*

Cl<sup>-</sup>/HCO<sub>3</sub><sup>-</sup> exchange function across the apical membrane of villous epithelial cells using BCECF microfluorimetry has not been previously demonstrated in intact duodenal mucosa. The horizontal Ussing chamber system used in this study allowed separate superfusion of the luminal (apical) and basolateral (serosal) sides of the mucosa. In the basolateral superfusate, Cl<sup>-</sup> was replaced by isethionate<sup>-</sup> to minimize the contribution of basolateral anion exchange activity and 1 μM EIPA was included in the solution to inhibit basolateral Na<sup>+</sup>/H<sup>+</sup> exchanger isoform 1 (NHE1). A standard experimental paradigm (see Figure 2.2A) to demonstrate Cl<sup>-</sup>/base exchange activity involves the replacement of luminal superfusate Cl<sup>-</sup> with the impermeant ion isethionate<sup>-</sup>, resulting in rapid alkalization of the pH<sub>i</sub> as the exchange process runs in reverse mode (Cl<sup>-</sup><sub>out</sub>/HCO<sub>3</sub><sup>-</sup><sub>in</sub>). Return of luminal superfusate Cl<sup>-</sup> rapidly acidifies (i.e., recovers) pH<sub>i</sub> to baseline values as the exchanger process runs in forward mode (Cl<sup>-</sup><sub>in</sub>/HCO<sub>3</sub><sup>-</sup><sub>out</sub>). To investigate the Cl<sup>-</sup> dependence of the anion exchange process, Cl<sup>-</sup> was not returned to the luminal superfusate after maximal alkalization by Cl<sup>-</sup> removal. As shown in Figure 2.2B, the pH<sub>i</sub> acidified very little for the duration of the experiment (> 10 min). To determine whether the anion exchange process was dependent on HCO<sub>3</sub><sup>-</sup>, CO<sub>2</sub>/HCO<sub>3</sub><sup>-</sup> was removed from the superfusates and the duodenum was treated with 100 μM methazolamide to inhibit endogenous carbonic anhydrase activity during the Cl<sup>-</sup> substitution protocol. As shown in Figure 2.2C, Cl<sup>-</sup>-dependent alkalization and recovery was greatly diminished during removal of CO<sub>2</sub>/HCO<sub>3</sub><sup>-</sup> from the superfusing solutions. Addition of CO<sub>2</sub>/HCO<sub>3</sub><sup>-</sup> to the superfusates re-established anion exchange activity. Thus, the process of

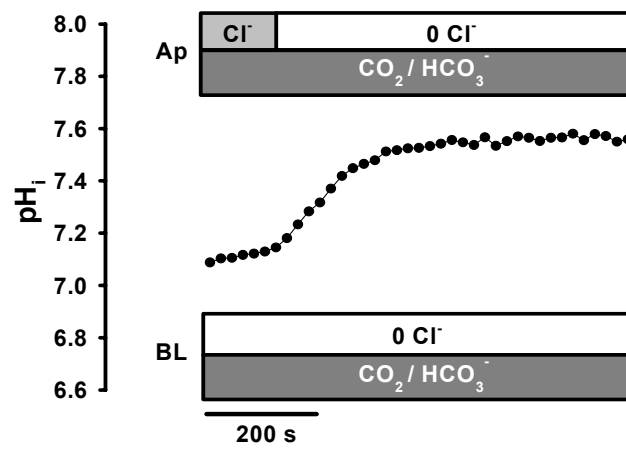
**Figure 2.2.** Anion exchange in duodenal villous epithelium exhibits  $\text{Cl}^-$  and  $\text{HCO}_3^-$  dependence. **A.** Standard experimental paradigm demonstrating  $\text{pH}_i$  change as a result of  $\text{Cl}^-$ /base exchange activity in duodenal villous epithelial cells during changes in extracellular  $\text{Cl}^-$  concentration ( $\text{Cl}^-_o$ ). **B.** Representative  $\text{pH}_i$  trace of duodenal villous epithelial cells during luminal  $\text{Cl}^-$  removal (replacement with isethionate). Following alkalization,  $\text{pH}_i$  remains constant for the duration of the experiment (>10 min) demonstrating a dependence on  $\text{Cl}^-_o$  for recovery from alkalization. Trace representative of  $n = 3$  experiments. **C.** Representative  $\text{pH}_i$  trace of duodenal villous epithelial cells during luminal  $\text{Cl}^-$  removal and replacement in the presence and absence of  $\text{HCO}_3^-/\text{CO}_2$ . In the absence of  $\text{HCO}_3^-/\text{CO}_2$ , villous epithelial cells exhibit minimal  $\text{Cl}^-$ /base activity (~20% of the activity in the presence of  $\text{HCO}_3^-/\text{CO}_2$ ). Trace representative of  $n = 3$  experiments.

Figure 2.2

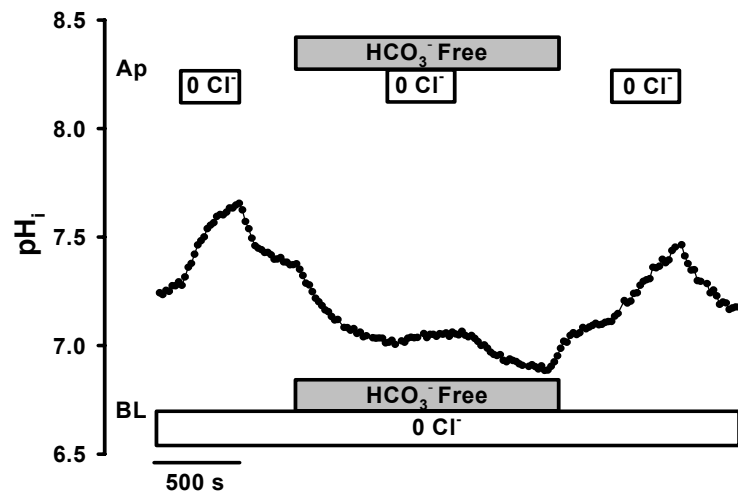
**A**



**B**



**C**



Cl<sup>-</sup>-dependent alkalization and recovery in the duodenal villus epithelium is primarily dependent on the presence of HCO<sub>3</sub><sup>-</sup>, indicating dominance of Cl<sup>-</sup>/HCO<sub>3</sub><sup>-</sup> rather than Cl<sup>-</sup>/OH<sup>-</sup> exchange.

*Reduced Cl<sup>-</sup>/HCO<sub>3</sub><sup>-</sup> exchange activity in the villous epithelium of CF mouse duodenum*

Under basal conditions, both WT and CF intestine exhibit a finite rate of transepithelial HCO<sub>3</sub><sup>-</sup> secretion that involves the activity of an apical membrane Cl<sup>-</sup>/base exchange process (25;26;84;87). Several studies show that the rate of HCO<sub>3</sub><sup>-</sup> secretion across CF duodenum is reduced relative to the WT intestine (26;84;87). Therefore, we compared the rates of Cl<sup>-</sup>/HCO<sub>3</sub><sup>-</sup> exchange activity in the villous epithelium between CF and WT murine duodena. As shown by the experiment in Figure 2.3A, the basal pH<sub>i</sub> of the villous epithelium is elevated and the rates of alkalization and recovery during Cl<sup>-</sup> substitution/replacement are reduced in CF as compared to WT duodenum. Cumulative data for several experiments on CF and WT epithelia show that the baseline pH<sub>i</sub> (Figure 2.3B) is significantly more alkaline in the CF villi and both the rates of HCO<sub>3</sub><sup>-</sup> influx during Cl<sup>-</sup> removal and HCO<sub>3</sub><sup>-</sup> efflux during Cl<sup>-</sup> replacement are reduced relative to the WT villi (37% and 30%, respectively; Figures 2.3C and 2.3D). No differences in Cl<sup>-</sup>/HCO<sub>3</sub><sup>-</sup> exchange activity were found between duodenal epithelium from the CFTR knockout (cfr<sup>tm1UNC</sup>) and ΔF508 mCFTR (cfr<sup>tm1Kth</sup>) mice, although it was anticipated that differences in the latter mouse model might exist due to the potential for exchanger interaction with expressed mCFTR mutant protein (55). However, unlike some ΔF508 mCFTR mouse models (37), mRNA expression of the ΔF508 mCFTR is severely reduced (75 – 80%) in cfr<sup>tm1Kth</sup> mice resulting in intestinal transport properties that more closely resemble the mCFTR knockout intestine (126).

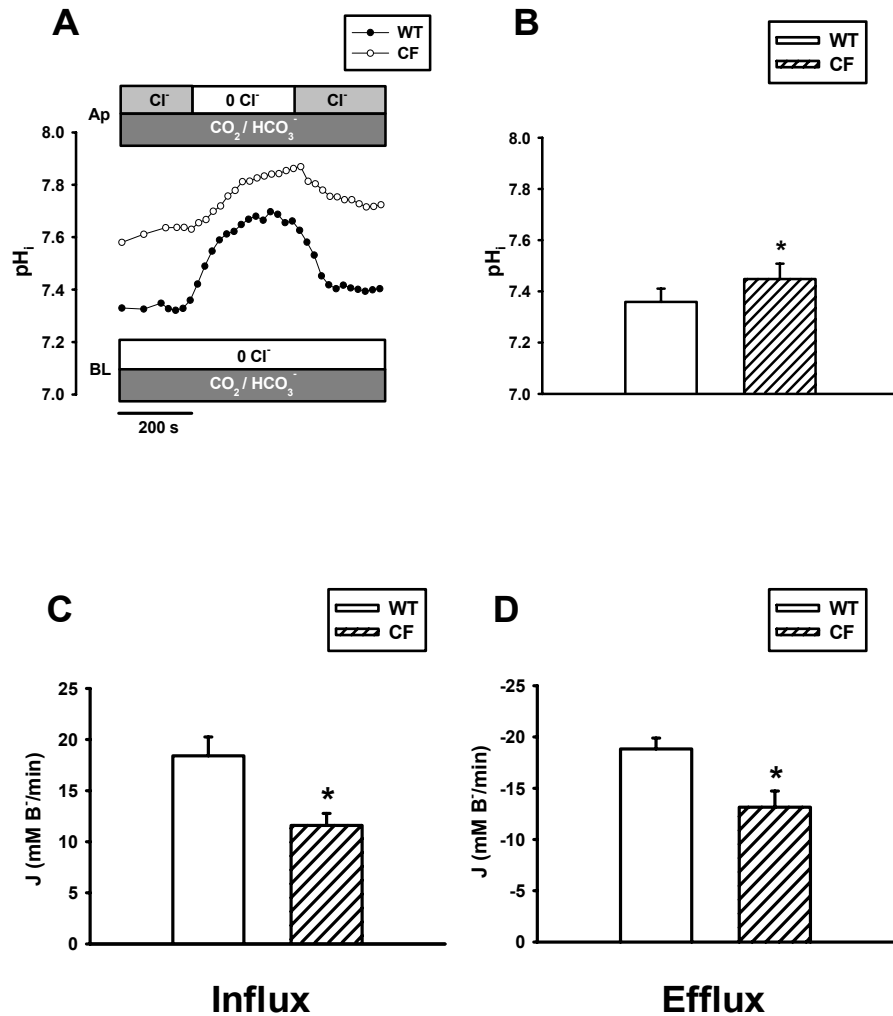


**Figure 2.3.** Comparison of pH<sub>i</sub> and Cl<sup>-</sup>/HCO<sub>3</sub><sup>-</sup> exchange in duodenal villous epithelium of WT and CF mice. **A.** Representative pH<sub>i</sub> trace of WT and CF duodenal villous epithelial cells during luminal Cl<sup>-</sup> removal and replacement. **B.** Summary of baseline pH<sub>i</sub> in duodenal villous epithelial cells of WT and CF mice (n = 11). The cumulative data show a significantly elevated baseline pH<sub>i</sub> in CF compared to WT. **C and D.** Summary of HCO<sub>3</sub><sup>-</sup> influx (C) and HCO<sub>3</sub><sup>-</sup> efflux rates (D) in duodenal villous epithelial cells from WT (n=9) and CF (n=8) mice. The cumulative data show reduced rates of Cl<sup>-</sup>/HCO<sub>3</sub><sup>-</sup> exchange following luminal Cl<sup>-</sup> removal and replacement in CF compared to WT. \*Significantly different from WT.

*Properties of apical membrane Cl<sup>-</sup>/HCO<sub>3</sub><sup>-</sup> exchange are similar in WT and CF villous epithelia*

To examine whether the characteristics of the Cl<sup>-</sup>/HCO<sub>3</sub><sup>-</sup> exchange are similar between CF and WT villi, we compared inhibitor sensitivity, transport electrogenicity and anion selectivity of the villous anion exchange process. In inhibitor studies, the effects of two inhibitors of anion exchange, the distilbene DIDS and NFA (8), on Cl<sup>-</sup>/HCO<sub>3</sub><sup>-</sup> exchange rate were examined in CF and WT villi (Figure 2.4). DIDS, at a concentration (1 mM) known to inhibit activity of recombinant isoforms of both the Slc26a and Slc4 transport families, had very little effect on the rates of villous epithelial anion exchange when applied to the luminal superfusate in either WT or CF duodenum (< 5 %). In contrast, NFA significantly inhibited the rate of Cl<sup>-</sup>/HCO<sub>3</sub><sup>-</sup> exchange to a similar degree (60 %) in both WT and CF intestine.

Recent studies have indicated that members of the Slc26a family of anion exchangers, i.e., DRA and PAT-1, possess electrogenic properties when examined in recombinant systems (55;72;124). To investigate electrogenic properties of the villous Cl<sup>-</sup>/HCO<sub>3</sub><sup>-</sup> exchange process, the K<sup>+</sup> concentration in both the luminal and basolateral superfusate was increased to 80 mM to depolarize the membrane potential of the villous epithelial cells. As shown in Figure 2.5, cell depolarization significantly increased the mean rate of HCO<sub>3</sub><sup>-</sup> influx during Cl<sup>-</sup> removal in both the WT and CF villous epithelium, whereas the mean rate of HCO<sub>3</sub><sup>-</sup> efflux during Cl<sup>-</sup> replacement was not significantly different in the high [K<sup>+</sup>] medium. Thus, the qualitative effect of membrane depolarization on Cl<sup>-</sup>/HCO<sub>3</sub><sup>-</sup> exchange is similar between WT and CF duodenal villi. In the case of the CF intestine, where the CFTR conductive pathway in the apical membrane



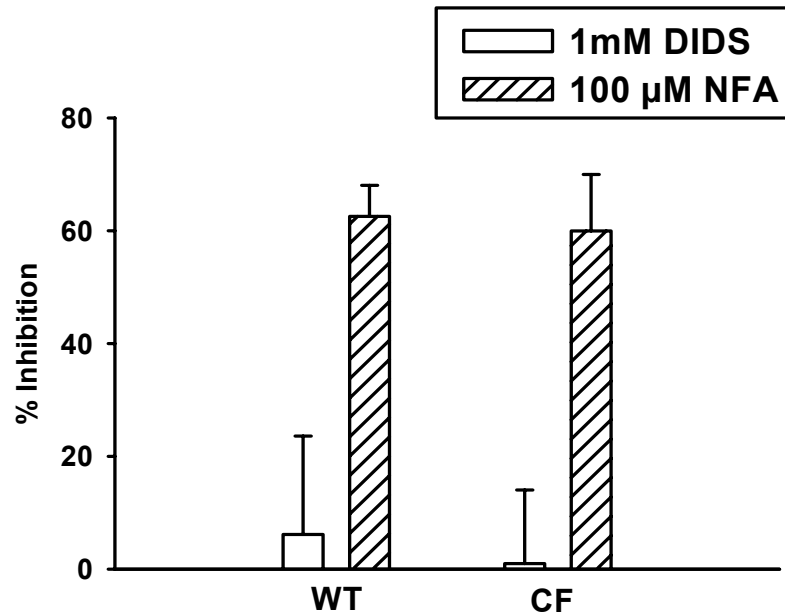


**Figure 2.4.** Effect of anion exchange inhibitors on  $\text{Cl}^-/\text{HCO}_3^-$  exchange rates in WT and CF villous epithelium. Intact duodenum was superfused in the luminal bath for 5 minutes with 1 mM DIDS or 100  $\mu\text{M}$  NFA prior to luminal  $\text{Cl}^-$  removal and replacement. In the presence of 1 mM DIDS, the rate of  $\text{HCO}_3^-$  efflux was minimally inhibited in both WT and CF duodena ( $n = 4$ ). In the presence of 100  $\mu\text{M}$  NFA,  $\text{HCO}_3^-$  efflux was reduced by ~60% in both WT ( $n=5$ ) and CF ( $n=4$ ) duodena.

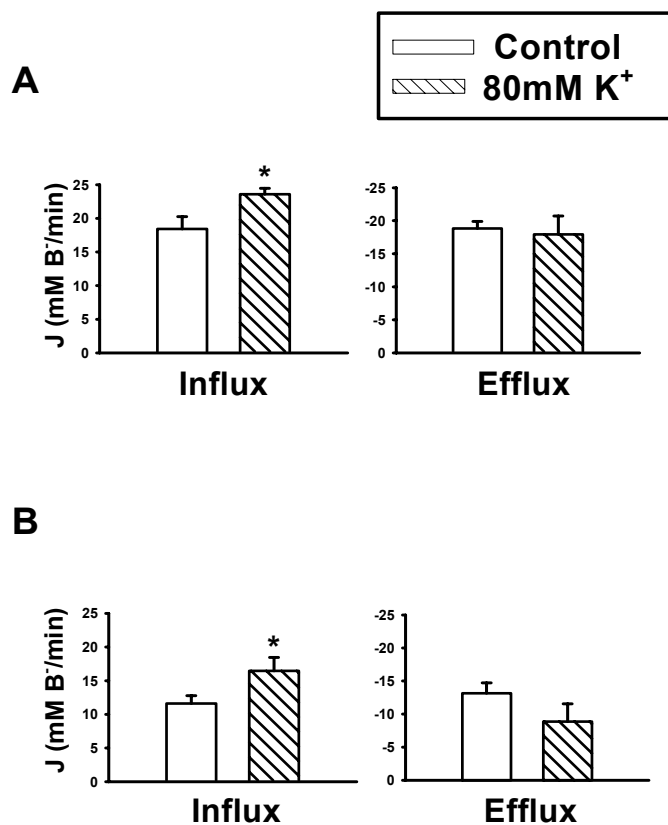


**Figure 2.5.** Effect of cell depolarization on  $\text{Cl}^-/\text{HCO}_3^-$  exchange rates in **A.** WT and **B.** CF villous epithelia. Intact duodenum was superfused bilaterally with medium containing 80 mM  $\text{K}^+$  during luminal  $\text{Cl}^-$  removal and replacement. In the presence of the high  $[\text{K}^+]$ , the rate of  $\text{HCO}_3^-$  influx during luminal  $\text{Cl}^-$  removal was significantly increased, whereas the rate of  $\text{HCO}_3^-$  efflux during  $\text{Cl}^-$  replacement was unaffected in WT (n=8) or CF (n=7) duodenal villous epithelia. \*Significantly different from WT (n=9) or CF (n=8) controls (i.e., normal IBR medium).

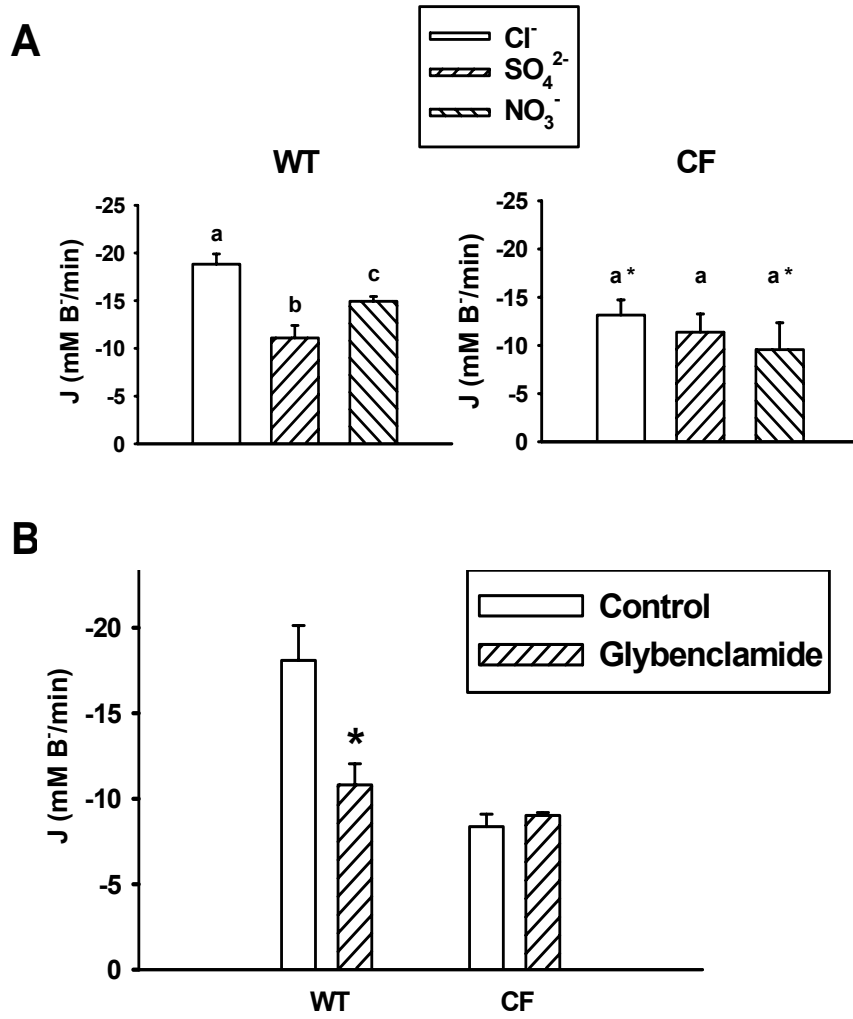
is not present, the stimulatory effect of depolarization on  $\text{HCO}_3^-$  influx suggests the dominance of an anion exchanger that hyperpolarizes the apical membrane upon  $\text{Cl}^-$  removal.

*Investigation of reduced  $\text{Cl}^-/\text{HCO}_3^-$  exchange in the CF villous epithelium*

The anion selectivity of CFTR has been well-characterized (62) and it is known that members of the Slc26a anion exchangers transport a number of monovalent and divalent anions (72). Therefore, we investigated the ability of selected anions to support CFTR-facilitated anion exchange. CFTR is essentially impermeant to  $\text{SO}_4^{2-}$  (47), whereas recombinant Slc26a anion exchangers, including DRA and PAT-1 (72), are capable of transporting  $\text{SO}_4^{2-}$  (although the rate of  $\text{SO}_4^{2-}$  transport by DRA may be very low (20). To compare  $\text{SO}_4^{2-}$  transport between WT and CF villous epithelium, we measured the rates of  $\text{SO}_4^{2-}$ -dependent  $\text{HCO}_3^-$  efflux ( $\text{SO}_4^{2-}_{\text{in}}/\text{HCO}_3^-_{\text{out}}$ ) following  $\text{pH}_i$  alkalization induced by luminal  $\text{Cl}^-$  removal. As shown in Figure 2.6A (left panel), the  $\text{SO}_4^{2-}$ -dependent  $\text{HCO}_3^-$  efflux in WT villous epithelium occurred at a significantly reduced rate as compared to recovery induced by luminal  $\text{Cl}^-$  addition. In contrast, the  $\text{SO}_4^{2-}$ -dependent  $\text{HCO}_3^-$  efflux after alkalization was not different from the rate of  $\text{Cl}^-$ -dependent  $\text{HCO}_3^-$  efflux in the CF villous epithelium (Figure 2.6A, right panel). Note also that the mean rates of  $\text{SO}_4^{2-}$ -dependent  $\text{HCO}_3^-$  efflux were nearly identical between WT and CF villous epithelium. Since  $\text{SO}_4^{2-}$  does not permeate CFTR (47), these findings suggest that CFTR facilitates  $\text{Cl}^-/\text{HCO}_3^-$  exchange in the WT duodenal villous epithelial cells by providing a “leak” pathway for intracellular  $\text{Cl}^-$ , whereas this pathway is not available for  $\text{SO}_4^{2-}$  and thus the rates of  $\text{SO}_4^{2-}/\text{HCO}_3^-$  exchange are similar to CF epithelial cells. As a test of this hypothesis, we measured the rate of  $\text{NO}_3^-$ -dependent

**Figure 2.6.** Effects of anion substitution or glybenclamide on  $\text{HCO}_3^-$  efflux in WT and CF duodenal villous epithelia. **A.** Comparison of  $\text{HCO}_3^-$  efflux rates during luminal superfusion with 55 mM  $\text{Cl}^-$ ,  $\text{SO}_4^{2-}$  or  $\text{NO}_3^-$  following  $\text{pH}_i$  alkalization induced by luminal  $\text{Cl}^-$  removal. In WT duodenal epithelium (left panel),  $\text{HCO}_3^-$  efflux rate was increased over CF duodenal epithelium only in the presence of luminal  $\text{Cl}^-$  or  $\text{NO}_3^-$ , but not  $\text{SO}_4^{2-}$  (n = 9). In CF duodena (right panel), similar rates of  $\text{HCO}_3^-$  efflux were measured with 55 mM  $\text{Cl}^-$ ,  $\text{SO}_4^{2-}$  or  $\text{NO}_3^-$  (n = 5 - 8). <sup>a,b,c</sup>Means with the same letters are not statistically different within either the WT or CF group. \*Significantly different from WT. **B.** Intact duodenum was treated for 5 minutes with 100  $\mu\text{M}$  glybenclamide (luminal superfusate) prior to luminal  $\text{Cl}^-$  removal and replacement.  $\text{HCO}_3^-$  efflux was significantly reduced in WT but unaffected in CF villous epithelium (n = 8 WT and 4 CF). Control WT and CF duodena were treated with 0.4 % DMSO vehicle (n = 8 WT and 3 CF). \*Significantly different from control.

Figure 2.6



$\text{HCO}_3^-$  efflux following epithelial alkalization. CFTR also conducts  $\text{NO}_3^-$  ions ( $G_{\text{Cl}} : G_{\text{NO}_3} = 0.8$ , (47) and, like  $\text{SO}_4^{2-}$ ,  $\text{NO}_3^-$  can support anion exchange by DRA and PAT-1 (32;124). As shown in Figure 2.6A, the rate of  $\text{NO}_3^-$ -dependent  $\text{HCO}_3^-$  efflux was significantly increased relative to  $\text{SO}_4^{2-}$ -dependent  $\text{HCO}_3^-$  efflux in WT villous epithelium. However, in CF epithelium, the rate of  $\text{NO}_3^-$ -dependent  $\text{HCO}_3^-$  efflux was equivalent to that measured for  $\text{Cl}^-$  and  $\text{SO}_4^{2-}$ . These data are consistent with CFTR facilitation of anion exchange by providing a  $\text{NO}_3^-$  leak pathway. Next, as a further test of the hypothesis, we measured the rates of  $\text{Cl}^-$ -dependent  $\text{pH}_i$  alkalization and recovery during treatment of the intestine with the CFTR-selective channel blocker, glybenclamide (30). Preliminary studies using murine duodenum mounted in Ussing chambers indicated that 1 mM glybenclamide in the luminal bath inhibited the forskolin-induced short-circuit current by 78 % (Vehicle  $\Delta\text{Isc} = 187.8 \pm 44.1$ ; Glybenclamide  $\Delta\text{Isc} = 41.2 \pm 8.6 \mu\text{A}/\text{cm}^2$ ,  $n = 4$ ,  $p < 0.05$ ). As shown in Figure 2.6B, the rate of  $\text{Cl}^-/\text{HCO}_3^-$  exchange in WT villous epithelium pretreated with glybenclamide was significantly reduced relative to the vehicle (DMSO)-treated epithelium, whereas no change in the rates of  $\text{Cl}^-/\text{HCO}_3^-$  exchange were apparent in the CF villous epithelium.

The above studies are consistent with the hypothesis that the CFTR facilitation of apical membrane  $\text{Cl}^-/\text{HCO}_3^-$  exchange requires the anion conductive properties of CFTR. However, an alternative hypothesis is that both  $\text{SO}_4^{2-}$  and glybenclamide reduce the rate of  $\text{HCO}_3^-$  efflux by blocking a  $\text{HCO}_3^-$  current mediated by CFTR. While this alternative hypothesis may be consistent with the action of glybenclamide, previous studies using *extracellular*  $\text{SO}_4^{2-}$  have not demonstrated blockade of the CFTR channel pore

(35;77). Since it is possible that *intracellular*  $\text{SO}_4^{2-}$  may block the CFTR channel, we investigated whether the rate of  $\text{Cl}^-$ -dependent  $\text{HCO}_3^-$  efflux was reduced in WT epithelium following a period of  $\text{SO}_4^{2-}$  uptake resulting from  $\text{SO}_4^{2-}$ <sub>in</sub>/ $\text{HCO}_3^-$ <sub>out</sub> exchange. As shown in Figure 2.7, initial exposure of the epithelium to  $\text{SO}_4^{2-}$  induced a finite rate of  $\text{HCO}_3^-$  efflux but replacement of  $\text{SO}_4^{2-}$  with  $\text{Cl}^-$  rapidly increased the rate to levels typical of  $\text{Cl}^-$ -dependent  $\text{HCO}_3^-$  efflux. Since  $\text{SO}_4^{2-}$  uptake did not alter the subsequent rate of  $\text{Cl}^-/\text{HCO}_3^-$  exchange in WT epithelium, this finding suggests that intracellular  $\text{SO}_4^{2-}$  accumulation in the villous epithelium does not affect the anion conductive properties of CFTR.

The anion substitution studies indicated the presence of apical membrane anion exchanger(s) that can readily perform  $\text{SO}_4^{2-}$ <sub>in</sub>/ $\text{HCO}_3^-$ <sub>out</sub> exchange. If recent studies indicating very limited  $\text{SO}_4^{2-}$  transport by hDRA (20) are also true for murine DRA (mDRA), it is possible that a drastic reduction in mDRA expression in the CF mouse intestine could explain the reduced rates of  $\text{Cl}^-/\text{HCO}_3^-$  exchange. In other words, if both mDRA and mPAT-1 contribute to  $\text{Cl}^-/\text{HCO}_3^-$  exchange but only mPAT-1 contributes to  $\text{SO}_4^{2-}/\text{HCO}_3^-$  exchange, then loss of mDRA expression in the CF intestine would result in reduced  $\text{Cl}^-/\text{HCO}_3^-$  exchange and unchanged  $\text{SO}_4^{2-}/\text{HCO}_3^-$  exchange relative to WT intestine. This possibility is strengthened by studies of recombinant proteins that show a positive correlation between the expression of CFTR and the anion exchangers, DRA and PAT-1 (42). Therefore, we investigated the mRNA expression of DRA and PAT-1 in the WT and CF proximal intestine. As shown in Figure 2.8, Northern blot analysis indicated only a slight, non-significant decrease in DRA (~25%) and essentially no change in PAT-1 mRNA expression in the CF as compared to the WT duodenum. Although measures

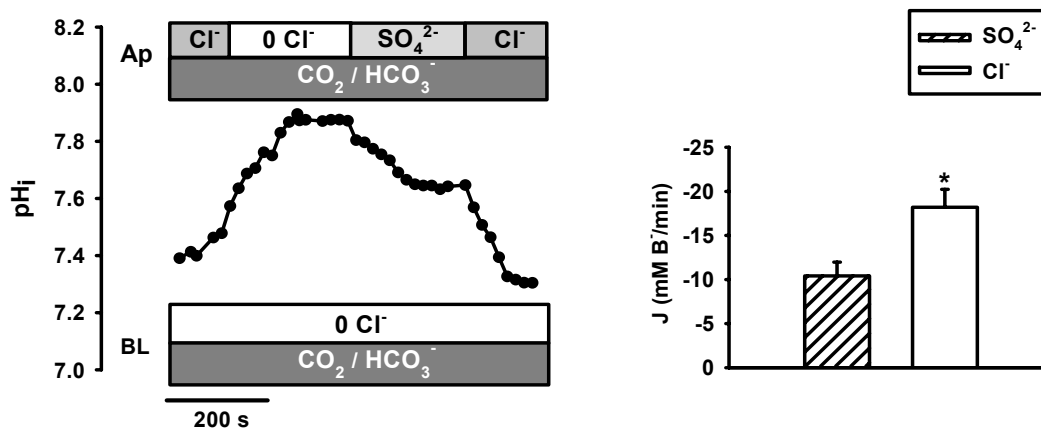


**Figure 2.7.** Effect of a preceding period of  $\text{SO}_4^{2-}$  uptake on  $\text{Cl}^-/\text{HCO}_3^-$  exchange in WT duodenal villous epithelium. **Left panel**, representative  $\text{pH}_i$  trace of WT duodenal villous epithelial cells. Following alkalization secondary to luminal  $\text{Cl}^-$  removal, 55 mM  $\text{SO}_4^{2-}$  was introduced in the luminal superfusate to allow  $\text{SO}_4^{2-}$  uptake by  $\text{SO}_4^{2-}_{\text{in}}/\text{HCO}_3^-_{\text{out}}$  exchange. This period was immediately followed by equimolar replacement of luminal  $\text{SO}_4^{2-}$  with  $\text{Cl}^-$ , resulting in a typical rate of  $\text{Cl}^-/\text{HCO}_3^-$  exchange ( $\text{HCO}_3^-$  efflux). **Right panel**, summary of  $\text{HCO}_3^-$  efflux rates (mean  $\pm$  SE) induced by luminal  $\text{SO}_4^{2-}$  followed by luminal  $\text{Cl}^-$  in duodenal villous epithelial cells ( $n = 6$  mice), indicating that a preceding period of  $\text{SO}_4^{2-}$  uptake by the epithelium does not decrease the rate of  $\text{Cl}^-$ -dependent  $\text{HCO}_3^-$  efflux. \*Significantly different from  $\text{SO}_4^{2-}$ .



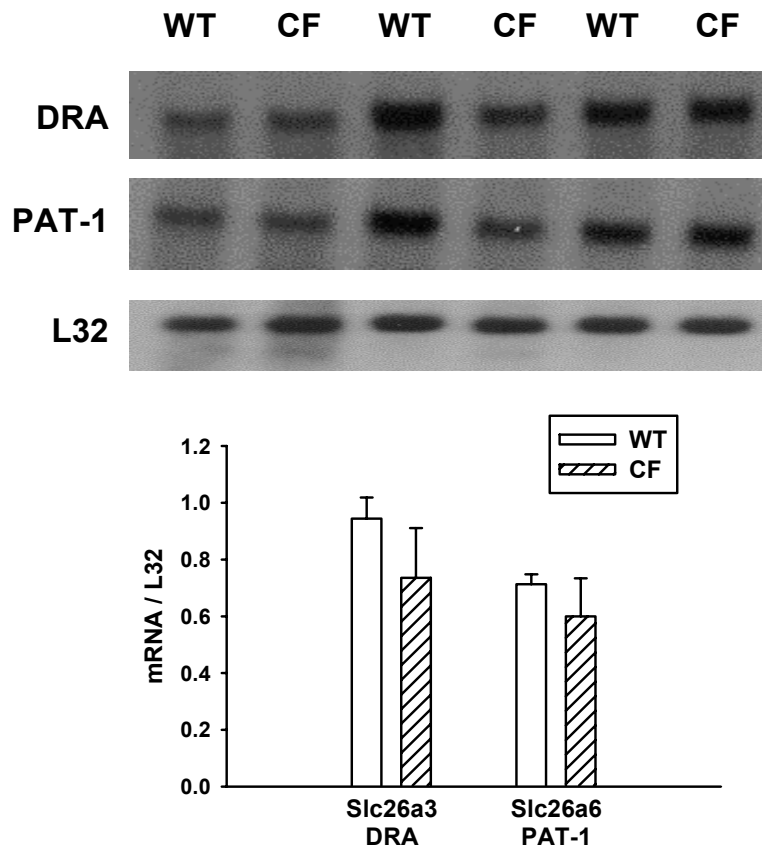


**Figure 2.8.** mRNA expression of Slc26a3 (mDRA) and Slc26a6 (mPAT-1) in the small intestine of gender-matched littermate WT and CF mouse pairs. **A.** Representative Northern blot of mDRA, mPAT-1, and L32 ribosomal protein (as a loading control) in the small intestine of 3 pairs of gender-matched WT and CF littermate mice. **B.** Densitometric analysis of mRNA expression for mDRA and mPAT-1 normalized to the mRNA expression of L32 ribosomal protein (n = 3 mouse pairs).

of protein expression or functional studies in knockout mice will be necessary to confirm these findings, the present data do not indicate a major reduction in the expression of DRA in the CF duodenum.

## Discussion

In the present study, *in situ* measurements of epithelial cells from the mid-region of duodenal villi demonstrated robust activity of  $\text{Cl}^-/\text{HCO}_3^-$  exchange across the apical membrane. Dependence of anion exchange activity on luminal  $\text{Cl}^-$  was shown by sustained intracellular alkalization during substitution of  $\text{Cl}^-$  with the impermeant anion, isethionate $^-$ . The process was also found to be primarily  $\text{HCO}_3^-$ -dependent in studies where  $\text{CO}_2/\text{HCO}_3^-$  was removed from the luminal and basolateral bathing media. The rates of alkalization and recovery in the absence of  $\text{CO}_2/\text{HCO}_3^-$ , i.e.,  $\text{Cl}^-/\text{OH}^-$  exchange, were less than 15 % and 24 %, respectively, of the rates in the presence of  $\text{CO}_2/\text{HCO}_3^-$ . An important observation was the finding that the  $\text{Cl}^-/\text{HCO}_3^-$  exchange activity in CF duodenal villous epithelial cells was reduced by approximately one-third relative to WT cells. Despite reduced activity, investigations of inhibitor sensitivity and responses during membrane depolarization did not reveal overt differences in the characteristics of the anion exchange process between WT and CF duodenum.

In the inhibitor studies, treatment with the distilbene DIDS reduced  $\text{Cl}^-/\text{HCO}_3^-$  exchange by less than 5 % in both WT and CF villous epithelium. DIDS resistance is consistent with properties reported for recombinant mDRA (69) but not for recombinant mPAT-1 or rat AE4 proteins (49;54;124). In contrast to the effect of DIDS, NFA treatment substantially reduced villous  $\text{Cl}^-/\text{HCO}_3^-$  activity by an equivalent degree in both

WT and CF duodenum. Studies of recombinant hDRA, hPAT-1 and mPAT-1 have demonstrated that these proteins are sensitive to NFA ((20), Chernova MN, Alper SL, et al, manuscript submitted); however, we are unaware of similar studies performed on the mDRA ortholog. Membrane depolarization using high  $[K^+]$  media also produced similar effects on the  $Cl^-/HCO_3^-$  exchange process in WT and CF duodena. In both cases, depolarization enhanced the rate of  $HCO_3^-$  influx during luminal  $Cl^-$  removal. Recent studies of recombinant mDRA and hPAT-1, but not rat AE4, indicate the transport activity of these proteins exhibit electrogenic properties (49;54;55;124). In the case of hPAT-1, removal of extracellular  $Cl^-$  induces membrane hyperpolarization and has led to the proposal that the apparent stoichiometry of the protein is  $1 Cl^- / \geq 2 HCO_3^-$  (55). In contrast, removal of extracellular  $Cl^-$  from cells expressing recombinant mDRA caused membrane depolarization, suggesting an apparent stoichiometry of  $\geq 2 Cl^- / 1 HCO_3^-$ . It has been further proposed that equal expression of these two exchangers would result in electroneutral activity because of their opposing effects on membrane potential (55). However, this hypothesis was not supported in our studies of villous epithelium because membrane depolarization significantly increased the rate of  $HCO_3^-$  influx during luminal  $Cl^-$  substitution.

Previous studies of cAMP regulation of  $HCO_3^-$  secretion in pancreatic ducts led to the proposal that the presence of a chloride channel in the apical membrane facilitates  $Cl^-/HCO_3^-$  exchange by recycling or leaking  $Cl^-$  back to the extracellular milieu, thereby providing a favorable  $Cl^-$  concentration gradient for exchange activity. Several lines of evidence suggest that this model also explains the present observation that  $Cl^-/HCO_3^-$  exchange activity is greater in WT versus CF villous epithelium under basal conditions.

First, only anions that permeate CFTR, i.e.,  $\text{Cl}^-$  and  $\text{NO}_3^-$  but not  $\text{SO}_4^{2-}$ , produced greater rates of anion exchange in WT villous epithelium. In contrast, the rate of  $\text{SO}_4^{2-}/\text{HCO}_3^-$  exchange in the WT cells was equivalent to that in the CF epithelium. Because neither  $\text{SO}_4^{2-}$  nor  $\text{NO}_3^-$  reduced the rate of anion exchange in the CF duodenum, the results indicate that these anions fully support the activity of the anion exchanger(s). Secondly, the lower rate of  $\text{SO}_4^{2-}$ -dependent  $\text{HCO}_3^-$  efflux in the WT epithelium did not result from  $\text{SO}_4^{2-}$  blockade of a CFTR-mediated  $\text{HCO}_3^-$  conductance because the rate of  $\text{Cl}^-$ -dependent  $\text{HCO}_3^-$  efflux was not reduced by preceding the experiment with a period of  $\text{SO}_4^{2-}$  uptake across the apical membrane. Third, treatment of the WT epithelium with the CFTR-selective channel blocker glybenclamide also reduced the rate of  $\text{Cl}^-/\text{HCO}_3^-$  exchange to a level equivalent with that in CF epithelium. Since the rate of  $\text{Cl}^-/\text{HCO}_3^-$  exchange was not reduced in the CF epithelium treated with glybenclamide, it is unlikely that the effect of the channel blocker in the WT epithelium was due to non-specific effects of the compound. The above data support the conclusion that the  $\text{Cl}^-$  channel function of CFTR facilitates the activity of  $\text{Cl}^-/\text{HCO}_3^-$  exchange in the villous epithelium of the murine duodenum under basal conditions. However, it should be emphasized that this conclusion only applies to the basal, unstimulated condition and, specifically, to  $\text{Cl}^-_{\text{in}}/\text{HCO}_3^-_{\text{out}}$  exchange, a physiologically-relevant transport mode in duodenal villous epithelium.

Although the transport studies support the hypothesis that CFTR  $\text{Cl}^-$  conduction supports  $\text{Cl}^-/\text{HCO}_3^-$  exchange in duodenal villi, the possibility was raised that reduced  $\text{Cl}^-/\text{HCO}_3^-$  exchange in the CF epithelium may result from decreased expression of an anion exchanger that does not transport  $\text{SO}_4^{2-}$ , e.g., DRA (20). However, the mRNA expression

of mDRA was not significantly reduced in the CF duodenum. These data are consistent with previous studies which found only slight or no decrease in DRA mRNA expression in the distal intestine of CFTR-null mice (20), but contrary to the effect of recombinant CFTR expression on native DRA and PAT-1 expression in pancreatic duct cell lines (42). Although large changes in DRA expression sufficient to account for the differences in  $\text{Cl}^-/\text{HCO}_3^-$  exchange activity in the CF duodenum were not apparent from the Northern blot analysis, additional studies measuring surface protein levels will be necessary to fully evaluate the contribution of changes in DRA expression to the reduced rates of  $\text{Cl}^-/\text{HCO}_3^-$  exchange in the CF duodenum.

It was interesting that basal  $\text{pH}_i$  in the CF duodenal epithelium was significantly more alkaline than WT under the conditions of our study. Previous reports of CF pancreatic duct epithelial cell lines have found  $\text{pH}_i$  to be alkaline relative to CFTR-corrected cells, whereas no  $\text{pH}_i$  difference was apparent in primary CF airway epithelial cells (34;123). Important to the present discussion, no differences from WT were found in measurements of  $\text{pH}_i$  of isolated enterocytes from both human and murine CF duodena (82;84), nor in *in vivo* preparations of intact duodenum from CFTR-deficient mice (44). However, in the latter study, exposure of the murine duodenum to luminal acid revealed differences in the  $\text{CO}_2/\text{HCO}_3^-$ -dependent buffering power in the CF epithelium that was tentatively ascribed to the imbalance resulting from intact  $\text{HCO}_3^-$ -loading processes and the absence of CFTR-mediated  $\text{HCO}_3^-$ -unloading mechanism. Likewise, in the present study, the condition of disabling basolateral “house-keeping”  $\text{pH}_i$  regulation by NHE1 (EIPA treatment) and AE2 (basolateral  $\text{Cl}^-$  removal) potentially accentuated  $\text{CO}_2/\text{HCO}_3^-$ -dependent buffering power in the CF duodenal epithelium.  $\text{HCO}_3^-$ -loading processes of

NaHCO<sub>3</sub> cotransport and intracellular carbonic anhydrase activity were left intact. Thus, an imbalance resulting in increased pH<sub>i</sub> may have been created in the CF villous epithelium which lacked CFTR facilitation of basal Cl<sup>-</sup>/HCO<sub>3</sub><sup>-</sup> exchange activity.

Our studies indicate that the Cl<sup>-</sup> channel activity of CFTR is necessary for increased rates of Cl<sup>-</sup><sub>in</sub>/HCO<sub>3</sub><sup>-</sup><sub>out</sub> exchange in WT epithelium under basal conditions. The efficiency of this interaction may require a close association between the Cl<sup>-</sup>/HCO<sub>3</sub><sup>-</sup> exchanger(s) and CFTR either by direct binding or through scaffolding protein co-localization (55;56;59;63). Interestingly, Figure 2.5 shows that even under membrane depolarizing conditions (high [K<sup>+</sup>]), that the rate of HCO<sub>3</sub><sup>-</sup> influx during luminal Cl<sup>-</sup> removal remains greater in WT than CF epithelium (WT = 23.6 ± 0.9 vs. CF = 16.5 ± 2.0 mM/min, p < 0.05). These data suggest that CFTR also facilitates Cl<sup>-</sup><sub>out</sub>/HCO<sub>3</sub><sup>-</sup><sub>in</sub> exchange, a process not predicted to require a Cl<sup>-</sup> leak pathway. Although the observation may be indirect evidence of a functional intermolecular interaction between the Cl<sup>-</sup>/HCO<sub>3</sub><sup>-</sup> exchanger(s) and CFTR, other explanations for increased alkalization in WT epithelium during luminal Cl<sup>-</sup> removal can be offered including additive effects of luminal Cl<sup>-</sup> removal and high [K<sup>+</sup>] medium on membrane depolarization and increased HCO<sub>3</sub><sup>-</sup> influx via CFTR in the nominal absence of luminal Cl<sup>-</sup> (89). Nonetheless, given earlier estimates of luminal ionic content (81), it seems unlikely that the luminal Cl<sup>-</sup> concentration in the duodenum would decrease to levels sufficiently low for sustained Cl<sup>-</sup><sub>out</sub>/HCO<sub>3</sub><sup>-</sup><sub>in</sub> exchange activity *in vivo*.

The present data are sufficient to allow a tentative conclusion regarding the identity of the predominant apical membrane Cl<sup>-</sup>/HCO<sub>3</sub><sup>-</sup> exchanger in the duodenal villous epithelium. A major difficulty with this exercise is that the characteristics of the

anion exchangers are almost exclusively based on studies of recombinant proteins expressed in heterologous cell systems. Although necessary to isolate the protein's activity, the knowledge derived from those investigations are limited by factors such as expression level, lack of native binding partners, experiments performed at non-physiological temperatures and the use of a single splice variant of the proteins. Given these limitations, some comparisons of recombinant protein studies can be drawn with characteristics of  $\text{Cl}^-/\text{HCO}_3^-$  exchange activity in the villous epithelium. The inhibitor studies indicated a transport process insensitive to DIDS but significantly inhibited by NFA. Although this characteristic is consistent with a report on recombinant murine DRA which showed less than 25% inhibition by DIDS (69), additional studies on this and other murine orthologs of anion exchangers may be necessary because the effect of DIDS on the human DRA has remained controversial despite five studies reporting experiments (16;20;69;71;92). Another identifying characteristic was shown by studies inducing membrane depolarization with high  $[\text{K}^+]$  medium which increased the rate of  $\text{HCO}_3^-$  influx during luminal  $\text{Cl}^-$  removal. Membrane depolarization would favor the activity of murine PAT-1, which has been shown to hyperpolarize the cell during  $\text{Cl}^-$  removal (72). Since the rate of  $\text{HCO}_3^-$  influx was also increased by membrane depolarization in CF epithelium, the aforementioned switching effect of luminal  $\text{Cl}^-$  removal on CFTR permeability to  $\text{HCO}_3^-$  would not be a consideration. Finally, the high rate of  $\text{SO}_4^{2-}/\text{HCO}_3^-$  exchange in the villous epithelium is also consistent with the activity of murine PAT-1. Studies of murine PAT-1 have shown robust  $\text{SO}_4^{2-}$  transport (72). In contrast, although DRA has been reported as a sulfate transporter (92),  $^{35}\text{SO}_4^{2-}$  uptake studies of human and murine recombinant DRA show transport rates that are at least 3 orders of

magnitude less than the  $\text{SO}_4^{2-}/\text{HCO}_3^-$  exchange rates measured in the present study, which would be too low to appreciably alter  $\text{pH}_i$  ((20); J. Simpson, unpublished observations). Thus, based on the effects of membrane depolarization and high rates of  $\text{SO}_4^{2-}$  transport, the data suggests that mPAT-1 provides a major portion of the anion exchange activity in the villous epithelium of the murine duodenum. Thus, based on the effects of membrane depolarization and high rates of  $\text{SO}_4^{2-}$  transport, the data suggests that mPAT-1 provides a major portion of the anion exchange activity in the villous epithelium of the murine duodenum. However, it should be emphasized that this conclusion only applies to the villous epithelium located in the upper one-half of murine duodenal villi. The contribution of villous PAT-1  $\text{Cl}^-/\text{HCO}_3^-$  exchange to the absolute rates of transepithelial  $\text{HCO}_3^-$  secretion and  $\text{Cl}^-$  absorption across murine duodenum is yet unknown. Previous studies have indicated that DRA  $\text{Cl}^-/\text{HCO}_3^-$  exchange provides a major contribution to electroneutral  $\text{HCO}_3^-$  secretion in the duodenum of several species (48). Other members of the Slc26a family of anion transporters and AE4 also likely contribute to transepithelial anion transport. Thus, the activity of these anion exchange proteins in the lower villous and crypt epithelia, where CFTR expression is greatest, may have a dominant role in transepithelial  $\text{HCO}_3^-$  secretion and  $\text{Cl}^-$  absorption in the duodenum. Additional studies of recombinant proteins and Slc26a anion exchanger knockout mice will be necessary to evaluate these hypotheses.

The results of the present study suggest that CFTR facilitates anion exchange activity in the villous epithelium by providing a  $\text{Cl}^-$  'leak' channel that enables sustained  $\text{Cl}^-_{\text{in}}/\text{HCO}_3^-_{\text{out}}$  exchange activity under basal (non-stimulated) conditions.

Physiologically, this mechanism may be important in restoring the alkaline mucus barrier



during interdigestive periods. The  $\text{HCO}_3^-$  secretory mechanism is compromised in the CF duodenum but the adverse effects of this deficiency may be compensated by increased  $\text{CO}_2/\text{HCO}_3^-$ -dependent intracellular buffering power which protects the epithelial cell from acid insult (44). In WT epithelium, the efficiency of  $\text{Cl}^-$  recycling for anion exchange is likely increased by co-localization of CFTR with the anion exchanger(s) at the apical membrane. However, it was unnecessary in these studies to postulate a direct regulatory interaction between CFTR and the anion exchangers to explain the passive role of CFTR in facilitating  $\text{Cl}^-_{\text{in}}/\text{HCO}_3^-_{\text{out}}$  exchange. Although CFTR may have a different, perhaps direct, regulatory relationship during the  $\text{Cl}^-_{\text{out}}/\text{HCO}_3^-_{\text{in}}$  transport mode, the reduced expression of CFTR in the villous epithelium (104) makes it difficult to envision a one-to-one molecular interaction with the anion exchanger(s). Based on the relative equality of macroscopic flux rates (24;40), it would be anticipated that the number of CFTR channels which transport  $\sim 1 \times 10^6$  ions/sec may be 1 - 2 orders of magnitude less than the number of anion exchangers which transport at  $1 - 5 \times 10^4$  ions/sec (1). Thus, the current model for interactions between CFTR and the Slc26a anion exchangers may require modification for epithelia where low-levels of CFTR expression provide indirect regulation of  $\text{Cl}^-/\text{HCO}_3^-$  exchange activity.

## **Chapter 3**

# **PAT-1 IS THE PREDOMINANT APICAL MEMBRANE $\text{Cl}^-/\text{HCO}_3^-$ EXCHANGER IN THE UPPER VILLOUS EPITHELIUM OF MURINE DUODENUM**

### **Introduction**

Duodenal epithelial bicarbonate secretion plays a critical role in the protection of the epithelium against damage from acidic chyme entering into the proximal duodenum (36). The process of active  $\text{HCO}_3^-$  secretion across the duodenum involves the apical membrane activities of the cystic fibrosis (CF) transmembrane conductance regulator (CFTR) and anion exchanger protein(s), which mediate  $\text{Cl}^-$  absorption in exchange for luminal  $\text{HCO}_3^-$  secretion (25;84;99). Under basal (unstimulated) conditions, studies in several species indicate that  $\text{Cl}^-/\text{HCO}_3^-$  exchange dominates duodenal  $\text{HCO}_3^-$  secretion and, in the CFTR(-) intestine, affords a degree of protection against acidic luminal pH (25;26;83;99). However, the identity of the anion exchange protein(s) involved in duodenal bicarbonate secretion and their functional contribution along the crypt-villus axis has yet to be resolved.

The principal candidates for this process are two members of the multifunctional anion exchanger (Slc26a) family, i.e., Slc26a3 [known as downregulated in adenoma (DRA)] and Slc26a6 [known as the putative anion exchanger (PAT-1) or chloride formate exchanger], and one member of the bicarbonate transporter family (Slc4a), i.e., Slc4a9 (known as anion exchanger isoform 4 (AE4)]. All three anion exchangers have been immunolocalized to the apical membrane of the intestinal epithelium, especially

along the villous axis (48;54;120;125). Studies utilizing recombinant proteins have shown that DRA transports  $\text{HCO}_3^-$  in exchange for luminal  $\text{Cl}^-$ ,  $\text{SO}_4^{2-}$ , or oxalate (72). PAT-1 is more versatile, demonstrating  $\text{Cl}^-$ , oxalate,  $\text{SO}_4^{2-}$ , formate,  $\text{HCO}_3^-$ , and hydroxyl transport in *Xenopus* oocytes (72). Less well characterized is AE4, but functional expression studies show AE4 exhibits  $\text{Cl}^-/\text{HCO}_3^-$  exchange (125).

Disease causing loss-of-function mutations have not been reported for human PAT-1 (SLC26A6) or AE4 (SLC4A9). However, loss-of-function mutations in DRA (SLC26A3) are the causal factor in the inherited disease congenital chloride-losing diarrhea (CLD). These patients have defective intestinal  $\text{Cl}^-/\text{HCO}_3^-$  exchange and the symptoms of diarrhea with high  $\text{Cl}^-$  content and systemic alkalization (51;71). Likewise, initial reports of clinical disease in the DRA knockout mouse model (i.e., diarrhea, chloride stool concentration, and growth retardation) closely resemble that of human CLD (17). The severe intestinal manifestations of CLD may reflect interaction between DRA and the major apical membrane  $\text{Na}^+/\text{H}^+$  exchangers (NHE2 and NHE3) responsible for electroneutral NaCl absorption, as based on evidence of functional coupling of these exchangers in recombinant cell systems and changes in DRA expression in the NHE3 knockout intestine (69;73).

Duodenal villi are directly exposed to gastric acid chyme emptying from the stomach, but little is known regarding the physiology of bicarbonate transport in the villous epithelium where DRA, PAT-1, and AE4 are reportedly expressed. Therefore, in the present study, we specifically evaluate the basal activity of anion exchange across the apical membrane of epithelial cells in the upper half of villi in intact duodenal mucosa. Using mice with gene-targeted deletions of PAT-1, DRA, and AE4 and their wild-type

(WT) littermates, rates of anion exchange are measured by BCECF-AM microfluorimetry of intracellular pH ( $\text{pH}_i$ ) to assess the relative contributions of each exchanger to the process of apical  $\text{Cl}^-/\text{HCO}_3^-$  exchange across the duodenal upper villous epithelium.

## **Material and Methods**

### *Animals*

The experiments in this study were performed on mice with the gene-targeted disruptions of the murine homologs of PAT-1 (119), DRA (17), and AE4. All comparisons were made with gender- and age-matched (+/+) siblings (WT). The mutant mice were identified by using a PCR based analysis of tail snip DNA, as previously described (24). All mice were maintained *ad libitum* on standard laboratory chow (Formulab 5008 Rodent Chow; Ralston Purina) and tap water. The mice were housed singly in a temperature (22-26°C) and light (12:12-h light-dark cycle)-controlled room in the AAALAC accredited animal facility at the Dalton Cardiovascular Research Center. Intestinal tissues for experiments were obtained from mice 2-4 months of age. These mice were fasted overnight prior to experimentation but were provided with water *ad libitum*. All experiments involving animals were approved by the University of Missouri Animal Care and Use Committee.

### *Fluorescence Measurement of Intracellular pH and Image Analysis*

The method used for imaging villous epithelial cells in intact murine intestine has been previously described (39;93). Briefly, after euthanasia of the mouse, the proximal duodenum was isolated, stripped of the outer muscle layers by blunt dissection and mounted luminal side up in a horizontal Ussing-type perfusion chamber where luminal

and serosal surfaces of the tissue were independently bathed. The luminal superfusate was an isethionate-bicarbonate Ringer solution (IBR) containing (in mmol/L): 140.0 Na<sup>+</sup>, 55.0 Cl<sup>-</sup>, 55.0 isethionate<sup>-</sup>, 25.0 HCO<sub>3</sub><sup>-</sup>, 5.2 K<sup>+</sup>, 5.0 N-tris methyl-2-aminoethanesulfonic acid (TES), 4.8 gluconate<sup>-</sup>, 2.8 PO<sub>4</sub><sup>2-</sup>, 1.2 Ca<sup>2+</sup>, 1.2 Mg<sup>2+</sup>, 10.0 glucose, and 6.8 mannitol that was gassed with 95% O<sub>2</sub>: 5% CO<sub>2</sub> at 37°C (pH 7.4). The serosal superfusate was a Cl<sup>-</sup>-Free IBR (Cl<sup>-</sup> replaced with isethionate) gassed with 95% O<sub>2</sub>: 5% CO<sub>2</sub> at 37°C (pH 7.4). All duodena were treated with indomethacin (1 μM), bilateral and tetrodotoxin (TTX, 0.1 μM), serosal to minimize the effect of endogenous prostaglandins and neural tone, respectively (13;90). During superfusion, the duodenum was treated on the serosal side with 1 μM 5-(N-ethyl-n-isopropyl)-amiloride (EIPA) to block the activity of Na<sup>+</sup>/H<sup>+</sup> exchanger isoform 1 (NHE1). Villi immobilized by a fine nylon mesh overlay were incubated for 5 minutes with a luminal solution containing 100 μM DL-dithiothreitol to remove mucus and then incubated on the luminal side with 16 μmol/L of 2',7'-bis-(2-carboxyethyl)-5-(and-6)-carboxyfluorescein acetoxymethyl ester BCECF-AM for 10 minutes before superfusion of the luminal surface. Using a 40 X water immersion objective (Olympus, Melville, NY), epithelial cells from the mid to upper-region of a single villus were selected for ratiometric analysis. Changes in intracellular pH (pH<sub>i</sub>) were measured by dual excitation wavelength technique (440 and 495 nm), and the villi were imaged at 535 nm emission. Ratiometric images were obtained at 20 second intervals with a Sensi-Cam digital camera (Cooke, Auburn Heights, MI) and processed using Axon Imaging Workbench 2.2 (Axon Instruments, Union City, CA). The 495 :440 nm ratios were converted to pH<sub>i</sub> using a standard curve generated by the K<sup>+</sup>/nigericin technique (12;108). Intrinsic buffering capacity (β<sub>i</sub>) of duodenal villous cells was

estimated by the ammonium prepulse technique and the total buffering capacity ( $\beta_{\text{total}}$ ) was calculated from the equation  $\beta_{\text{total}} = \beta_i + \beta_{\text{HCO}_3^-} = \beta_i + 2.3 \times [\text{HCO}_3^-]_i$ , where  $\beta_{\text{HCO}_3^-}$  is the buffering capacity of the  $\text{HCO}_3^-/\text{CO}_2$  system and  $[\text{HCO}_3^-]_i$  is the intracellular concentration of  $\text{HCO}_3^-$ . The rate of  $\text{pH}_i$  change during the initial 90-s period of linear  $\Delta\text{pH}/\Delta t$  change was converted to transmembrane net flux (J) of  $\text{HCO}_3^-$  or  $\text{H}^+$  measured in mM/min using the equation  $J = \Delta\text{pH}/\Delta t \times \beta_{\text{total}}$  (121).

*Measurement of apical  $\text{Cl}^-/\text{HCO}_3^-$  and  $\text{Na}^+/\text{H}^+$  exchange*

For measurement of  $\text{Cl}^-/\text{HCO}_3^-$  exchange, duodenal preparations were superfused with IBR on the luminal side and  $\text{pH}_i$  alkalization was induced by replacement of  $\text{Cl}^-$  with isethionate $^-$  on an equimolar basis. After attaining a stable  $\text{pH}_i$  (approximately 2 min),  $\text{pH}_i$  recovery was initiated by readdition of  $\text{Cl}^-$  to the luminal superfusate. In some experiments,  $\text{SO}_4^{2-}$  was used to replace  $\text{Cl}^-$  on an equimolar basis during  $\text{pH}_i$  recovery. For methazolamide studies, 100  $\mu\text{M}$  methazolamide was initially added to the superfusate from a 10-mM stock in water. For bilateral Krebs's bicarbonate Ringer (KBR) studies, the luminal superfusate was KBR containing, in mM: 140.0  $\text{Na}^+$ , 5.2  $\text{K}^+$ , 25  $\text{HCO}_3^-$ , 5 TES, 2.8  $\text{PO}_4^{2-}$ , 110  $\text{Cl}^-$ , 1.2  $\text{Ca}^{2+}$ , 1.2  $\text{Mg}^{2+}$ , 4.8 gluconate $^-$ , 16.8 mannitol, and gassed with 95%  $\text{O}_2/5\% \text{CO}_2$  at 37°C (pH 7.4). The serosal perfusate was similar in composition to the luminal solution except 10 mM mannitol was replaced equimolar with glucose. Rates of anion exchange during alkalization and recovery ( $\Delta\text{pH}_i/\text{min}$ ) were calculated from a linear regression of the values from the first 90 sec of the initial  $\text{pH}_i$  changes during  $\text{Cl}^-$  removal and replacement, respectively, and these rates were converted to net  $J(\text{HCO}_3^-)$ .

For measurement of apical membrane  $\text{Na}^+/\text{H}^+$  exchange activity, the proximal duodenum was superfused with nominally  $\text{HCO}_3^-$ -free solutions where  $\text{NaHCO}_3^-$  was

replaced equimolar with NaTES and gassed with 100% O<sub>2</sub>. Experiments to measure Na<sup>+</sup>/H<sup>+</sup> exchange consisted of pH<sub>i</sub> acidification induced by replacement of luminal Na<sup>+</sup> with NMDG<sup>+</sup> on an equimolar basis. After a stable pH<sub>i</sub> was obtained (approximately 2 min), pH<sub>i</sub> recovery was initiated by replacing NMDG<sup>+</sup> with Na<sup>+</sup>. Rates of anion exchange during Na<sup>+</sup>/H<sup>+</sup> exchange were calculated from a linear regression of the values from the first 90 sec of the initial pH<sub>i</sub> changes during Na<sup>+</sup> replacement, and these rates were converted to net J(H<sup>+</sup>).

#### *Studies of recombinant mDRA*

mDRA (gift of J. Melvin, University of Rochester) was inserted into the multiple cloning site of a bicistronic pIRES plasmid (Invitrogen) containing DSRed2, a red fluorescent protein (RFP). The resulting plasmid was transformed into DH5α competent cells (Invitrogen) by heat shock and single colonies were picked for plasmid isolation (after overnight growth) by the alkaline lysis method. Plasmid was digested with HincII to confirm the proper orientation of the DRA insert. Plasmid containing mDRA or empty vector (control) was transfected using Superfect transfection reagent (Qiagen) according to the manufacturer's directions into Chinese hamster ovary (CHO) cells grown on coverslips (50% confluent). Cells expressing RFP were selected for pH<sub>i</sub> studies 24 hours after transfection.

#### *Isolation of villous epithelium and RT-PCR*

Duodenal segments were resected, opened longitudinally along the anti-mesenteric border and washed in oxygenated, physiologic Ringer's solution containing 100 μM dithiothreitol. Under a dissecting microscope, the segment was placed mucosal-side up over a parallel ridge (1 mm height) on a plastic surface and drawn

beneath a #11 scalpel blade (perpendicular to the villi), thereby scraping the villous epithelium from the villous cores. The isolated villi were dispersed in a small volume (0.5 mL) of oxygenated Ringer's solution containing (800U/ml) RNase inhibitor (Qiagen) using a large bore transfer pipette and immediately frozen in liquid nitrogen. Total RNA was isolated using TRI-Reagent (Molecular Research Center, Inc.), according to manufacturer's instructions, and dissolved in 100 µl RNase-free water. The Superscript pre-amplification system (Invitrogen) was used for first-strand cDNA synthesis, according to the manufacturer's instructions. Each PCR of 25µl contained 1µl of cDNA, 1X PCR Mg<sup>2+</sup> Free Buffer, 2 mM MgCl<sub>2</sub>, 0.2 mM dNTP, 0.4 mM primer, and 0.5 U/rxn Taq DNA polymerase (Promega). A master mix was made and added to 0.2 ml reaction tubes containing either cDNA or water (as RT control). Primers for DRA, PAT-1, and AE4 were designed based on murine sequences from the National Center for Biotechnology Information (NCBI) database. Primers for DRA were 5' GGTTTAGCATTGCTCTGCTGG 3' and 5' TTACAGTCATGATGAGTTCGATG 3'. Primers for PAT-1 were 5' GCGACTCTCTGAAAGAGAAGTG 3' and 5' TCAGAGTTTGGTGGCCAAAACA 3'. Primers for AE4 were 5' CATGCCTGGTCAAGAAAGCTAG 3' and 5' CACTCATGTTACTGGGCCTGGTGG 3'. RT-PCR was performed on samples using RT-PCR cycles consisting of a 5.0 min denaturation at 94°C followed by 60 cycles of 94°C for 30 sec, 60°C for 1.0 min, and 72°C for 1.0 min and ended with 7.0 min at 72°C utilizing a MWG Primus 96 plus thermocycler (MWG-Biotech Inc., Highpoint, NC). RT-PCR products were electrophoresed on a 2% agarose gel for analysis. To evaluate genomic DNA contamination of the RNA samples, RT-PCR was performed on samples using primers



specific for  $\beta$ -actin, 5' TGTTACCAACTGGGACGACA 3' and 5' TCTCAGCTGTGGTGGTGAAG 3'. mRNA expression for each exchanger was compared against a similarly-treated tissue control reported to express high levels of the specific transcript.

#### *Western Blot Analysis of NHE3*

For Western blot analysis, duodenal microsomal membranes were prepared from age-matched PAT-1 (-) and WT adult mice as previously described (9;109;120). Briefly, the membrane preparations were separated by SDS-PAGE and transferred to nitrocellulose membranes, blocked with 5% milk proteins, and probed with affinity-purified primary antibodies against NHE3 or  $\beta$ -actin. The monoclonal anti-NHE3 antibody was directed against the C-terminal 131 aa of rabbit NHE3 (109), and  $\beta$ -actin monoclonal antibodies were purchased from Alpha Diagnostics (San Antonio, TX). The secondary antibody was an anti-rabbit immunoglobulin G (IgG) conjugated to horseradish peroxidase (GIBCO BRL, Gaithersburg, Md.), which was visualized using chemiluminescence (SuperSignal Substrate, Pierce) and captured on light-sensitive imaging film (Kodak). Bands corresponding to NHE3 and  $\beta$ -actin proteins were quantified by densitometric analysis (UN-SCAN-IT gel software, Silk Scientific, Inc., Orem, Utah, USA) and were expressed as percentages of control. The equity in protein loading in all blots was verified by gel staining using Coomassie brilliant blue R-250 (Bio-Rad, Hercules, CA, USA).

#### *Materials*

The fluorescent dye BCECF acetomethyl ester was obtained from Invitrogen (Carlsbad, CA). Tetrodotoxin was obtained from Biomol International L.P. (Plymouth

Meeting, PA). All other materials were obtained from either Sigma Aldrich (St. Louis, MO) or Fisher Scientific (Springfield, NJ).

### *Statistics*

All values were reported as mean  $\pm$  SEM. Data between two treatment groups was compared using a 2-tailed unpaired Student t-test assuming equal variances between groups. A probability value of  $p < 0.05$  was considered statistically significant.

## **Results**

### *Expression of DRA, PAT-1, and AE4 in the isolated duodenal villous epithelium*

DRA, PAT-1, and AE4 previously have been localized to the apical membrane of the intestinal epithelia (48;54;120;125). To verify expression in murine duodenal villi, mRNA expression in isolated murine duodenal villi was determined by RT-PCR and compared against a tissue control with high expression levels of the particular transcript (colon for DRA; kidney for PAT-1 and AE4) (53;54;69;120;124). As shown in Figure 3.1, RT-PCR of microdissected villous epithelium from murine duodenum shows prominent expression of DRA and PAT-1, and lesser expression of AE4 as compared to high-expressing tissue controls.

### *Anion exchange in the AE4 (-) upper villous epithelium of murine duodenum*

Functional studies in *Xenopus* oocytes indicate that AE4 exhibits Cl/HCO<sub>3</sub><sup>-</sup> exchange activity (125). Therefore, we compared anion exchange activity in the AE4 (-) duodenal villous epithelium to that in WT littermate epithelium. As shown in Figure 3.2A and B, there is no significant difference in the rates of HCO<sub>3</sub><sup>-</sup> influx during Cl<sup>-</sup> removal (i.e., Cl<sub>out</sub><sup>-</sup>/HCO<sub>3</sub><sup>-</sup><sub>in</sub> exchange) and HCO<sub>3</sub><sup>-</sup> efflux during Cl<sup>-</sup> replacement



**Figure 3.1.** mRNA expression of DRA, PAT-1, and AE4 in microdissected murine duodenal villi. RT-PCR showing mRNA expression of DRA, PAT-1, and AE4 in isolated villous epithelium (v) from WT duodena (representative of 3 experiments). Positive tissue controls (tc) are cDNA from cecum (ce) for DRA, and kidney (k) for PAT-1 and AE4. Water (w) and no RT (-) are negative controls. A single band for β-actin mRNA indicates minimal contamination of the samples with genomic DNA.

(i.e.,  $\text{Cl}^-_{\text{in}}/\text{HCO}_3^-_{\text{out}}$  exchange) in the AE4 (-) as compared to the WT epithelia. These experiments did not detect significant differences in the baseline  $\text{pH}_i$  of the upper villous epithelium in the AE4 (-) as compared to the WT (Figure 3.2C). Anion substitution studies in murine duodenal villi have indicated the presence of apical membrane anion exchanger(s) that can readily perform  $\text{SO}_4^{2-}_{\text{in}}/\text{HCO}_3^-_{\text{out}}$  exchange (93). Therefore, we examined this property in the AE4 (-) as compared to the WT epithelia. These studies also did not demonstrate a significant difference in the rate of  $\text{SO}_4^{2-}$  dependent- $\text{HCO}_3^-$  efflux in the AE4 (-) as compared to that in WT duodena (Figure 3.2D).

*Anion exchange in the DRA (-) upper villous epithelium of murine duodenum*

Previous studies have indicated that DRA is a major contributor to electroneutral  $\text{HCO}_3^-$  secretion in the duodenum of several species (48); therefore, we examined apical  $\text{Cl}^-/\text{HCO}_3^-$  exchange in the DRA (-) upper duodenal villous epithelium. Cumulative data for several  $\text{pH}_i$  experiments on DRA (-) and WT epithelia demonstrate that the rates of  $\text{HCO}_3^-$  influx during  $\text{Cl}^-$  removal and  $\text{HCO}_3^-$  efflux during  $\text{Cl}^-$  replacement are significantly reduced in the DRA (-) relative to the WT villi by 30-40% (Figure 3.3A and B). Interestingly, the baseline  $\text{pH}_i$  is significantly increased in the DRA (-) villi under the conditions of our study (Figure 3.3C), which may reflect unopposed activity of apical  $\text{Na}^+/\text{H}^+$  exchange (NHE3) if DRA is coupled to NHE3 for electroneutral NaCl absorption in the upper villous epithelium.

Examination of apical membrane  $\text{SO}_4^-/\text{HCO}_3^-$  exchange between the DRA (-) epithelium as compared to the WT reveals no significant difference in the rate of  $\text{SO}_4^{2-}$ -dependent  $\text{HCO}_3^-$  efflux (Figure 3.3D). These findings suggest that the degree of  $\text{SO}_4^{2-}/\text{HCO}_3^-$  exchange attributable to murine DRA may be minimal as suggested previously

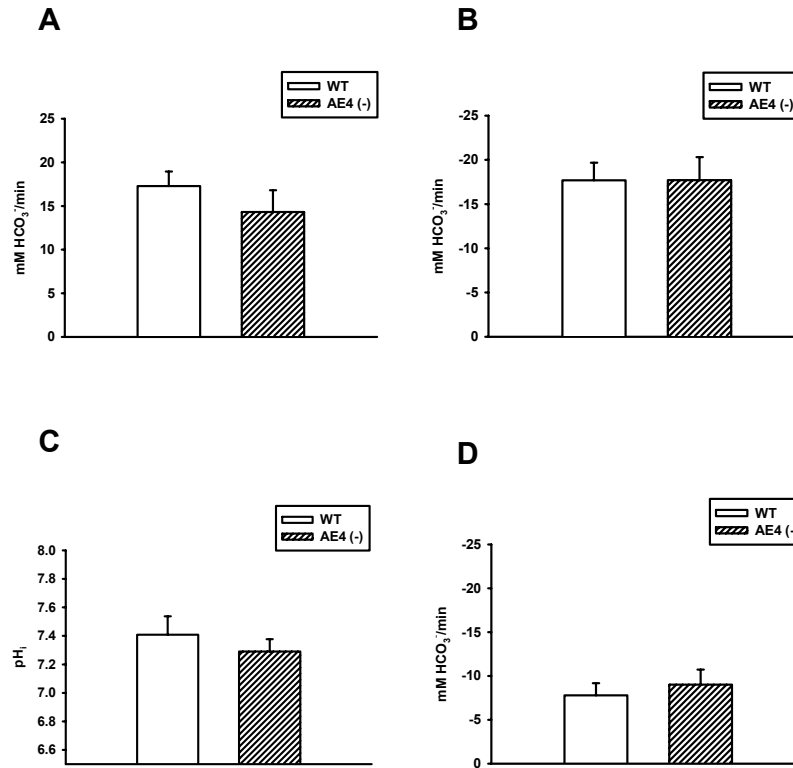
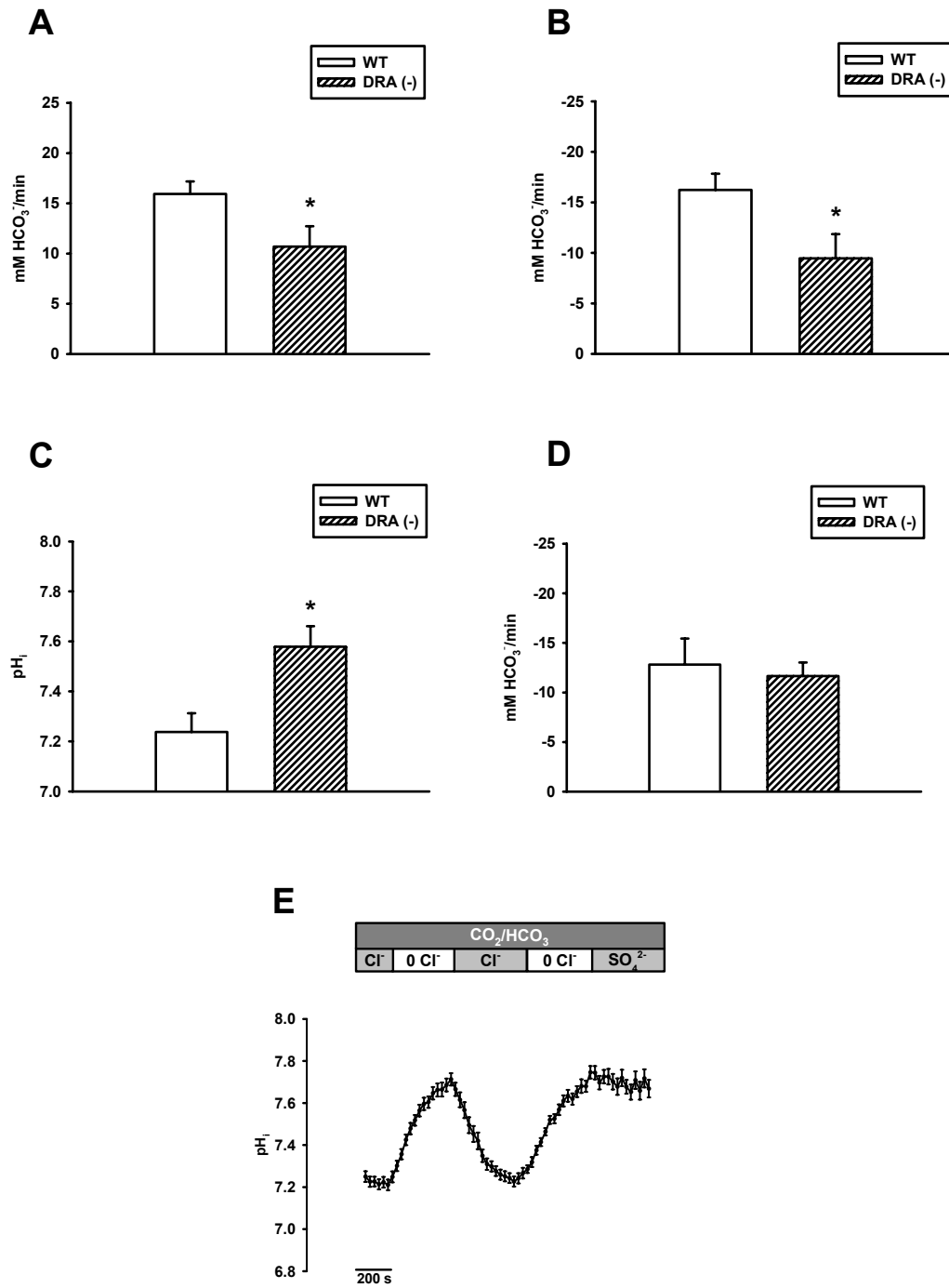


**Figure 3.2.** Anion exchange activity in the duodenal villous epithelium of WT and AE4 (-) mice. **A.** and **B.** Summary of HCO<sub>3</sub><sup>-</sup> influx (**A**) and HCO<sub>3</sub><sup>-</sup> efflux (**B**) rates during luminal Cl<sup>-</sup> removal and replacement, respectively, in duodenal villous epithelial cells from WT and AE4 (-) mice (n = 5). Cumulative data show no significant difference between the rates of Cl<sup>-</sup>/HCO<sub>3</sub><sup>-</sup> exchange in the AE4 (-) compared to the WT. **C.** Summary of baseline pH<sub>i</sub> in duodenal villous epithelial cells of WT and AE4 (-) mice (n = 5). Cumulative data show no significant difference between the baseline pH<sub>i</sub> in the AE4 (-) compared to the WT. **D.** Summary of SO<sub>4</sub><sup>2-</sup> dependent HCO<sub>3</sub><sup>-</sup> efflux rates in duodenal villous epithelial cells of WT and AE4 (-) mice (n = 3). Cumulative data show no significant difference between the rate of SO<sub>4</sub><sup>2-</sup>/HCO<sub>3</sub><sup>-</sup> exchange in the AE4 (-) compared to the WT.

**Figure 3.3.** Anion exchange activity in the duodenal villous epithelium of WT and DRA (-) mice. **A.** and **B.** Summary of  $\text{HCO}_3^-$  influx (**A**) and  $\text{HCO}_3^-$  efflux (**B**) rates in duodenal villous epithelial cells of WT (n = 10) and DRA (-) (n = 7) mice. The cumulative data show a moderate but significant reduction in the rate of  $\text{Cl}^-/\text{HCO}_3^-$  exchange following luminal  $\text{Cl}^-$  removal ( $\text{HCO}_3^-$  influx) and replacement ( $\text{HCO}_3^-$  efflux) in the DRA (-) compared to the WT. **C.** Summary of baseline  $\text{pH}_i$  in duodenal villous epithelial cells of WT (n = 10) and DRA (-) (n = 7) mice. Cumulative data show a significantly increased baseline  $\text{pH}_i$  in the DRA (-) compared to the WT. **D.** Summary of  $\text{SO}_4^{2-}$ -dependent  $\text{HCO}_3^-$  efflux rates in duodenal villous epithelial cells of WT and DRA (-) mice (n = 3). Cumulative data show no significant difference between the rate of  $\text{SO}_4^{2-}/\text{HCO}_3^-$  exchange in the DRA (-) compared to the WT. **E.** Representative  $\text{pH}_i$  trace from mDRA transfected CHO cells during extracellular  $\text{Cl}^-$  removal and replacement followed by a second  $\text{Cl}^-$  removal period and extracellular  $\text{SO}_4^{2-}$  addition (representative of 4 experiments). Removal of extracellular  $\text{Cl}^-$  resulted in intracellular alkalization and re-addition of  $\text{Cl}^-$  led to  $\text{pH}_i$  recovery demonstrating  $\text{Cl}^-/\text{HCO}_3^-$  exchange. However,  $\text{SO}_4^{2-}$  replacement following alkalization did not lead to appreciable  $\text{pH}_i$  recovery. \*Significantly different from WT.

Figure 3.3



(72). To investigate this possibility, we expressed recombinant murine DRA (mDRA) in CHO fibroblasts. <sup>1</sup>As shown by the representative experiment in Figure 3.3E, CHO cells expressing mDRA alkalize upon removal of extracellular Cl<sup>-</sup> and pH<sub>i</sub> recovery occurs upon readdition of extracellular Cl<sup>-</sup>, thus indicating robust Cl<sup>-</sup>/HCO<sub>3</sub><sup>-</sup> exchange mediated by mDRA. In contrast, following a second period of pH<sub>i</sub> alkalization induced by extracellular Cl<sup>-</sup> removal, the pH<sub>i</sub> does not significantly recover in the presence of extracellular SO<sub>4</sub><sup>2-</sup>, indicating murine DRA does not efficiently exchange SO<sub>4</sub><sup>2-</sup> for HCO<sub>3</sub><sup>-</sup>.

*Cl<sup>-</sup>/HCO<sub>3</sub><sup>-</sup> exchange in the PAT-1 (-) upper villous epithelium of murine duodenum*

Previous studies conducted in upper murine duodenal villous epithelia revealed characteristics of basal anion exchange (e.g., high rates of SO<sub>4</sub><sup>2-</sup> transport; enhanced Cl<sup>-</sup>/HCO<sub>3</sub><sup>-</sup> exchange activity during epithelial cell depolarization), that were most consistent with PAT-1 activity based upon recombinant protein expression studies (49;55;93;120;124). To evaluate the contribution of PAT-1, we compared rates of apical membrane Cl<sup>-</sup>/HCO<sub>3</sub><sup>-</sup> exchange activity between PAT-1 (-) and WT duodenal villi. As shown by the experiment in Figure 3.4A, the rates of alkalization and recovery during Cl<sup>-</sup> substitution/replacement are significantly reduced in PAT-1 (-) compared with WT duodenum. Cumulative data from several pH<sub>i</sub> experiments on PAT-1 (-) and WT epithelia demonstrate that the rates of HCO<sub>3</sub><sup>-</sup> influx during Cl<sup>-</sup> removal and HCO<sub>3</sub><sup>-</sup> efflux during Cl<sup>-</sup> replacement are significantly reduced by 65 and 80%, respectively in the PAT-1 (-) relative to the WT villi (Figure 3.4B and 3.4C). Paradoxically, the baseline

---

<sup>1</sup> No endogenous Cl<sup>-</sup>/HCO<sub>3</sub><sup>-</sup> exchange was observed in mock transfected CHO cells whereas inconsistent levels of activity were found when examining mock-transfected NIH 3T3 and HEK293 cells.



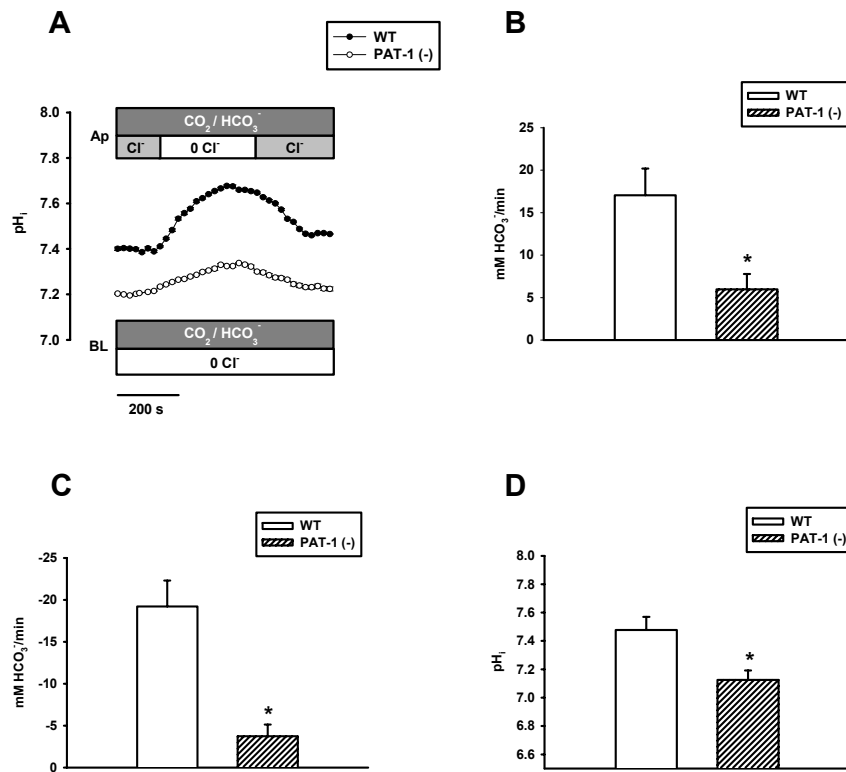


**Figure 3.4.** Comparison of Cl<sup>-</sup>/HCO<sub>3</sub><sup>-</sup> exchange activity and baseline pH<sub>i</sub> and in duodenal villous epithelium of WT and PAT-1 (-) mice. **A.** Representative pH<sub>i</sub> trace of WT and PAT-1 (-) duodenal villous epithelial cells during luminal Cl<sup>-</sup> removal and replacement. **B** and **C.** Summary of HCO<sub>3</sub><sup>-</sup> influx (**B**) and HCO<sub>3</sub><sup>-</sup> efflux (**C**) rates in duodenal villous epithelial cells from WT and PAT-1 (-) mice (n = 5). Cumulative data show significantly reduced rates of Cl<sup>-</sup>/HCO<sub>3</sub><sup>-</sup> exchange following luminal Cl<sup>-</sup> removal (HCO<sub>3</sub><sup>-</sup> influx) and replacement (HCO<sub>3</sub><sup>-</sup> efflux) in the PAT-1 (-) compared to WT. **D.** Summary of baseline pH<sub>i</sub> in duodenal villous epithelial cells of WT and PAT-1 (-) mice (n = 5). Cumulative data show a significantly reduced baseline pH<sub>i</sub> in PAT-1 (-) compared to WT. \*Significantly different from WT.

pH<sub>i</sub> is significantly more acidic in the PAT-1 (-) relative to the WT under the conditions of our study. (Figure 3.4D).

In order to assess the contribution of PAT-1 to SO<sub>4</sub><sup>2-</sup>/HCO<sub>3</sub><sup>-</sup> exchange, we measured SO<sub>4</sub><sup>2-</sup>-dependent HCO<sub>3</sub><sup>-</sup> transport rates in duodenal villous epithelium of PAT-1 (-) and WT mice. As shown by the experiment in Figure 3.5A, following pH<sub>i</sub> alkalization induced by luminal Cl<sup>-</sup> removal, luminal SO<sub>4</sub><sup>2-</sup> application resulted in pH<sub>i</sub> recovery in WT villous epithelium. In contrast, the PAT-1 (-) villous epithelium exhibited no discernable pH<sub>i</sub> recovery with SO<sub>4</sub><sup>2-</sup> application. Cumulative data for experiments on PAT-1 (-) and WT epithelia show that the rate of SO<sub>4</sub><sup>2-</sup>-dependent HCO<sub>3</sub><sup>-</sup> efflux (Figure 3.5B) is essentially abolished in the PAT-1 (-) epithelium. Thus PAT-1 is the major anion exchanger responsible for SO<sub>4</sub><sup>2-</sup> transport in the murine duodenal villous epithelium.

*Investigation of the reduced pH<sub>i</sub> in the PAT-1(-) upper villous epithelium of the murine duodenum*

As shown in Figure 3.4A and D, baseline pH<sub>i</sub> is significantly reduced in PAT-1 (-) duodenal villous epithelial cells under the conditions of our study. This result was surprising given that PAT-1 is considered a cellular base exporter (119). We hypothesized that the reduced pH<sub>i</sub> may result from the loss of a coupled interaction between PAT-1 and the apical membrane Na<sup>+</sup>/H<sup>+</sup> exchanger NHE3, resulting in inhibition of NHE3 expression and/or activity. Therefore, NHE3 protein expression and activity were measured in WT and PAT-1 (-) duodena. First, as shown in Figure 3.6A, Western blot analysis did not indicate that NHE3 protein expression was different between PAT-1 (-) and WT duodena. Second, apical membrane Na<sup>+</sup>/H<sup>+</sup> exchange

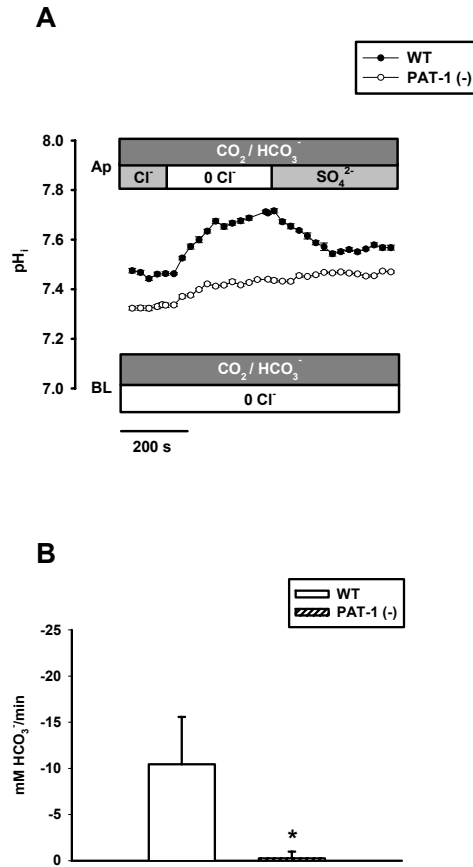


**Figure 3.5.** Comparison of  $\text{SO}_4^{2-}/\text{HCO}_3^-$  exchange in the duodenal villous epithelium of WT and PAT-1 (-) mice. **A.** Representative  $\text{pH}_i$  trace of WT and PAT-1 (-) duodenal villous epithelial cells. Following alkalinization secondary to luminal  $\text{Cl}^-$  removal,  $\text{SO}_4^{2-}$  was introduced in the luminal superfusate for  $\text{SO}_4^{2-}_{\text{in}}/\text{HCO}_3^-_{\text{out}}$  exchange. **B.** Summary of  $\text{HCO}_3^-$  efflux rates induced by luminal  $\text{SO}_4^{2-}$  application in duodenal epithelial cells from WT ( $n = 3$ ) and PAT-1 (-) ( $n = 5$ ) mice. Cumulative data show a significantly reduced rate of  $\text{SO}_4^{2-}/\text{HCO}_3^-$  exchange in the PAT-1 (-) compared to the WT.

\*Significantly different from WT.

activity was measured as the  $\text{Na}^+$ -dependent recovery of  $\text{pH}_i$  after cellular acidification in WT and PAT-1 (-) duodenal villi. These studies revealed no significant difference in the rates of  $\text{Na}^+/\text{H}^+$  exchange (i.e.,  $\text{H}^+$  efflux) between the PAT-1 (-) and WT duodenal villous epithelium (Figure 3.6B), indicating that the acidic  $\text{pH}_i$  in the PAT-1 (-) epithelium is not due to loss of NHE3 regulation. An alternative explanation for the acidic  $\text{pH}_i$  is that PAT-1 may act as a  $\text{HCO}_3^-$ -loading process ( $\text{Cl}^-_{\text{out}}/\text{HCO}_3^-_{\text{in}}$ ) in the villous epithelium under the conditions of our studies. To determine whether the process was  $\text{HCO}_3^-$  dependent, the baseline  $\text{pH}_i$  was measured in the absence of  $\text{CO}_2/\text{HCO}_3^-$  in the PAT-1 (-) and WT. This maneuver essentially eliminated the difference in baseline  $\text{pH}_i$  between the PAT-1 (-) and the WT villous epithelium as shown in Figure 3.7A. Since both a functional and physical relationship between cytosolic carbonic anhydrase CA II and PAT-1 has been shown (4;68), we also examined the effect of the carbonic anhydrase inhibitor methazolamide (100  $\mu\text{M}$ ) on baseline  $\text{pH}_i$  in PAT-1 (-) and WT duodenal villous epithelial cells in the presence of  $\text{CO}_2/\text{HCO}_3^-$ . As shown in Figure 3.7B, methazolamide treatment eliminated the difference between the baseline  $\text{pH}_i$  of the PAT-1 (-) and WT villous epithelium. Since isolation of the apical membrane transporters in our studies requires inhibition of basolateral transporters including the  $\text{Na}^+/\text{K}^+/2\text{Cl}^-$  cotransporter NKCC1 and the  $\text{Cl}^-/\text{HCO}_3^-$  exchanger AE2 (with basolateral  $\text{Cl}^-$  free conditions) and the  $\text{pH}_i$ -compensating effects of basolateral NHE1 (with 1  $\mu\text{M}$  EIPA), we asked whether removal of this inhibition would normalize  $\text{pH}_i$  in the PAT-1 (-) villous epithelium. Initially, the activity of NHE1 was restored by measuring  $\text{pH}_i$  in the absence of basolateral EIPA. As shown in Fig. 3.7C, baseline  $\text{pH}_i$  remains acidic in the PAT-1 (-) as compared to the WT epithelium. Finally, untreated duodenal mucosal preparations

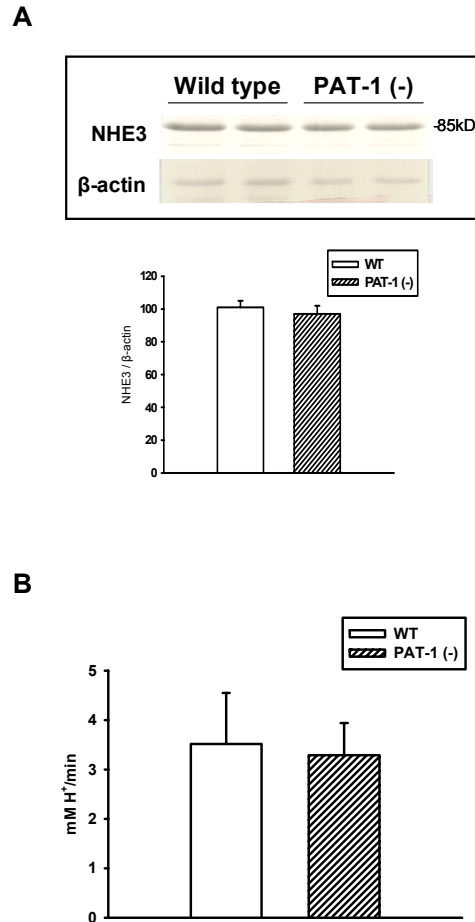
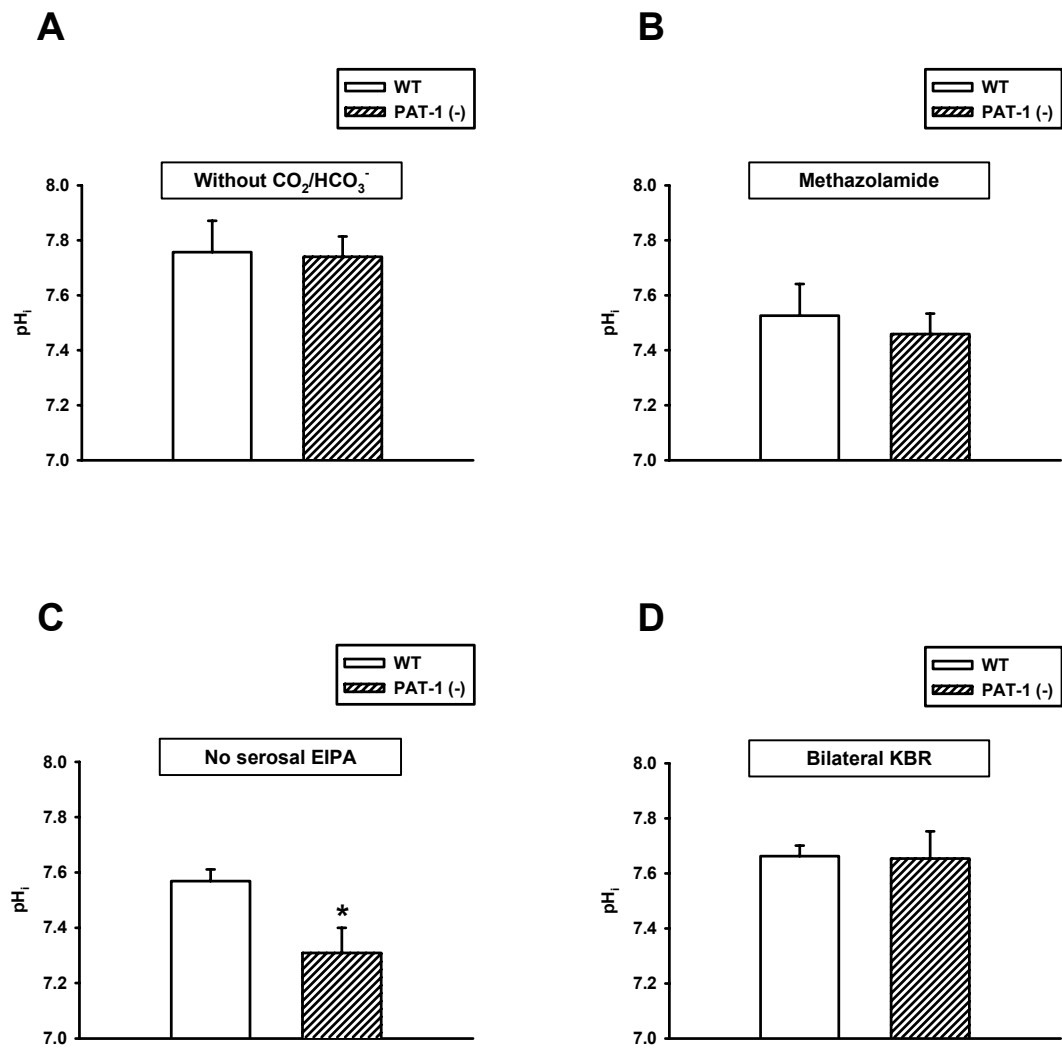


**Figure 3.6.** Comparison of NHE3 expression and apical membrane Na<sup>+</sup>/H<sup>+</sup> exchange activity in WT and PAT-1 (-) small intestine. **A.** (Upper panel) Representative Western blot of NHE3 and β-actin protein (as a loading control) in duodenal microsomes of gender-matched WT and PAT-1 (-) littermate pairs. (Lower panel) Densitometric analysis of protein expression for NHE3 normalized to expression of β-actin (n = 4 mouse pairs). These data show no significant difference of NHE3 protein expression in PAT-1 (-) brush border membrane vesicles compared to WT. **B.** Summary of Na<sup>+</sup>-dependent H<sup>+</sup> efflux rates in duodenal villous cells of WT and PAT-1 (-) (n = 3) mice. The cumulative data show no significant difference between the rate of Na<sup>+</sup>/H<sup>+</sup> exchange in PAT-1 (-) duodenal villi as compared to WT.

**Figure 3.7.** Baseline  $\text{pH}_i$  studies in the duodenal villous epithelium of WT and PAT-1 (-) mice. **A.** Summary of baseline  $\text{pH}_i$  in duodenal villous epithelial cells of WT and PAT-1 (-) ( $n = 3$ ) mice in the absence of  $\text{CO}_2/\text{HCO}_3^-$ . Cumulative data show no significant difference in the baseline  $\text{pH}_i$  of PAT-1 (-) as compared to WT. **B.** Summary of baseline  $\text{pH}_i$  in duodenal villous epithelial cells of WT and PAT-1 (-) ( $n = 3$ ) mice when performed in the presence of bilateral methazolamide ( $100 \mu\text{M}$ ) to inhibit carbonic anhydrase activity. Cumulative data show no significant difference in the baseline  $\text{pH}_i$  of PAT-1 (-) as compared to WT. **C.** Summary of baseline  $\text{pH}_i$  in duodenal villous epithelial cells of WT and PAT-1 (-) ( $n = 5$ ) mice when performed in the absence of serosal EIPA. Cumulative data show a significantly reduced baseline  $\text{pH}_i$  in PAT-1 (-) compared to WT. **D.** Summary of baseline  $\text{pH}_i$  in duodenal villous epithelial cells of WT and PAT-1 (-) ( $n = 3$ ) mice when performed with bilateral KBR. Cumulative data show no significant difference in baseline  $\text{pH}_i$  of PAT-1 (-) as compared to WT under physiologic conditions. \*Significantly different from WT.

Figure 3.7



were superfused with a physiologic Krebs's bicarbonate Ringer's solution (KBR) bilaterally. These studies revealed that under physiologic conditions,  $\text{pH}_i$  was similar between PAT-1 (-) and WT epithelium (Fig. 3.7D).

## Discussion

The process of basal  $\text{HCO}_3^-$  secretion across the duodenum has been shown in several species to principally involve the activity of apically located  $\text{Cl}^-/\text{HCO}_3^-$  exchanger(s) (25;84;99). Therefore, in an effort to resolve the identity of the anion exchangers involved in these processes, we examined the anion exchange properties in epithelial cells located on the upper one-half of duodenal villi in murine knockout models with deletions of the apical membrane transporters, PAT-1, DRA, and AE4 (48;54;120;125). RT-PCR of isolated murine duodenal villi demonstrated the expression of PAT-1 and DRA, and a low level of AE4 expression. Phenotypically, investigations of PAT-1 (-) (119) and AE4 (-) (G.E. Shull, unpublished observations) mice have revealed no overt disease and normal growth rates. In contrast, the DRA (-) mice have chronic mild diarrhea (i.e., soft feces), a propensity to rectal prolapse, decreased body weights, and a mortality rate that exceeds that of the PAT-1 (-) and AE4 (-) mice (17). In the present investigation, BCECF microfluorimetry studies of intact PAT-1 (-) duodena revealed that apical  $\text{Cl}^-/\text{HCO}_3^-$  exchange was significantly reduced by 65-80% as compared to WT. This finding confirms our previous study that revealed characteristics of anion exchange in the upper villus of the murine duodenum that were most consistent with PAT-1 activity, [i.e., capability for  $\text{SO}_4^{2-}/\text{HCO}_3^-$  exchange; an increased rate of  $\text{Cl}_{\text{out}}/\text{HCO}_3^-_{\text{in}}$  exchange during membrane consistent with the proposed stoichiometry of



PAT-1 (1 Cl<sup>-</sup>/≥2 HCO<sub>3</sub><sup>-</sup>) (93). In addition to PAT-1, a finite rate of Cl<sup>-</sup>/HCO<sub>3</sub><sup>-</sup> exchange was still present in the PAT-1 (-) duodena, indicating the contribution of other anion exchangers such as DRA and AE4. Examination of AE4 (-) as compared to WT mice revealed minimal involvement of the AE4 anion exchanger to basal Cl<sup>-</sup>/HCO<sub>3</sub><sup>-</sup> exchange in the upper villous epithelium. In contrast, examination of Cl<sup>-</sup>/HCO<sub>3</sub><sup>-</sup> exchange activity in DRA (-) as compared to WT mice demonstrated a 30-40% reduction in exchange rates. Thus these data indicate that PAT-1 is the principal Cl<sup>-</sup>/HCO<sub>3</sub><sup>-</sup> exchanger in the apical membrane of the upper villous epithelium with a smaller but significant contribution by DRA, and minimal contribution from AE4.

The present investigation found that a distinguishing feature of PAT-1 is its ability to transport SO<sub>4</sub><sup>2-</sup> because SO<sub>4</sub><sup>2-</sup>/HCO<sub>3</sub><sup>-</sup> exchange is essentially eliminated in the PAT-1 (-) villous epithelium as compared to WT. Both PAT-1 and DRA have been reported to be sulfate transporters (72); however, recent studies utilizing recombinant protein expression systems have shown that human DRA does not efficiently transport SO<sub>4</sub><sup>2-</sup>, i.e., the rate of SO<sub>4</sub><sup>2-</sup> transport is 2-3 orders of magnitude less than the rate of Cl<sup>-</sup>/HCO<sub>3</sub><sup>-</sup> exchange (20;72). In the present study, SO<sub>4</sub><sup>2-</sup>/HCO<sub>3</sub><sup>-</sup> exchange in the DRA (-) duodenal villus was not significantly different from that observed in WT villi indicating that murine DRA also does not transport SO<sub>4</sub><sup>2-</sup>. To verify that murine DRA like human DRA does not effectively transport SO<sub>4</sub><sup>2-</sup>, we measured SO<sub>4</sub><sup>2-</sup>/HCO<sub>3</sub><sup>-</sup> exchange activity of recombinant mDRA expressed in CHO fibroblasts. These studies revealed a robust Cl<sup>-</sup>/HCO<sub>3</sub><sup>-</sup> exchange but little evidence of SO<sub>4</sub><sup>2-</sup>/HCO<sub>3</sub><sup>-</sup> exchange in mDRA transfected cells. In addition, examination of SO<sub>4</sub><sup>2-</sup> transport in the surface epithelium of the cecum where DRA is the dominant apical membrane exchanger also revealed no detectable SO<sub>4</sub><sup>2-</sup>

transport (data not shown). Rates of  $\text{SO}_4^{2-}/\text{HCO}_3^-$  exchange were also measured in the AE4 (-) duodenal villous epithelium since studies examining AE4 exchange properties are limited (125). Like the studies with DRA (-) epithelium, these experiments revealed no significant difference in the  $\text{SO}_4^{2-}$ -dependent  $\text{HCO}_3^-$  efflux in the AE4 (-) as compared to WT villous epithelium. Thus, the data show that a distinguishing characteristic of PAT-1 is the capability for  $\text{SO}_4^{2-}/\text{HCO}_3^-$  exchange in the upper villous epithelium of murine duodenum.

Measurements of  $\text{pH}_i$  in the DRA (-) and PAT-1 (-) villous epithelium revealed opposite effects of these transporters on  $\text{pH}_i$  regulation. In the DRA (-) villous epithelium, baseline  $\text{pH}_i$  was significantly increased as compared to WT. This change is consistent with loss of a  $\text{Cl}^-/\text{HCO}_3^-$  exchanger that is normally coupled to the  $\text{Na}^+/\text{H}^+$  exchanger NHE3 for electroneutral  $\text{NaCl}$  absorption, i.e., continued proton efflux via NHE3 without concurrent  $\text{HCO}_3^-$  efflux would increase  $\text{pH}_i$ . Additional studies of DRA (-) mice using jejunum, where electroneutral  $\text{NaCl}$  absorption predominates, will be necessary to test this hypothesis. In contrast to the deletion of DRA, measurements of  $\text{pH}_i$  in the PAT-1 (-) villous epithelium revealed a significantly reduced baseline  $\text{pH}_i$  as compared to WT. This phenomenon was investigated further because cell acidification resulting from deletion of a base-exporter is counterintuitive. One potential explanation is that loss of a coupled interaction between PAT-1 and NHE3 reduces the activity or expression of the  $\text{Na}^+/\text{H}^+$  exchanger. However, apical membrane  $\text{Na}^+/\text{H}^+$  exchange activity and NHE3 protein expression were not different between PAT-1 (-) and WT epithelia. An alternative hypothesis is that PAT-1 acts as a base importer (i.e.,  $\text{Cl}^-_{\text{out}}/\text{HCO}_3^-_{\text{in}}$  exchange) under the conditions of our study. Consistent with this hypothesis

was the demonstration that removal of  $\text{CO}_2/\text{HCO}_3^-$  from the superfusate media normalized  $\text{pH}_i$  in the PAT-1 (-) and WT epithelium. Based on evidence that PAT-1 may functionally and physically interact with carbonic anhydrase II (4), the latter finding suggests a novel interaction between PAT-1 and intracellular carbonic anhydrase, i.e., the “ $\text{HCO}_3^-$  transport metabolon” (68;102) that facilitates  $\text{HCO}_3^-$  influx to protect the epithelial cell against intracellular acidification. This may be of physiologic importance as the upper villous epithelium of the duodenum is exposed to acid challenge not only from gastric effluent, but also from  $\text{H}^+$  influx during nutrient absorption (e.g., the apical  $\text{H}^+$ /peptide cotransporter PEPT1) (28). However, this hypothesis will need to be tested further during luminal acid exposure and PEPT1-mediated transport in the duodenal villous epithelium. Isolation of apical membrane acid-base transporters required inhibition of basolateral NHE1 by EIPA treatment and  $\text{Cl}^-/\text{HCO}_3^-$  exchange by removal of basolateral  $\text{Cl}^-$ , respectively. We first investigated whether the activity of NHE1 could normalize basal  $\text{pH}_i$  in the PAT-1 (-) epithelium by removing basolateral EIPA treatment. However, the PAT-1 (-) villous epithelium remained acidic as compared to the WT indicating that activity of NHE1 alone is apparently unable to compensate for the loss of PAT-1. Next, a physiological  $\text{Cl}^-$  concentration was included in the basolateral bath in addition to removing basolateral EIPA treatment. These changes resulted in the correction of the  $\text{pH}_i$  difference between the PAT-1 (-) and WT villous epithelium. Thus, under physiological conditions,  $\text{pH}_i$  of the upper villous epithelium can be normalized in the absence of PAT-1 by a complex process apparently requiring the activity of basolateral transporters.

Basal  $\text{HCO}_3^-$  secretion by the duodenum is largely mediated by the activity of anion exchangers and reduced rates of secretion have been reported for CF patients and CF mouse models (83;84). Consistent with these findings, our previous studies of the CFTR (-) mouse intestine found that rates of apical membrane  $\text{Cl}^-/\text{HCO}_3^-$  are reduced in the upper villous epithelium. The mechanism of the decrease was traced to the loss of a CFTR-mediated  $\text{Cl}^-$  “leak” pathway that effluxes  $\text{Cl}^-$  entering via an apical  $\text{Cl}^-/\text{HCO}_3^-$  exchanger (93). This conclusion followed from studies showing that 1) increased anion exchanger activity in wild-type (WT) duodenum was supported only by transport of CFTR-permeant anions ( $\text{Cl}^-$  and  $\text{NO}_3^-$  but not  $\text{SO}_4^{2-}$ ), and 2) glybenclamide blockade of CFTR reduced the rate of  $\text{Cl}^-/\text{HCO}_3^-$  exchange in WT epithelium to a level equivalent with CFTR(-) epithelium. Based upon the present data, it is reasonable to conclude that the CFTR  $\text{Cl}^-$  leak primarily facilitates PAT-1 function in the upper villous epithelium. However, loss of CFTR facilitation of PAT-1 activity may represent only one component of reduced basal  $\text{HCO}_3^-$  secretion in the CF intestine. Recent pH stat studies of PAT-1 (-) mouse duodenum estimate that PAT-1 contributes only 20% to basal  $\text{HCO}_3^-$  secretion in WT duodenum (114). Since the present studies were confined to the upper villous epithelium, most  $\text{HCO}_3^-$  secretion under basal conditions apparently comes from the lower villous and crypt epithelium where the activities of DRA or AE4 may provide a major contribution to basal  $\text{HCO}_3^-$  secretion.

In conclusion, our studies of PAT-1, DRA, and AE4 (-) mice indicate that PAT-1 is the major contributor to basal  $\text{Cl}^-/\text{HCO}_3^-$  and  $\text{SO}_4^{2-}/\text{HCO}_3^-$  exchange across the apical membrane of epithelial cells in the upper villous epithelium of the duodenum. Based on past studies of CFTR activity in this region of the villus, it is likely that PAT-1 activity is

facilitated indirectly by a CFTR Cl<sup>-</sup> “leak” pathway that sustains the driving force for Cl<sup>-</sup>/HCO<sub>3</sub><sup>-</sup> exchange. However, additional studies of the PAT-1 (-) duodenum revealed a propensity for PAT-1 to operate in Cl<sup>-</sup><sub>out</sub>/HCO<sub>3</sub><sup>-</sup><sub>in</sub> mode for HCO<sub>3</sub><sup>-</sup> influx, thereby providing a potentially important mechanism for protecting the upper villous epithelial cell from intracellular acidification during exposure to luminal acid. DRA was also found to contribute a smaller but significant portion of Cl<sup>-</sup>/HCO<sub>3</sub><sup>-</sup> exchange in the upper villous epithelium. DRA deletion resulted in intracellular alkalization which may be indicative of DRA’s involvement in coupled NaCl absorption in this locale. Therefore, DRA in the upper villous epithelium may not significantly contribute to net HCO<sub>3</sub><sup>-</sup> secretion under basal conditions. Nonetheless, it will be necessary to examine anion transport in the lower villus/crypt epithelium where CFTR is predominantly expressed in order to fully evaluate the contributions of AE4, DRA, and PAT-1 to transepithelial bicarbonate secretion.

## Chapter 4

# INHIBITION OF PAT-1 IMPAIRS THE ABILITY OF UPPER VILLOUS EPITHELIAL CELLS OF THE MURINE DUODENUM TO REGULATE $pH_i$ DURING $H^+$ -DIPEPTIDE TRANSPORT

### Introduction

The small intestinal enterocyte is the principal site for the absorption of dietary proteins that have been degraded enzymatically to free amino acids and small peptides. The majority of protein digestion products are absorbed in the form of di- and tripeptides by the intestinal oligopeptide transporter PEPT1 (28). PEPT1 expression is restricted to the apical membrane of the small intestine with greatest levels in the duodenum and jejunum where it is not detectable in the crypts but increases from the villous base to its highest levels in the villous tips (38). The PEPT1 protein has the ability to transport all the 400 different dipeptides and 8000 different tripeptides derived from luminal protein digestion regardless of net charge, molecular size, and solubility (57). In addition, many orally delivered drugs which have dipeptide and tripeptide structures, including  $\beta$ -lactam antibiotics and ACE inhibitors, and bacterial products, such as f-MLP and muramyl dipeptide, cross the absorption barrier by means of transport through PEPT1 (15;38;70;116).

Transport via PEPT1 is electrogenic and is coupled to an inwardly directed proton gradient that allows for transport of peptides against a concentration gradient (65).  $H^+$ /peptide influx exhibits a stoichiometry of 1:1, which occurs irrespective of the net

charge associated with the peptide, but there is a clear preference for non-charged species (57). Studies of intestinal cell lines have shown that proton di-/tripeptide uptake results in intracellular acidification, and this decrease in  $\text{pH}_i$  will diminish the driving force for PEPT1-mediated transport unless the proton load is reduced by means of intracellular buffering or proton efflux (110;111). Therefore, optimal peptide absorption must rely upon the coordination of a number of acid-base transport proteins present in intestinal epithelial cells. Studies performed in the absence of  $\text{CO}_2/\text{HCO}_3^-$  have revealed that the intracellular acidification resulting from PEPT1-mediated transport can be effectively minimized by means of apical membrane  $\text{Na}^+/\text{H}^+$  exchange activity (i.e., NHE2 and NHE3) (50;94;112;113). Further, in intestinal cell lines endogenously expressing PEPT1 and  $\text{Na}^+/\text{H}^+$  exchanger proteins, it has been shown that PEPT1-mediated transport activates NHE3, the major  $\text{Na}^+/\text{H}^+$  exchanger in the mammalian intestine (50;112;113). As a result,  $\text{H}^+$  can recycle across the apical membrane maintaining  $\text{pH}_i$  and the driving force for peptide absorption. Under physiologic conditions, (i.e., in the presence of  $\text{CO}_2/\text{HCO}_3^-$ ), one previous study performed in murine small intestinal villous epithelia has demonstrated that intracellular carbonic anhydrase (CA) activity facilitates diffusive  $\text{H}^+$  movement thereby maintaining a transmembrane ion gradient that allows for maximal absorption via PEPT1 (103). However, the contribution of acid-base transporters to the regulation of  $\text{pH}_i$  during  $\text{H}^+$  peptide transport has not been fully investigated under physiologic conditions.

In addition to  $\text{Na}^+/\text{H}^+$  exchangers and carbonic anhydrase,  $\text{Cl}^-/\text{HCO}_3^-$  exchangers contribute to acid/base transport across duodenal villous epithelium. Three anion exchangers that allow for  $\text{Cl}^-/\text{HCO}_3^-$  exchange have been localized to the apical

membrane in murine duodenum: down-regulated in adenoma (DRA, Slc26a3), the putative anion transporter-1 (PAT-1, Slc26a3), and anion exchanger 4 (AE4, Slc4a9) (48;54;120;125). In a recent study on mice with gene-targeted deletions of these exchangers, PAT-1 has been shown to be the dominant  $\text{Cl}^-/\text{HCO}_3^-$  exchanger in the apical membrane of epithelial cells in the upper half of the duodenal villi (Chapter 3), the site of primary expression for PEPT1 (38). However, recent pH stat studies in the PAT-1 (-) murine duodenum indicate that PAT-1 contributes only 20% to transepithelial basal bicarbonate secretion (114;119). In addition,  $\text{pH}_i$  measurements under conditions that isolate apical membrane acid-base transport in the PAT-1 (-) villous epithelium have revealed a significantly reduced baseline  $\text{pH}_i$  as compared to WT, a difference that is  $\text{HCO}_3^-$ -dependent (Chapter 3). This finding indicates a propensity for PAT-1 to act as a base importer (i.e.,  $\text{Cl}^-_{\text{out}}/\text{HCO}_3^-_{\text{in}}$ ) in native villous epithelium. The ability of PAT-1 to function as a base importer may be physiologically relevant as the upper villous epithelium of the duodenum is exposed to acid challenge not only from gastric effluent, but also from  $\text{H}^+$  influx during nutrient absorption, e.g., PEPT1-mediated absorption. Furthermore, PAT-1 has been shown to physically and functionally interact with cytosolic CAII, the most widely expressed isozyme of the small intestine (4). Therefore, we investigated the relative contributions of PAT-1 and CAII in the process of  $\text{pH}_i$  regulation in the duodenal upper villous epithelium during absorption of the PEPT1-dipeptide substrate glycyl-sarcosine (Gly-Sar) using mice with gene-targeted deletions of PAT-1 and CAII and their wild-type (WT) littermates.



## Materials and Methods

### *Animals*

The experiments in this study were performed on mice with gene-targeted disruptions of the murine homologs of PAT-1 (119) and CAII (98). All comparisons were made with gender- and age-matched (+/+) siblings (WT). The mutant mice were identified using a PCR based analysis of tail snip DNA, as previously described (24). All mice were maintained *ad libitum* on standard laboratory chow (Formulab 5008 Rodent Chow; Ralston Purina) and tap water. The mice were housed singly in a temperature (22-26°C) and light (12:12-h light-dark cycle)-controlled room in the AAALAC accredited animal facility at the Dalton Cardiovascular Research Center. Intestinal tissues for experiments were obtained from mice 2-4 months of age. These mice were fasted overnight prior to experimentation but were provided with water *ad libitum*. All experiments involving animals were approved by the University of Missouri Animal Care and Use Committee.

### *Short-circuit current measurement*

Freshly-excised duodenum or jejunum from WT mice was stripped of the underlying muscle layers and mounted on voltage-clamped Ussing chambers for the measurement of short-circuit current ( $I_{sc}$ ) as previously described (25). The apical surface of the duodenum was bathed with Krebs's bicarbonate Ringers (KBR) containing in mM: 140.0  $\text{Na}^+$ , 5.2  $\text{K}^+$ , 2.8  $\text{PO}_4^{2-}$ , 119.8  $\text{Cl}^-$ , 25.0  $\text{HCO}_3^-$ , 1.2  $\text{Ca}^{2+}$ , 1.2  $\text{Mg}^{2+}$ , 4.8 gluconate $^-$ , 10.0 mannitol, 1  $\mu\text{M}$  indomethacin and gassed with 95%  $\text{O}_2$ : 5%  $\text{CO}_2$  at 37°C (pH 7.4). The basolateral perfusate was similar in composition to the apical solution except 10 mM mannitol was replaced equimolar with glucose and contained 1  $\mu\text{M}$

indomethacin, and 0.1  $\mu\text{M}$  tetrodotoxin. Prior to experimentation, the apical surface of the tissue was treated with 100  $\mu\text{M}$  5-(N-ethyl-n-isopropyl)-amiloride (EIPA) or 100  $\mu\text{M}$  niflumic acid (NFA) from a 100 mM stock in DMSO. Following a 20 min equilibration period, 20 mM Gly-Sar was added to the luminal bath, and the change in  $I_{\text{sc}}$  was recorded after five minute intervals.

#### *Fluorescence Measurement of Intracellular pH and Image Analysis*

The method used for imaging villous epithelial cells in intact murine intestine has been previously described (39;93). Briefly, after euthanasia of the mouse, the proximal duodenum or jejunum was isolated, stripped of the outer muscle layers by blunt dissection and mounted luminal side up in a horizontal Ussing-type perfusion chamber where luminal and serosal surfaces of the tissue were independently bathed. All tissues were treated with indomethacin (1  $\mu\text{M}$ ) bilaterally and tetrodotoxin (TTX, 0.1  $\mu\text{M}$ ) serosally to minimize the effect of endogenous prostaglandins and neural tone, respectively. Villi immobilized by a fine nylon mesh overlay were incubated for 5 minutes with a KBR or isethionate<sup>-</sup> bicarbonate Ringer (IBR) luminal solution containing 100  $\mu\text{M}$  DL-dithiothreitol to remove mucus and followed by incubation on the luminal side with 16  $\mu\text{mol/L}$  of 2',7'-bis-(2-carboxyethyl)-5-(and-6)-carboxyfluorescein acetoxymethyl ester (BCECF-AM) for 10 minutes. Using a 40 X water immersion objective (Olympus, Melville, NY), 10 epithelial cells from the mid to upper-region of a single villus were selected for ratiometric analysis. Changes in intracellular pH ( $\text{pH}_i$ ) were measured by the dual excitation wavelength technique (440 and 495 nm), and imaged at 535 nm emission. Ratiometric images were obtained at 20 second intervals with a Sensi-Cam digital camera (Cooke, Auburn Heights, MI) and processed using Axon

Imaging Workbench 2.2 (Axon Instruments, Union City, CA). The 495: 440 nm ratios were converted to  $\text{pH}_i$  using a standard curve generated by the  $\text{K}^+$ /nigericin technique (12;108). Intrinsic buffering capacity ( $\beta_i$ ) of duodenal villous cells was estimated by the ammonium prepulse technique and the total buffering capacity ( $\beta_{\text{total}}$ ) was calculated from the equation  $\beta_{\text{total}} = \beta_i + \beta_{\text{HCO}_3^-} = \beta_i + 2.3 \times [\text{HCO}_3^-]_i$ , where  $\beta_{\text{HCO}_3^-}$  is the buffering capacity of the  $\text{HCO}_3^-/\text{CO}_2$  system and  $[\text{HCO}_3^-]_i$  is the intracellular concentration of  $\text{HCO}_3^-$  (121). The rate of  $\text{pH}_i$  change during the initial 90-s period of linear  $\Delta\text{pH}/\Delta t$  change was converted to transmembrane net flux (J) of  $\text{HCO}_3^-$  or  $\text{H}^+$  measured in mM/min using the equation  $J = \Delta\text{pH}/\Delta t \times \beta_{\text{total}}$ .

#### *Measurement of Gly-Sar induced $\text{H}^+$ influx*

For studies measuring Gly-Sar induced  $\text{H}^+$  influx, the luminal superfusate was a KBR solution containing (in mmol/L): 140.0  $\text{Na}^+$ , 110.0  $\text{Cl}^-$ , 25.0  $\text{HCO}_3^-$ , 5.2  $\text{K}^+$ , 5.0 N-tris methyl-2-aminoethanesulfonic acid (TES), 4.8 gluconate $^-$ , 2.8  $\text{PO}_4^{2-}$ , 1.2  $\text{Ca}^{2+}$ , 1.2  $\text{Mg}^{2+}$ , and 16.8 mannitol that was gassed with 95%  $\text{O}_2$ : 5%  $\text{CO}_2$  at 37°C (pH 7.4). The serosal perfusate was similar in composition to the luminal solution except 10 mM mannitol was replaced equimolar with glucose. After attaining a stable  $\text{pH}_i$  measurement (approximately 2 min), the tissue was exposed to 20 mM Gly-Sar on the luminal side. Following measurement of Gly-Sar-induced acidification,  $\text{pH}_i$  recovery was induced by removing Gly-Sar from the luminal superfusate. For methazolamide studies, 100  $\mu\text{M}$  methazolamide was initially added to the luminal and serosal perfusates from a 10 mM stock in water. In  $\text{HCO}_3^-$ -free studies, a TES buffered Ringer (TBR) was used in which 25 mM  $\text{HCO}_3^-$  was replaced with 25 mM TES, and the luminal and serosal solutions were gassed with 100%  $\text{O}_2$ . For inhibitor studies, 100  $\mu\text{M}$  EIPA or 100  $\mu\text{M}$  NFA was added to

the luminal superfusate from a 100 mM stock in DMSO. For Cl<sup>-</sup> free studies, Cl<sup>-</sup> was replaced equimolar with isethionate<sup>-</sup>. Rates of Gly-Sar-induced acidification and recovery ( $\Delta\text{pH}_i/\text{min}$ ) were calculated from a linear regression of the values from the first 90 sec of the initial pH<sub>i</sub> changes during luminal Gly-Sar addition and removal, respectively.

*Measurement of apical Cl<sup>-</sup>/HCO<sub>3</sub><sup>-</sup> exchange*

For studies measuring Cl<sup>-</sup>/HCO<sub>3</sub><sup>-</sup> exchange in the murine duodenal preparations, the luminal superfusate was an IBR solution containing (in mmol/L): 140.0 Na<sup>+</sup>, 55.0 Cl<sup>-</sup>, 55.0 isethionate<sup>-</sup>, 25.0 HCO<sub>3</sub><sup>-</sup>, 5.2 K<sup>+</sup>, 5.0 TES, 4.8 gluconate<sup>-</sup>, 2.8 PO<sub>4</sub><sup>2-</sup>, 1.2 Ca<sup>2+</sup>, 1.2 Mg<sup>2+</sup>, 10.0 glucose, and 6.8 mannitol that was gassed with 95% O<sub>2</sub>: 5% CO<sub>2</sub> at 37°C (pH 7.4). The serosal superfusate was a Cl<sup>-</sup>-Free IBR (Cl<sup>-</sup> replaced with isethionate) gassed with 95% O<sub>2</sub>: 5% CO<sub>2</sub> at 37°C (pH 7.4). Duodenal preparations were superfused with IBR on the luminal side and pH<sub>i</sub> alkalization was induced by replacement of Cl<sup>-</sup> with isethionate<sup>-</sup> on an equimolar basis. After attaining a stable pH<sub>i</sub> measurement (approximately 2 min), pH<sub>i</sub> recovery was initiated by readdition of Cl<sup>-</sup> to the luminal superfusate. For Gly-Sar studies, 20 mM Gly-Sar was added to the luminal superfusate. For methazolamide studies, 100 μM methazolamide was initially added to luminal and serosal superfusates from a 10 mM stock in water. Rates of anion exchange during alkalization and recovery ( $\Delta\text{pH}_i/\text{min}$ ) were calculated from a linear regression of the values from the first 90 sec of the initial pH<sub>i</sub> changes during Cl<sup>-</sup> removal and replacement, respectively.

## *Materials*

The fluorescent dye BCECF acetoxymethyl ester was obtained from Invitrogen (Carlsbad, CA). Tetrodotoxin was obtained from Biomol International L.P. (Plymouth Meeting, PA). All other materials were obtained from either Sigma Aldrich (St. Louis, MO) or Fisher Scientific (Springfield, NJ).

## *Statistics*

All values are reported as mean  $\pm$  SEM. Data between two treatment groups were compared using a 2-tailed unpaired Student *t*-test assuming equal variances between groups. Data from multiple treatment groups were compared using a one-way analysis of variance with a *post hoc* Tukey's *t*-test. A probability value of  $p < 0.05$  was considered statistically significant.

## **Results**

### *The role of apical Na<sup>+</sup>/H<sup>+</sup> exchangers in peptide absorption under physiologic conditions*

In the absence of CO<sub>2</sub>/HCO<sub>3</sub><sup>-</sup> in the medium, the apical membrane Na<sup>+</sup>/H<sup>+</sup> exchangers NHE3 and NHE2 can effectively minimize pH<sub>i</sub> acidification during proton di-/tripeptide transport (50;94;112;113). However, relatively little is currently known regarding the role of apical membrane Na<sup>+</sup>/H<sup>+</sup> exchangers in pH<sub>i</sub> maintenance during peptide absorption under physiologic conditions (i.e., in the presence of CO<sub>2</sub>/HCO<sub>3</sub><sup>-</sup>). Therefore, we investigated transepithelial absorption of Gly-Sar, a non-metabolized dipeptide substrate for PEPT1, as indexed by I<sub>sc</sub> across the murine duodenum. As shown in Figure 4.1A, these studies demonstrate that robust Gly-Sar absorption occurs under physiologic conditions, and that with apical application of 100  $\mu$ M EIPA, a reduced but

substantial amount of dipeptide absorption persists. To further investigate  $\text{pH}_i$  regulation during dipeptide uptake under physiologic conditions,  $\text{pH}_i$  of murine duodenal villous epithelial cells was measured in the presence and absence of  $\text{CO}_2/\text{HCO}_3^-$ . In  $\text{HCO}_3^-$ -free conditions (i.e., TBR), addition of 20 mM Gly-Sar to the luminal bath results in intracellular acidification ( $\text{H}^+$  influx) as  $\text{H}^+$  is transported along with Gly-Sar into the cell via PEPT1 (Figure 4.1B and 1C). Following removal of Gly-Sar from the luminal bath,  $\text{pH}_i$  returns toward baseline value in the villous epithelium (Figure 4.1B). In contrast, under physiologic conditions (i.e., KBR), villous epithelia exhibit minimal  $\text{H}^+$  influx with luminal Gly-Sar addition. Furthermore, with apical application of 100  $\mu\text{M}$  EIPA to inhibit NHE2 and NHE3 activity, minimal  $\text{H}^+$  influx is observed (Figure 4.1C). Taken together, these data indicate that, under physiologic conditions, villous epithelia are able to maintain stable  $\text{pH}_i$  allowing for sustained peptide absorption by mechanisms other than  $\text{H}^+$  efflux via apical membrane  $\text{Na}^+/\text{H}^+$  exchange.

#### *Involvement of carbonic anhydrase II in $\text{pH}_i$ regulation during peptide absorption*

A previous study has shown that carbonic anhydrase functions in small intestinal enterocytes to facilitate intracellular acid diffusion during  $\text{H}^+$ /dipeptide transport (103). Therefore, we investigated the role of carbonic anhydrase activity in the regulation of  $\text{pH}_i$  during luminal peptide absorption. First,  $\text{pH}_i$  was measured in murine duodenal villous epithelial cells in the presence of methazolamide to inhibit the activity of both intracellular and extracellular carbonic anhydrases. As shown in Figure 4.2A and B, the rates of  $\text{H}^+$  influx and efflux during luminal Gly-Sar addition and removal, respectively, are significantly increased in the methazolamide-treated as compared to vehicle control. To investigate the specific CA involved in  $\text{pH}_i$  regulation during peptide absorption,

**Figure 4.1.** Measurement of  $H^+$ /peptide absorption and  $H^+$ /peptide-induced acidification in murine duodena during inhibition of apical  $Na^+/H^+$  exchange. **A.** Transepithelial Gly-Sar absorption as indexed by short circuit current ( $I_{sc}$ ) for WT duodena in the presence ( $n = 5$ ) or absence of 100  $\mu$ M EIPA ( $n = 8$ ) to inhibit apical  $Na^+/H^+$  exchange. Cumulative data show that under physiologic conditions (i.e., in the presence of  $CO_2/HCO_3^-$ ), robust Gly-Sar absorption occurs, and with apical application of EIPA, a reduced but substantial amount of Gly-Sar absorption persists. \*Significantly different from vehicle control. **B.** Representative trace of  $pH_i$  in the absence of  $CO_2/HCO_3^-$  (i.e., TBR) in WT duodenal villous epithelial cells during luminal addition and removal of Gly-Sar. Addition of Gly-Sar results in intracellular acidification as  $H^+$  is transported along with Gly-Sar into the cell through PEPT1. Following removal of Gly-Sar from the luminal bath, a recovery in the  $pH_i$  of the villous epithelia is observed. **C.** Comparison of  $H^+$  influx rates during apical Gly-Sar addition for WT duodenal villous epithelia in TBR ( $n = 6$ ), under physiologic conditions (i.e., KBR) ( $n = 3$ ), and in KBR with luminal addition of 100  $\mu$ M EIPA (i.e., KBR + 100  $\mu$ M EIPA) ( $n = 3$ ). Cumulative data show that in TBR, duodenal villous epithelial cells acidify in response to Gly-Sar uptake; however, in KBR and KBR +EIPA, villous epithelia exhibit minimal  $H^+$  influx with apical Gly-Sar addition.

<sup>a,b</sup>Means with the same letters are not statistically different.

Figure 4.1

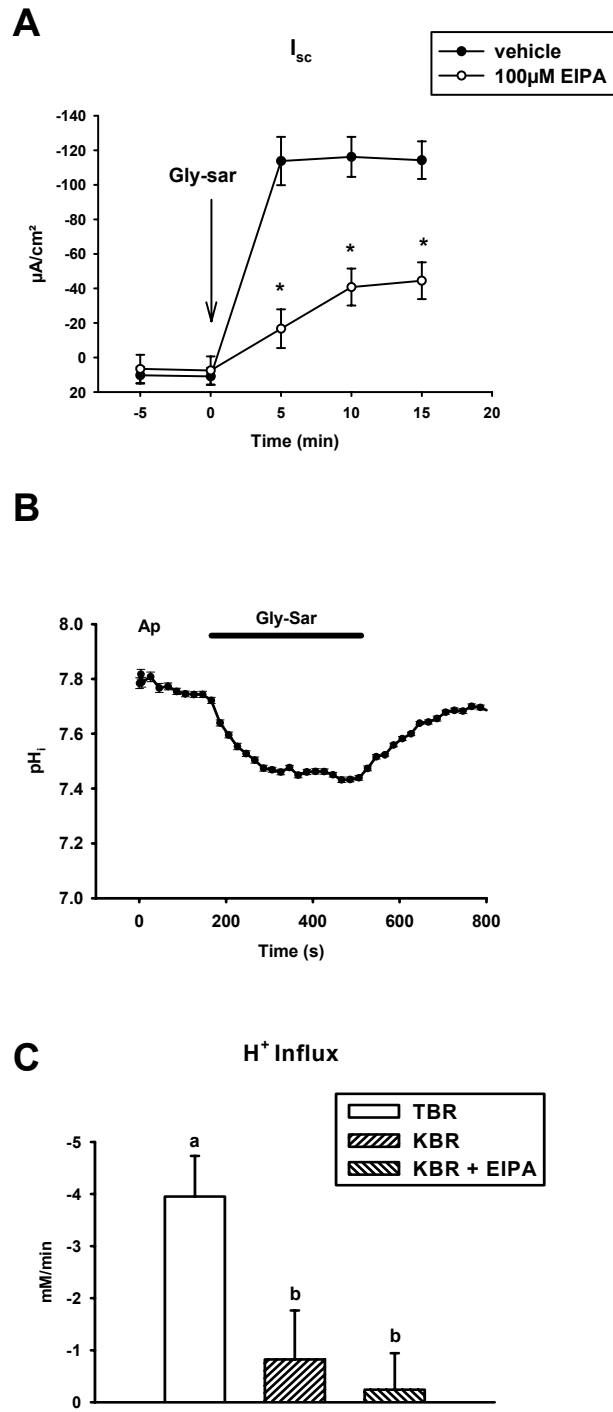
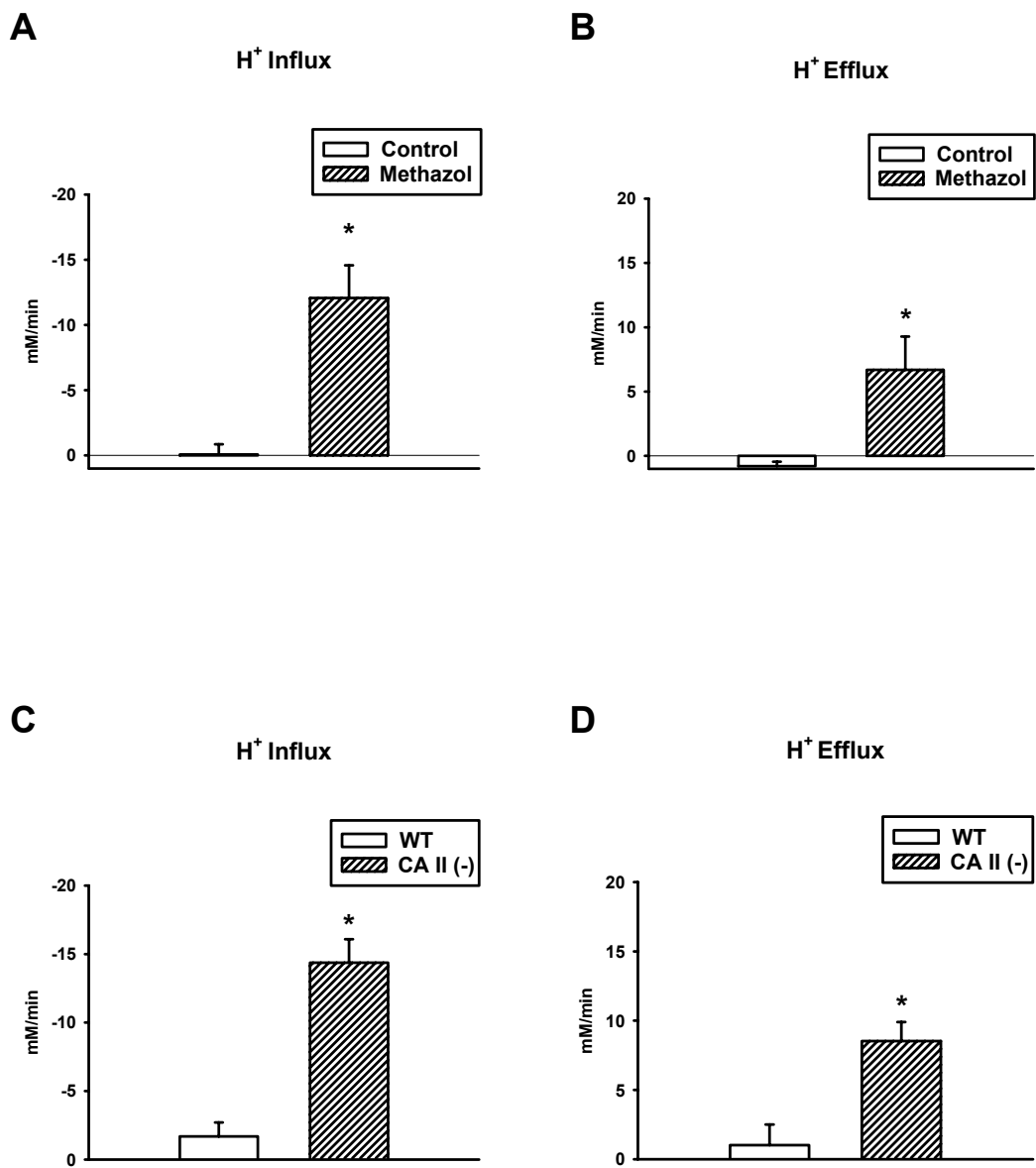




**Figure 4.2.** Regulation of  $\text{pH}_i$  during Gly-Sar uptake during inhibition of carbonic anhydrases. **A** and **B.** Summary of  $\text{H}^+$  influx (**A**) and  $\text{H}^+$  efflux (**B**) rates for WT duodenal villous epithelial cells in the presence ( $n = 3$ ) or absence of  $100 \mu\text{M}$  methazolamide ( $n = 3$ ) to inhibit carbonic anhydrases during luminal addition and removal of Gly-Sar. The cumulative data show a significant acidification ( $\text{H}^+$  influx) during luminal Gly-Sar application in the presence of methazolamide; and following Gly-Sar removal the villous epithelial cells do exhibit a significant rate of  $\text{pH}_i$  recovery ( $\text{H}^+$  efflux). \*Significantly different from vehicle control. **C** and **D.** Summary of  $\text{H}^+$  influx (**C**) and  $\text{H}^+$  efflux (**D**) rates for jejunal villous epithelial cells from WT and CAII (-) mice ( $n = 4$ ) during luminal addition and removal of Gly-Sar. Cumulative data show a significant acidification ( $\text{H}^+$  influx) during luminal Gly-Sar application in the CAII (-) compared to the WT, and following Gly-Sar removal the CAII (-) villous epithelial cells do exhibit a significant rate of  $\text{pH}_i$  recovery ( $\text{H}^+$  efflux). \*Significantly different from WT.

Figure 4.2



studies were then performed utilizing small intestine from mice lacking the cytosolic carbonic anhydrase II (CAII), the major isozyme of the villous epithelium (78). As shown in Figure 4.2C, small intestinal villous epithelia of CAII (-) mice demonstrate an impaired ability to maintain  $\text{pH}_i$ , as evidenced by an increased rate of  $\text{H}^+$  influx upon luminal Gly-Sar addition as compared to WT. Following removal of Gly-Sar from the luminal bath, a complete recovery of the  $\text{pH}_i$  was observed in the CAII (-) villous epithelium (Figure 4.2D). The above studies indicate that CAII by regulating the reversible hydration of  $\text{CO}_2$  facilitates the rate of  $\text{H}^+$  movement within the enterocyte during peptide absorption.

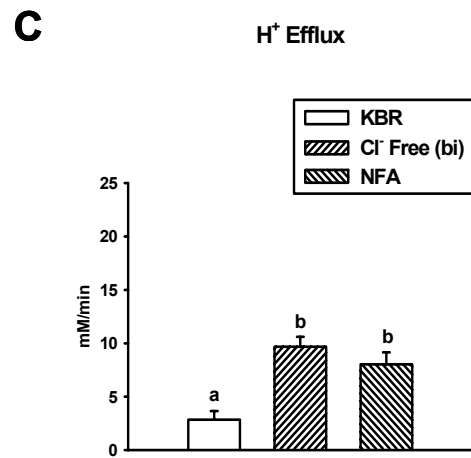
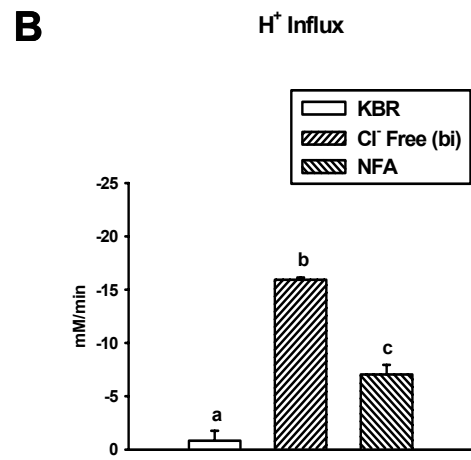
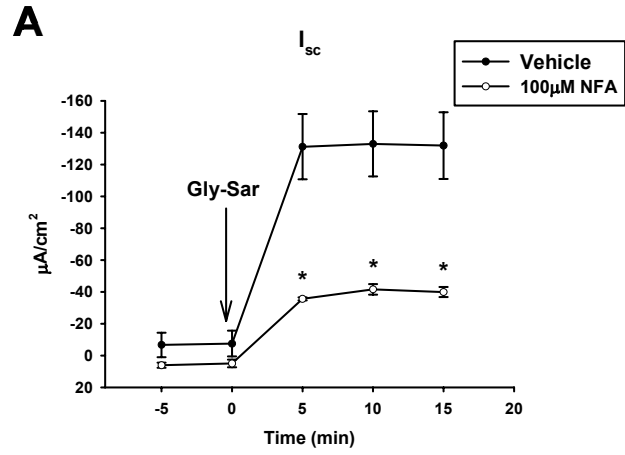
*Role of apical membrane  $\text{Cl}^-/\text{HCO}_3^-$  exchange in the  $\text{pH}_i$  regulation during peptide absorption*

Previous studies have shown high levels of expression and functional activity of Slc26a  $\text{Cl}^-/\text{HCO}_3^-$  exchangers in the villous epithelium of the upper small intestine (Chapters 2 and 3). Therefore, we investigated the contribution of apical membrane  $\text{Cl}^-/\text{HCO}_3^-$  exchange to  $\text{H}^+$  dipeptide absorption. Transepithelial absorption of Gly-Sar as indexed by  $I_{sc}$  in the murine jejunum was measured during inhibition of apical membrane  $\text{Cl}^-/\text{HCO}_3^-$  exchange with apical application of 100  $\mu\text{M}$  NFA, a dose previously shown to inhibit approximately 60% of villous  $\text{Cl}^-/\text{HCO}_3^-$  exchange NFA (Chapter 2) (Figure 4.3A). These results demonstrate that, under physiologic conditions, a significant reduction in Gly-Sar absorption (~70%) occurs in the presence of NFA compared to vehicle control. To investigate the role of  $\text{Cl}^-/\text{HCO}_3^-$  exchange activity during luminal peptide absorption, we performed studies to measure  $\text{pH}_i$  during the inhibition of apical membrane  $\text{Cl}^-/\text{HCO}_3^-$  exchange by  $\text{Cl}^-$  substitution or NFA treatment.

**Figure 4.3.** Regulation of  $\text{pH}_i$  during Gly-Sar uptake and  $\text{H}^+$ /peptide absorption in murine duodena during inhibition of apical  $\text{Cl}^-/\text{HCO}_3^-$  exchange. **A.** Transepithelial Gly-Sar absorption as indexed by  $I_{\text{sc}}$  for WT duodena in the presence or absence of NFA (n = 4) to inhibit apical  $\text{Cl}^-/\text{HCO}_3^-$  exchange. Cumulative data show a significant reduction in Gly-Sar absorption with apical application of NFA compared to control. \*Significantly different from vehicle control. **B** and **C.** Summary of  $\text{H}^+$  influx (**B**) and  $\text{H}^+$  efflux (**C**) rates for WT duodenal villous epithelial cells during apical Gly-Sar addition for WT duodenal villous epithelia in KBR, in the absence  $\text{Cl}^-$  bilateral ( $\text{Cl}^-$  Free (bi)), and in the presence of NFA (n = 3). Cumulative data show in  $\text{Cl}^-$  Free (bi) a significantly increased rate of acidification ( $\text{H}^+$  influx) with luminal Gly-Sar addition as compared to KBR, and luminal application of NFA results in an acidification rate intermediate to that observed with KBR and  $\text{Cl}^-$  free conditions. With luminal Gly-Sar removal an equivalent rate of  $\text{pH}_i$  recovery ( $\text{H}^+$  efflux) was observed under both  $\text{Cl}^-$  free (bi) and NFA conditions.

<sup>a,b,c</sup>Means with the same letters are not statistically different.

Figure 4.3



As shown in Figure 4.3B, in the absence of  $\text{Cl}^-$ , duodenal villous epithelia exhibit a significantly increased rate of acidification with apical Gly-Sar addition as compared to KBR. Apical application of NFA results in an acidification rate intermediate to that observed with KBR and  $\text{Cl}^-$  free conditions. Following Gly-Sar removal from the luminal bath, an equivalent rate of  $\text{pH}_i$  recovery is observed during inhibition of  $\text{Cl}^-/\text{HCO}_3^-$  exchange with bilateral  $\text{Cl}^-$  free conditions or during apical NFA treatment (Figure 4.3C).

#### *Role of apical membrane PAT-1 in $\text{pH}_i$ regulation during peptide absorption*

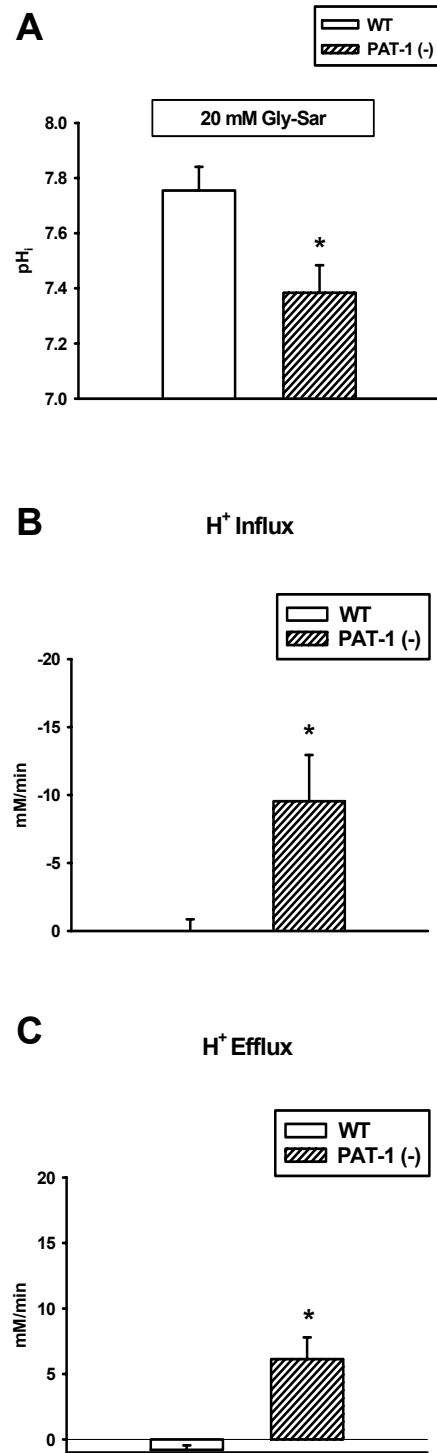
Previous studies have demonstrated that PAT-1 is the primary apical membrane  $\text{Cl}^-/\text{HCO}_3^-$  exchanger in the upper villus of the duodenum and that it may principally act as a  $\text{HCO}_3^-$  importer (Chapter 3). Furthermore, separate studies have revealed that cytosolic CAII can physically and functionally interact with PAT-1 (4). Therefore, we next examined the specific involvement of PAT-1 during PEPT1 transport. Utilizing duodena from mice deficient for PAT-1, small intestinal villous epithelia of PAT-1 (-) mice demonstrate a significantly reduced  $\text{pH}_i$  (Fig. 4.4A) and an increased rate of  $\text{H}^+$  influx with luminal Gly-Sar addition as compared to WT (Fig. 4.4B), and following removal of Gly-Sar from the luminal bath, a partial recovery of the  $\text{pH}_i$  is observed in the PAT-1 (-) villous epithelium (Fig. 4.4C).

#### *Specific effect of Gly-Sar absorption on apical membrane $\text{Cl}^-/\text{HCO}_3^-$ exchange activity in duodenal villous epithelium*

To examine the role of PAT-1 in regulating  $\text{pH}_i$  during Gly-Sar absorption, the rate of  $\text{Cl}^-/\text{HCO}_3^-$  exchange was measured in the presence of luminal Gly-Sar. First, studies of WT upper duodenal villous epithelium reveal that the mean rate of

**Figure 4.4.** Comparison of baseline  $\text{pH}_i$  and  $\text{pH}_i$  regulation in duodenal villous epithelium of WT and PAT-1 (-) mice during Gly-Sar absorption. **A.** Summary of baseline  $\text{pH}_i$  in duodenal villous epithelial cells of WT and PAT-1 (-) ( $n = 4$ ) mice during luminal Gly-Sar exposure. Cumulative data show a significantly reduced baseline  $\text{pH}_i$  in the PAT-1 (-) compared to the WT. **B** and **C.** Summary of  $\text{H}^+$  influx (**B**) and  $\text{H}^+$  efflux (**C**) rates for duodenal villous epithelial cells from WT and PAT-1 (-) ( $n = 3$ ) mice during luminal addition and removal of Gly-Sar. Cumulative data show a significant acidification ( $\text{H}^+$  influx) during luminal Gly-Sar application in the PAT-1 (-) compared to the WT, and following Gly-Sar removal the PAT-1 (-) villous epithelial cells do exhibit a significant rate of  $\text{pH}_i$  recovery ( $\text{H}^+$  efflux). \*Significantly different from WT.

Figure 4.4



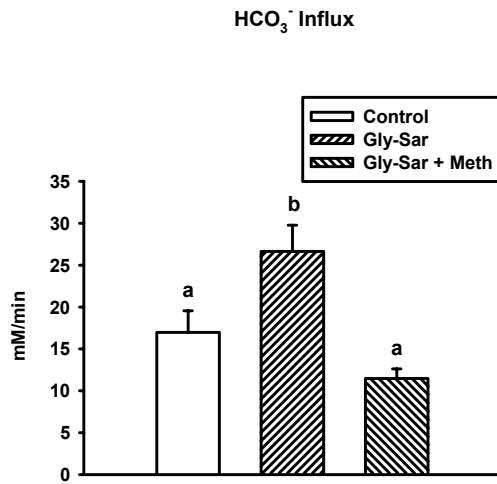


$\text{Cl}^-_{\text{out}}/\text{HCO}_3^-_{\text{in}}$  exchange (i.e.,  $\text{HCO}_3^-$  influx) during  $\text{Cl}^-$  removal is increased in the presence of Gly-Sar as compared to control (Fig. 4.5A). In contrast, the mean rate of  $\text{Cl}^-_{\text{in}}/\text{HCO}_3^-_{\text{out}}$  exchange (i.e.,  $\text{HCO}_3^-$  efflux) during  $\text{Cl}^-$  replacement is unaffected (Fig. 4.5B). The increased rate of  $\text{HCO}_3^-$  influx in the presence of Gly-Sar is consistent with the activity of a  $\text{HCO}_3^-$  importing process that predominates in the upper villous epithelium during peptide absorption. However, these results must be discerned from a simple pH gradient favorable for dipeptide absorption. Previous studies have demonstrated that dipeptide uptake across the intestinal apical membrane is enhanced by an inwardly-directed pH gradient (111); therefore, an enhanced rate of  $\text{HCO}_3^-$  influx would help support this gradient (50). However, if the maintenance of this gradient is responsible for the enhanced rate of  $\text{Cl}^-_{\text{out}}/\text{HCO}_3^-$  exchange in the presence of Gly-Sar, a parallel decrease in  $\text{Cl}^-_{\text{in}}/\text{HCO}_3^-_{\text{out}}$  exchange would be expected. When bilateral methazolamide (100  $\mu\text{M}$ ) is applied to inhibit carbonic anhydrase activity, the increased rate of  $\text{HCO}_3^-$  influx in the presence of Gly-Sar is abolished, which supports the presence of a functional interaction between carbonic anhydrase and apical  $\text{Cl}^-/\text{HCO}_3^-$  exchange (Fig. 4.5A and B). Finally, to examine whether PAT-1 activity is specifically required for this process, the rates of  $\text{Cl}^-/\text{HCO}_3^-$  exchange during Gly-Sar exposure were compared between PAT-1 (-) and WT mice. As shown in Fig. 4.5C and D, there is no significant difference in the rates of  $\text{HCO}_3^-$  influx and efflux in the PAT-1 (-) upper villous epithelium in the presence or absence of Gly-Sar revealing a dependence on PAT-1 activity for increased rate of  $\text{Cl}^-_{\text{out}}/\text{HCO}_3^-_{\text{in}}$  during luminal peptide uptake.

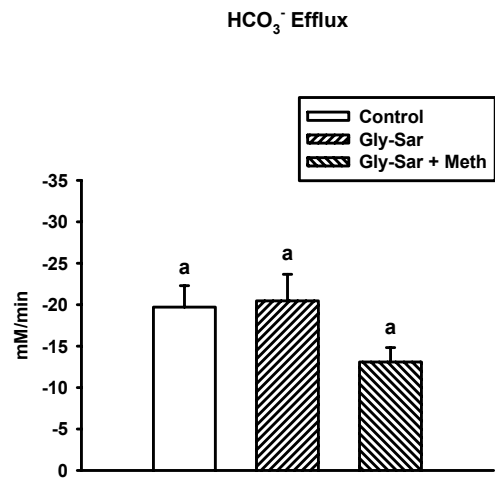
**Figure 4.5.** Comparison of  $\text{Cl}^-/\text{HCO}_3^-$  exchange activity in duodenal villous epithelium of WT and PAT-1 (-) mice during luminal Gly-Sar absorption. **A - D.** Intact duodenum was superfused in the luminal bath for 20 minutes with 20 mM Gly-Sar with or without 100  $\mu\text{M}$  methazolamide prior to luminal  $\text{Cl}^-$  removal and replacement. **A and B.** In WT duodenal epithelium, the rate of  $\text{HCO}_3^-$  influx (mean  $\pm$  SE) (**A**) was increased in the presence of luminal Gly-Sar ( $n = 5$ ), but not with luminal Gly-Sar with methazolamide ( $n = 3$ ) compared to the control ( $n = 6$ ), whereas the rate of  $\text{HCO}_3^-$  efflux (**B**) during  $\text{Cl}^-$  replacement was unaffected. <sup>a,b,c</sup> Means with the same letters are not statistically different. **C and D.** In PAT-1 (-) duodenal villous epithelium,  $\text{HCO}_3^-$  influx (**C**) and  $\text{HCO}_3^-$  efflux (**D**) rates during luminal  $\text{Cl}^-$  removal and replacement were not significantly different in the presence or absence of Gly-Sar ( $n = 3$ ). \*Significantly different from WT.

Figure 4.5

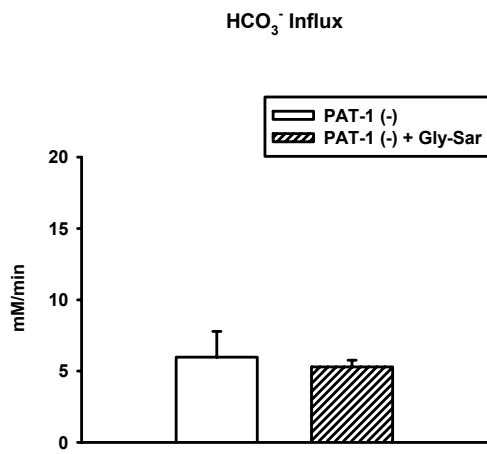
**A**



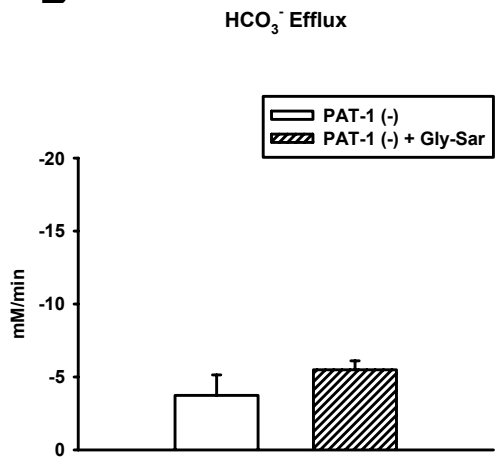
**B**



**C**



**D**



## Discussion

Uptake of peptides via the small intestinal transporter PEPT1 is driven by an inward  $H^+$  electrochemical gradient that is established by the acid microclimate of the lumen (67). The maintenance of the transepithelial pH gradient during nutrient absorption is critical for efficient absorption. Based upon studies in intestinal cell lines and intact villous epithelium, the driving force for absorption is sustained in part by  $H^+$  efflux via apical membrane NHE activity (50;94;112;113). However, the role of other acid-base transporters, including apical membrane  $Cl^-/HCO_3^-$  exchangers and carbonic anhydrases, in  $pH_i$  regulation during peptide absorption has not been fully evaluated. Therefore, we investigated  $pH_i$  regulation during absorption of the PEPT1 dipeptide substrate Gly-Sar across the villous epithelia of intact intestinal mucosa from CAII (-) and PAT-1 (-) and WT mice to determine the nature of  $pH_i$  regulation under physiologic conditions.

In the present investigation,  $I_{sc}$  studies indexing transepithelial absorption of Gly-Sar in the murine duodena revealed that substantial Gly-Sar absorption occurs under physiologic conditions. With application of EIPA to inhibit apical membrane NHE activity, the absorption was reduced by approximately 60% indicating that the chemical driving force for peptide absorption can be maintained by additional acid-base transporters. In addition, measurement of acidification rates during Gly-Sar absorption during inhibition of apical membrane NHE activity in the presence of  $CO_2/HCO_3^-$  showed that villous epithelial cells are able to maintain  $pH_i$ , demonstrating the apparent involvement of a  $HCO_3^-$ -dependent process.

Previous studies implicate the participation of carbonic anhydrase in facilitating the diffusion of  $H^+$  away from the subapical space after entry into enterocytes (103). However, the identity of the participating carbonic anhydrase isozyme(s) has yet to be resolved. In the present investigation, we initially measured changes in  $pH_i$  induced by peptide absorption during carbonic anhydrase inhibition with methazolamide (a broad spectrum inhibitor) in intact duodenal mucosa. These studies revealed a significantly increased rate of acidification in the methazolamide-treated villous epithelial cells as compared to control. We advanced these studies by utilizing intestine from mice deficient of CAII, the most widely expressed isozyme of the small intestine. Phenotypically, the CAII (-) mouse has been associated with growth retardation as well as renal acidification supporting its involvement in the regulation of  $pH_i$  during peptide absorption (98). Measurement of  $H^+$  influx during Gly-Sar absorption in the CAII (-) intestine demonstrated a significantly increased rate of acidification compared to the WT, which was similar in magnitude to the rate observed with the methazolamide-treated intestine. Thus, these findings indicated that CAII is the principal carbonic anhydrase isozyme involved in the maintenance of  $pH_i$  during peptide absorption.

Carbonic anhydrase catalyzes the reversible hydration of  $CO_2$  to  $HCO_3^-$  and  $H^+$ , a reaction limited by the relative concentrations of components in the  $CO_2$  buffer system (i.e.,  $HCO_3^-$ ,  $CO_2$ , and  $H_2CO_3$ ). Since  $HCO_3^-$  is reasonably cell-impermeant, we hypothesized that a  $Cl^-/HCO_3^-$  exchanger may contribute to the import of  $HCO_3^-$  across the apical membrane that could neutralize  $H^+$  entering via PEPT1. In addition, several lines of evidence have demonstrated associations between cytosolic CAII and apical  $Cl^-/HCO_3^-$  exchange proteins, which includes members of the Slc26a family (DRA and

PAT-1) and the Slc4 family (AE4) (4;68;100-102). Initial  $\text{pH}_i$  measurements were performed during inhibition of apical membrane  $\text{Cl}^-/\text{HCO}_3^-$  exchange by the removal of bilateral  $\text{Cl}^-$  or treatment with NFA. These studies indicated an impaired ability of the duodenal villous epithelia to regulate  $\text{pH}_i$  in the presence of Gly-Sar during inhibition of  $\text{Cl}^-/\text{HCO}_3^-$  exchange. Ussing chamber studies also showed a significant reduction in Gly-Sar absorption during inhibition of apical  $\text{Cl}^-/\text{HCO}_3^-$  exchange with NFA. Together, these studies demonstrate that functional  $\text{Cl}^-/\text{HCO}_3^-$  exchange in the apical membrane is required for optimal absorption of dipeptides across the intestinal epithelium under physiologic conditions. Based on evidence that PAT-1 is the principal apical  $\text{Cl}^-/\text{HCO}_3^-$  exchanger of the upper duodenal villus (Chapter 3) where PEPT1 is expressed at highest levels, we examined the specific role of PAT-1 in regulating  $\text{pH}_i$  during peptide absorption. These investigations revealed a significantly reduced  $\text{pH}_i$  and an increased rate of  $\text{H}^+$  influx in the PAT-1 (-) upper villus during Gly-Sar transport as compared to WT. The rate of acidification observed in the PAT-1 (-) epithelium is comparable to the rate observed during inhibition of  $\text{Cl}^-/\text{HCO}_3^-$  exchange with bilateral  $\text{Cl}^-$  free conditions indicating that PAT-1 is the principal  $\text{Cl}^-/\text{HCO}_3^-$  exchanger involved in the regulation of  $\text{pH}_i$  during peptide absorption. It is interesting to note that PAT-1 (-) mice do not demonstrate growth retardation (119). However, these observations were made during the provision of a well-balanced diet fed *ad libitum*. Therefore, growth rates should be measured in PAT-1 (-) and WT mice during challenge with a restricted protein diet. In contrast to the PAT-1 (-) mouse, the DRA (-) mouse, which is a model for human congenital chloride-losing diarrhea, does exhibit significant growth retardation, which previously has been attributed to a persistent secretory diarrhea and a resultant failure to

thrive (17;51;71); however, the involvement of DRA in nutrient absorption has not been investigated. Furthermore, DRA does demonstrate a significant contribution (30-40%) to apical  $\text{Cl}^-/\text{HCO}_3^-$  exchange in the murine upper duodenal villus. Therefore, studies of DRA (-) mice also are warranted to investigate the contribution of DRA to PEPT1-mediated absorption.

Previous studies in cell lines transfected with PAT-1 have demonstrated that inhibition of endogenous CAII reduces the anion exchange activity of PAT-1 (4). In addition, analysis of amino acid sequences of the carboxy-terminus of PAT-1 has revealed the presence of a CAII binding motif (4). This evidence suggests an interaction between PAT-1 and intracellular carbonic anhydrase, i.e., the “ $\text{HCO}_3^-$  transport metabolon” (68) that facilitates  $\text{HCO}_3^-$  influx to protect the epithelial cell against intracellular acidification. However, relatively little is known regarding the relationship of PAT-1 with CAII in native intestinal epithelia. In murine duodenal villi, there is an indication that PAT-1 may function as a base importer (i.e.,  $\text{Cl}^-_{\text{out}}/\text{HCO}_3^-_{\text{in}}$  exchange) as based on the specific condition of studies in PAT-1 (-) intestine (Chapter 3). Therefore, we hypothesized a novel derivation to the  $\text{HCO}_3^-$  metabolon whereby PAT-1 and CAII mediate  $\text{HCO}_3^-$  uptake during  $\text{H}^+$ /peptide transport to minimize intracellular acidification and sustain peptide absorption (Figure 4.6). To test this hypothesis, we measured the rate of apical membrane  $\text{Cl}^-/\text{HCO}_3^-$  exchange in murine duodenal villous epithelia in the presence of Gly-Sar. These studies indicated that the rate of  $\text{Cl}^-_{\text{out}}/\text{HCO}_3^-_{\text{in}}$  exchange was significantly increased in the presence of Gly-Sar as compared to control, whereas, there was no change in the rate of  $\text{Cl}^-_{\text{in}}/\text{HCO}_3^-_{\text{out}}$  exchange. These results support the possibility that activity of an apical membrane  $\text{Cl}^-/\text{HCO}_3^-$  exchanger facilitates  $\text{HCO}_3^-$

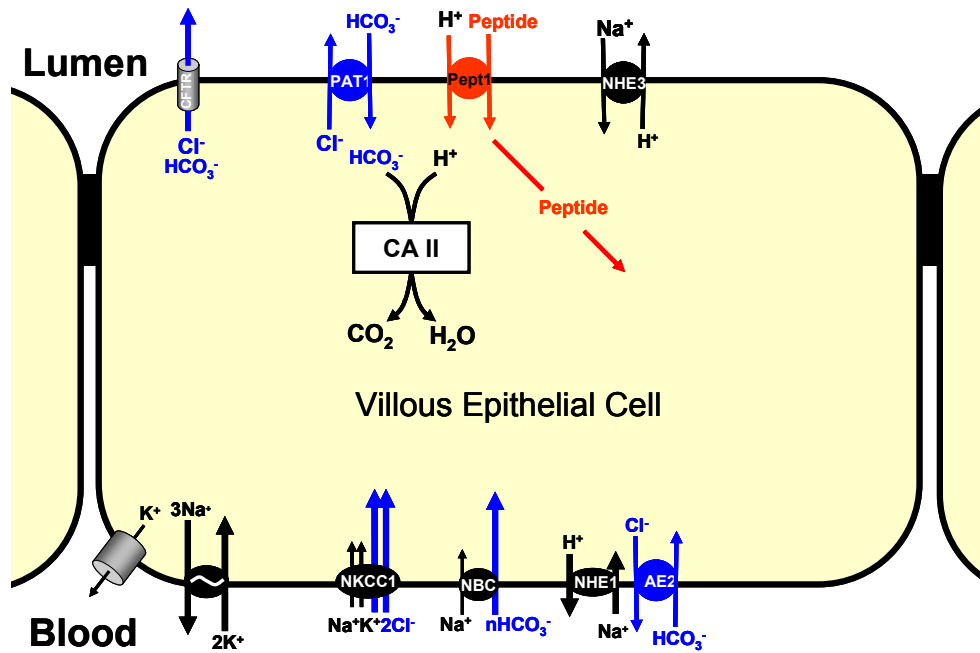


**Figure 4.6.** Cell model depicting the proposed activity of PAT-1 and CAII in the presence of peptide absorption.



import during peptide absorption. Since PAT-1 is the major  $\text{Cl}^-/\text{HCO}_3^-$  exchanger of upper duodenal villous epithelia, we expanded these studies to evaluate  $\text{Cl}^-/\text{HCO}_3^-$  exchange in the PAT-1 (-) villous epithelia during apical Gly-Sar exposure. In the PAT-1 (-) epithelium, enhancement of  $\text{Cl}^-_{\text{out}}/\text{HCO}_3^-_{\text{in}}$  exchange was abolished, suggesting that  $\text{Cl}^-/\text{HCO}_3^-$  exchange activity of PAT-1 is exclusively involved in the  $\text{HCO}_3^-$  import process. Finally, to evaluate the interaction between carbonic anhydrase and apical  $\text{Cl}^-/\text{HCO}_3^-$  exchange activity, bilateral methazolamide was applied to murine duodena in the presence of Gly-Sar. This maneuver also reduced  $\text{Cl}^-_{\text{out}}/\text{HCO}_3^-_{\text{in}}$  exchange to the level of the control, supporting the existence of a functional coupling between PAT-1 and carbonic anhydrase during PEPT1 transport.

In conclusion, our studies indicate that optimal dipeptide absorption through PEPT1 in the murine duodena depends not only on the activity of apical membrane  $\text{Na}^+/\text{H}^+$  exchange, but also on the coordinated activities of  $\text{HCO}_3^-$ -dependent acid-base transporters. Examination of CAII and PAT-1 (-) mice indicate that both PAT-1 and CAII contribute to  $\text{pH}_i$  regulation during peptide absorption. PAT-1 was found to principally function in  $\text{Cl}^-_{\text{out}}/\text{HCO}_3^-_{\text{in}}$  exchange during the presence of Gly-Sar in duodenal villous epithelia, thus allowing for transmembrane movement of membrane-impermeant  $\text{HCO}_3^-$ . By forming a  $\text{HCO}_3^-$  transport metabolon with CAII, this mode of transport by PAT-1 could effectively buffer the intracellular  $\text{H}^+$  influx that occurs during peptide absorption.

## Chapter 5

### CONCLUSIONS AND FUTURE STUDIES

#### **CFTR Facilitation of Basal $\text{Cl}^-/\text{HCO}_3^-$ Exchange in the Villous Epithelium of Intact Murine Duodenum**

##### *Summary and Conclusions*

Basal  $\text{HCO}_3^-$  secretion by the duodenum is largely mediated by the activity of anion exchangers and reduced rates of secretion have been reported for CF patients and CF mouse models (84). Investigation of the basal activity of anion exchange across the apical membrane of epithelial cells in the upper to mid-region of villi of intact duodenal mucosa from wild-type (WT) and PAT-1(-), DRA(-), and AE4(-) mice indicates that PAT-1 is the principal  $\text{Cl}^-/\text{HCO}_3^-$  exchanger in the apical membrane of the upper villous epithelium with a smaller but significant contribution by DRA (30-40%), and minimal contribution from AE4 (<5%) (Chapter 3). Examination of  $\text{Cl}^-/\text{HCO}_3^-$  exchange in the CF mouse intestine suggests that CFTR facilitates this anion exchange activity by providing a  $\text{Cl}^-$  'leak' channel that enables sustained  $\text{Cl}^-_{\text{in}}/\text{HCO}_3^-_{\text{out}}$  exchange activity under basal (non-stimulated) conditions (Figure 5.1A) based upon the evidence that 1) CFTR(-) intestine has lower rates of villous  $\text{Cl}^-/\text{HCO}_3^-$  exchange as compared to WT and 2) WT anion exchange is reduced to the level measured in the CF duodenum when either a CFTR-impermeant anion ( $\text{SO}_4^{2-}$ ) is used for exchange or CFTR channel activity is blocked with glybenclamide (Chapter 2). However, recent studies show that the CFTR blocker glybenclamide may also inhibit human DRA (58). Further, as shown in our

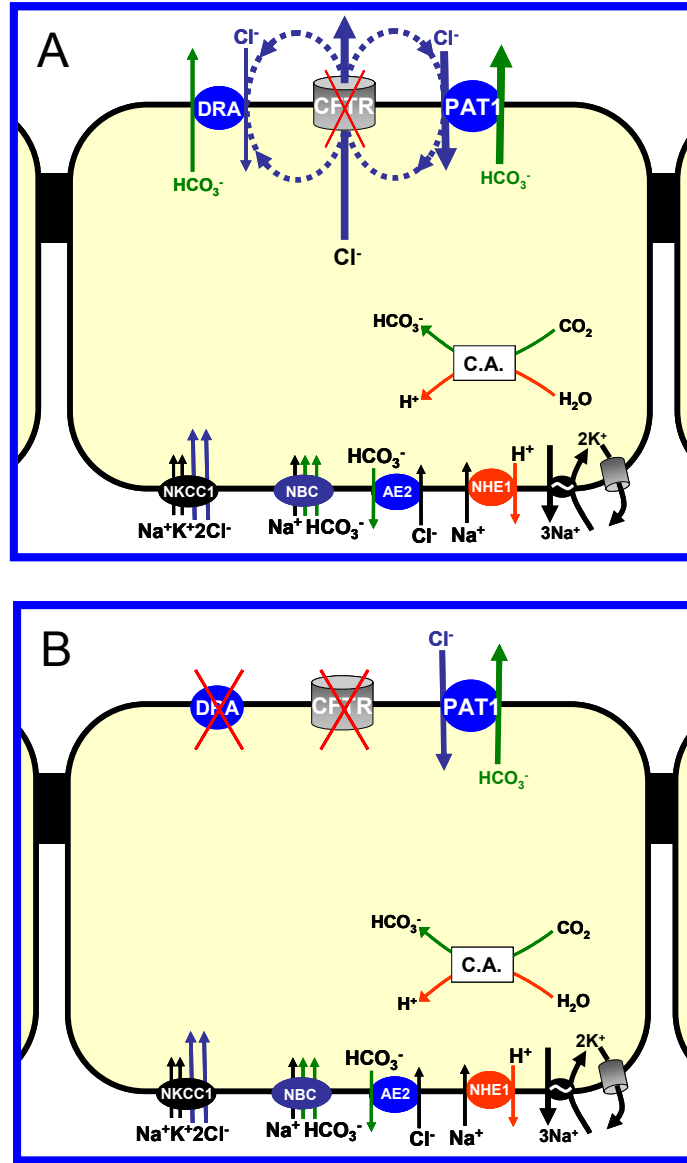


**Figure 5.1.** Two proposed models for reduced  $\text{Cl}^-/\text{HCO}_3^-$  exchange in the CFTR (-) upper duodenal villus. One model (A) supports indirect facilitation of  $\text{Cl}^-/\text{HCO}_3^-$  exchange by CFTR. The second model (B) suggests that DRA is inactive in the CF upper villus.

subsequent studies (Chapter 3), murine DRA does not participate in  $\text{SO}_4^{2-}/\text{HCO}_3^-$  exchange, thus indicating a caveat to our conclusion based on the requirement for CFTR-permeant anions. In addition, ~30% of  $\text{Cl}^-/\text{HCO}_3^-$  exchange in the upper villus was found to be due to DRA activity, which is almost equivalent to the reduction in  $\text{Cl}^-/\text{HCO}_3^-$  exchange seen in the CF mouse intestine (Chapter 3). Therefore, these findings raise the alternative hypothesis that the reduction in  $\text{Cl}^-/\text{HCO}_3^-$  exchange in the CF upper villus is due to decreased activity of DRA and not CFTR  $\text{Cl}^-$  conductance (Figure 5.1B).

#### *Supplemental Studies*

To investigate the possibility that DRA expression is reduced or that DRA is inactive in CF duodenal villus, we first examined the ability of glybenclamide to inhibit DRA activity in the murine cecum where DRA is the predominant apical  $\text{Cl}^-/\text{HCO}_3^-$  exchanger (Figure 5.2, left panel). These studies revealed that glybenclamide had very little effect on the rate of  $\text{Cl}^-/\text{HCO}_3^-$  exchange activity in the murine cecum where DRA activity is "isolated" (Figure 5.2, right panel). Next "isolated" DRA was examined in the presence and absence of CFTR activity by comparing  $\text{Cl}^-/\text{HCO}_3^-$  exchange rates between PAT-1 (-)/CFTR (+) and PAT-1 (-)/CFTR (-) double knockout mice in the upper duodenal villus (Figure 5.3). These studies revealed no significant difference in the rate of  $\text{Cl}^-/\text{HCO}_3^-$  exchange in the presence or absence of CFTR indicating that DRA is indeed active in the murine CF intestine, adding further credence to the Model A (Figure 5.1) that CFTR recycles  $\text{Cl}^-$  back to the extracellular milieu to provide a favorable  $\text{Cl}^-$  concentration gradient for exchange activity. We have, however, demonstrated a trend towards reduced DRA mRNA expression in the CFTR (-) duodenum (Chapter 2); therefore, it is still necessary to measure the level of DRA expression in the upper villous

**Large Intestine: Cl<sup>-</sup>/HCO<sub>3</sub><sup>-</sup> Exchange**

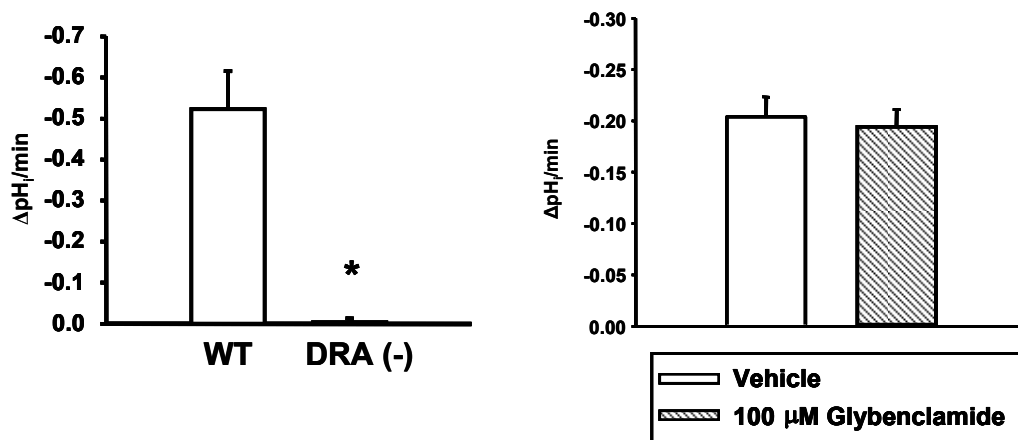


**Figure 5.2.** The effect of glybenclamide on DRA Cl<sup>-</sup>/HCO<sub>3</sub><sup>-</sup> exchange activity. (Right) Cl<sup>-</sup>/HCO<sub>3</sub><sup>-</sup> exchange activity in the cecal surface epithelium of DRA (-) and WT (n = 5) mice. \* Significantly different from WT. (Left) Cl<sup>-</sup>/HCO<sub>3</sub> exchange in the murine cecum in the presence and absence of glybenclamide (n = 3).

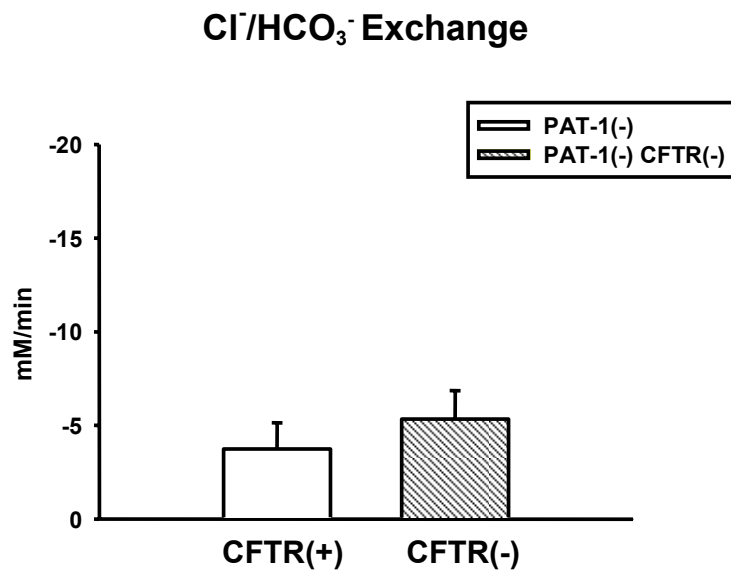


**Figure 5.3.** Isolation of DRA activity in the presence and absence of CFTR. Cl<sup>-</sup>/HCO<sub>3</sub><sup>-</sup> exchange in the upper duodenal villus from PAT (-) (n = 5) and PAT (-)/CFTR (-) (n = 2).

epithelium of CF and WT mice, and this will be determined through the use of laser capture dissection and quantitative RT-PCR. Finally, the ability of CFTR to specifically facilitate PAT-1 exchange will be investigated. For these studies, the DRA (-) intestine will be used to isolate PAT-1, which will allow us to compare the rates of  $\text{anion}_{\text{in}}/\text{HCO}_3^-$   $_{\text{out}}$  exchange between CFTR-permeant anions ( $\text{Cl}^-$ ,  $\text{NO}_3^-$ ) and the CFTR-impermeant anion  $\text{SO}_4^{2-}$  in the luminal bath. Increased PAT-1 activity during  $\text{Cl}^-/\text{HCO}_3^-$  or  $\text{NO}_3^-/\text{HCO}_3^-$  exchange as compared to  $\text{SO}_4^{2-}/\text{HCO}_3^-$  exchange would support the hypothesis that CFTR specifically facilitates PAT-1 activity by providing a  $\text{Cl}^-$  leak pathway.

### **Identification of the Apical Membrane Anion Exchanger(s) Responsible for Basal Bicarbonate Secretion**

#### *Summary and Conclusions*

Loss of CFTR facilitation of basal  $\text{Cl}^-/\text{HCO}_3^-$  exchange by PAT-1 in the upper villous epithelium of the duodenum may represent only one component of reduced basal  $\text{HCO}_3^-$  secretion in the CF intestine. Recent pH stat studies of PAT-1 (-) murine duodenum estimate that PAT-1 contributes only 20% to basal  $\text{HCO}_3^-$  secretion in WT duodenum (Figure 5.4, left panel). Because our examination of basal anion exchange was restricted to the upper villus, it appears that the majority of duodenal  $\text{HCO}_3^-$  secretion under basal conditions comes from the lower villous and crypt epithelium where that activities of DRA or AE4 may provide a major contribution to basal  $\text{HCO}_3^-$  secretion. Therefore, a thorough examination of  $\text{Cl}^-/\text{HCO}_3^-$  exchange in the lower villus/crypt epithelium where CFTR is predominantly expressed is warranted in order to fully evaluate the contributions of AE4, DRA, and PAT-1 to transepithelial bicarbonate secretion.

### Transepithelial HCO<sub>3</sub><sup>-</sup> Secretion

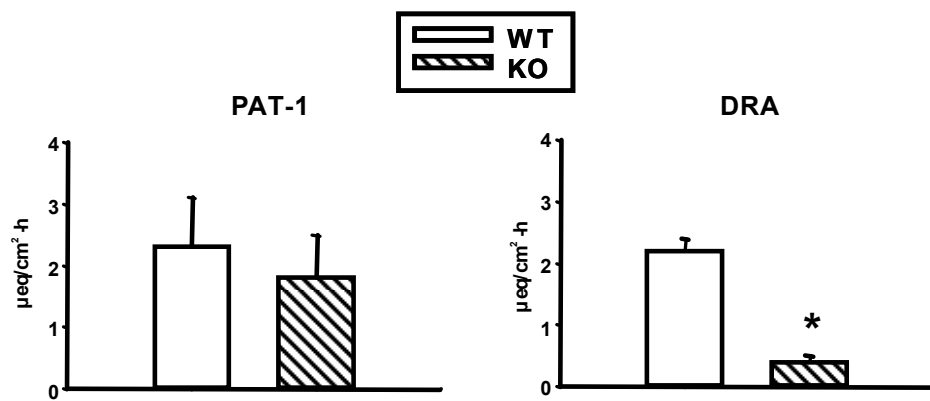


**Figure 5.4.** Transepithelial HCO<sub>3</sub><sup>-</sup> secretion across duodena from PAT-1 (-) (left panel, n = 3) and DRA (-) (right panel, n = 8 - 10) and WT mice as measured by pH stat.

\*Significantly different from WT.



### *Supplemental Studies*

Initial studies indicate that DRA is responsible for ~80% of basal  $\text{HCO}_3^-$  secretion across the murine duodenum (Figure 5.4, right panel). Further, *in situ* hybridization studies of rabbit duodenum have shown greatest mRNA expression of DRA in the lower villous and crypt epithelia (48). These findings indicate significant DRA activity in the duodenum; therefore, we investigated the possibility that DRA function is primarily localized to the lower villus (near crypt openings) by comparing rates of apical membrane  $\text{Cl}^-/\text{HCO}_3^-$  exchange activity in the duodena of mice with gene-targeted deletions of DRA, PAT-1 and AE4. Examination of  $\text{Cl}^-/\text{HCO}_3^-$  exchange in the lower duodenal villus revealed no significant difference in the rates of  $\text{HCO}_3^-$  influx and efflux during  $\text{Cl}^-$  removal and replacement as compared to the upper villus (Figure 5.5). Comparison of the rates of apical membrane  $\text{Cl}^-/\text{HCO}_3^-$  exchange activity in the lower duodenal villus of mice with gene-targeted deletions of DRA, PAT-1 and AE4 reveal that PAT-1 and AE4 do not significantly contribute to  $\text{Cl}^-/\text{HCO}_3^-$  exchange in lower villous epithelium (Figure 5.6). In distinct contrast to the upper villus,  $\text{Cl}^-/\text{HCO}_3^-$  exchange activity is eliminated in the lower villous epithelium of the DRA (-) intestine (Figure 5.7). In addition, it is interesting to note that epithelial cells from the DRA (-) lower villus paradoxically *acidify* upon luminal  $\text{Cl}^-$  removal and *alkalize* after  $\text{Cl}^-$  replacement (Figure 5.7 and 5.8). It is known that CFTR conducts  $\text{HCO}_3^-$  in addition to  $\text{Cl}^-$ , but its permeability is significantly less (1:4) (80;105). In addition, recent research has shown that recombinant CFTR  $\text{HCO}_3^-$  permeability may be regulated by the  $\text{Cl}^-$  content of the extracellular medium (89). Therefore, to investigate whether this observation is due to changes in the  $\text{HCO}_3^-$  permeability of CFTR during removal of luminal  $\text{Cl}^-$ ,  $\text{Cl}^-/\text{HCO}_3^-$

## Cl/HCO<sub>3</sub> Exchange

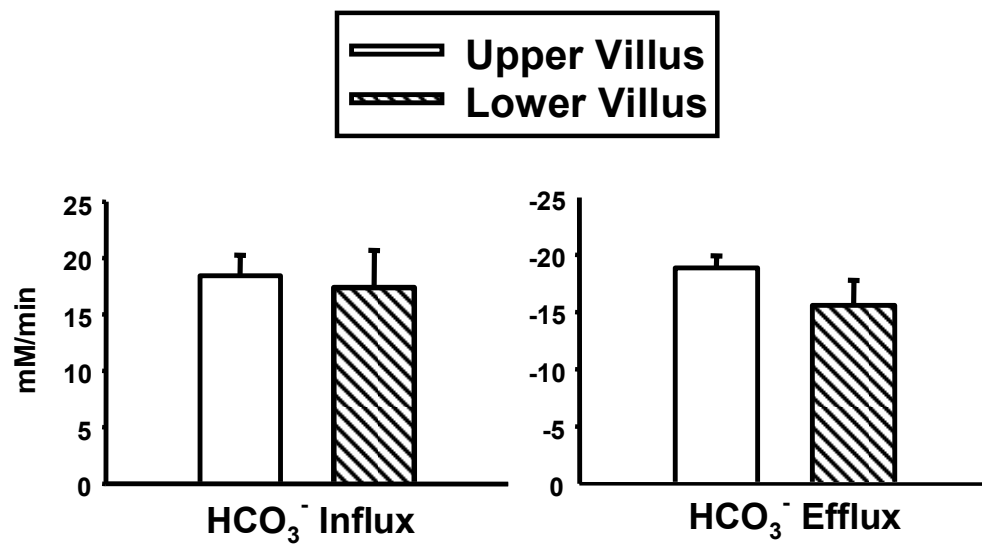


**Figure 5.5.** Rates of HCO<sub>3</sub><sup>-</sup> influx and efflux in upper and lower villous epithelia of WT duodenum (n = 5 - 9).

## Cl<sup>-</sup>/HCO<sub>3</sub><sup>-</sup> Exchange

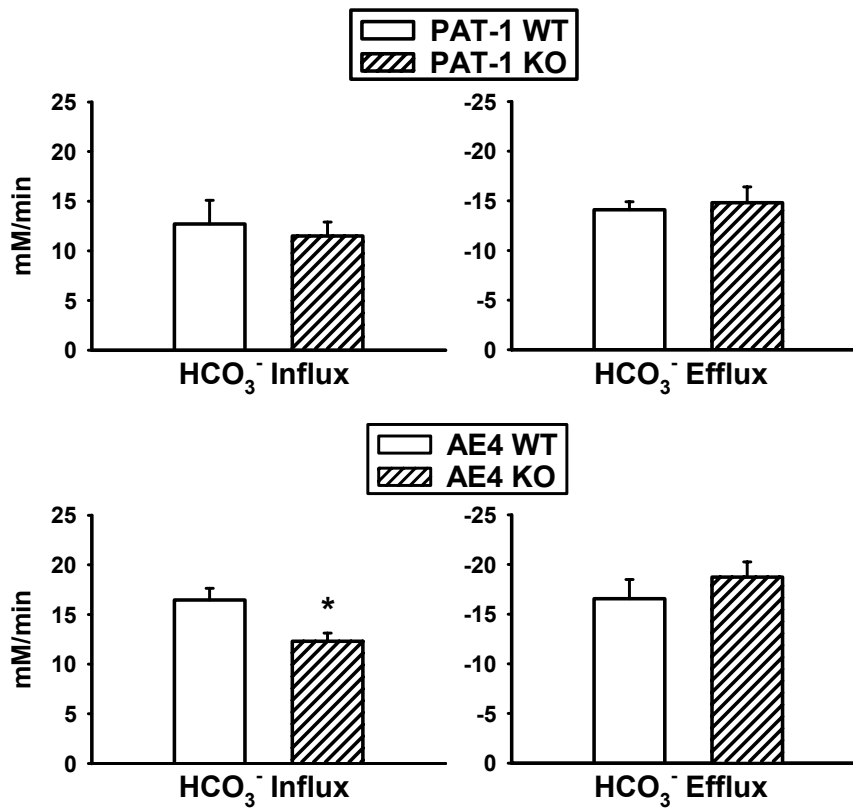


**Figure 5.6.** HCO<sub>3</sub><sup>-</sup> influx and efflux of PAT-1 (-) and WT (upper panel, n = 5) and AE4 (-) and WT (lower panel, n = 3 - 4) lower villous epithelium. In contrast to upper villous epithelium, loss of PAT-1 has no effect on the rate of Cl<sup>-</sup>/HCO<sub>3</sub><sup>-</sup> exchange, while loss of AE4 results in a small (~25%) reduction in HCO<sub>3</sub><sup>-</sup> influx but no change in HCO<sub>3</sub><sup>-</sup> efflux. \*Significantly different than WT.

## Cl<sup>-</sup>/HCO<sub>3</sub><sup>-</sup> Exchange

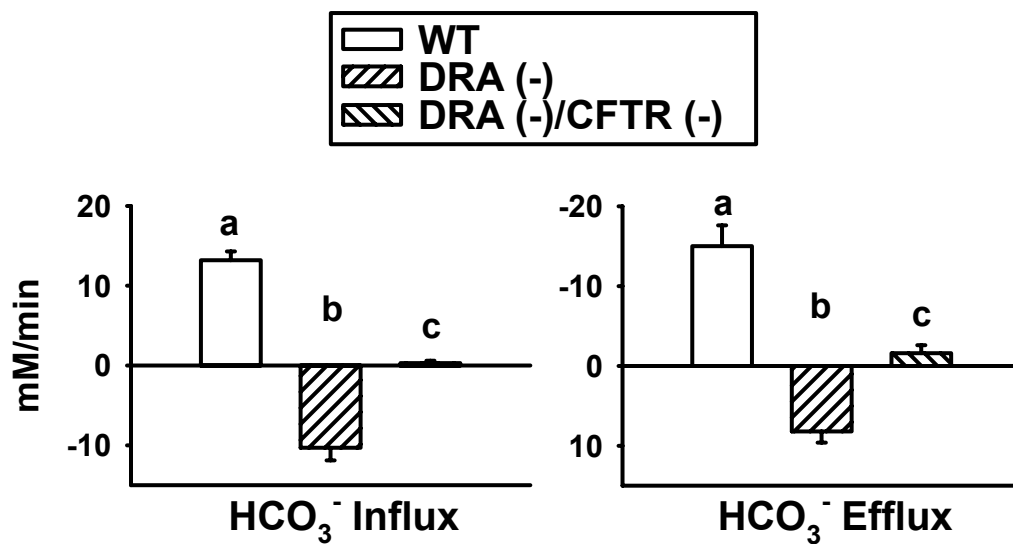


**Figure 5.7.** Rates of Cl<sup>-</sup>/HCO<sub>3</sub><sup>-</sup> exchange in WT, DRA (-), and DRA (-)/CFTR (-) duodenal lower villous epithelia (n = 3). Intracellular acidification during Cl<sup>-</sup> removal in the DRA (-) was eliminated in the DRA (-)/CFTR (-). <sup>a,b,c</sup>Means with the same letter are not statistically different.

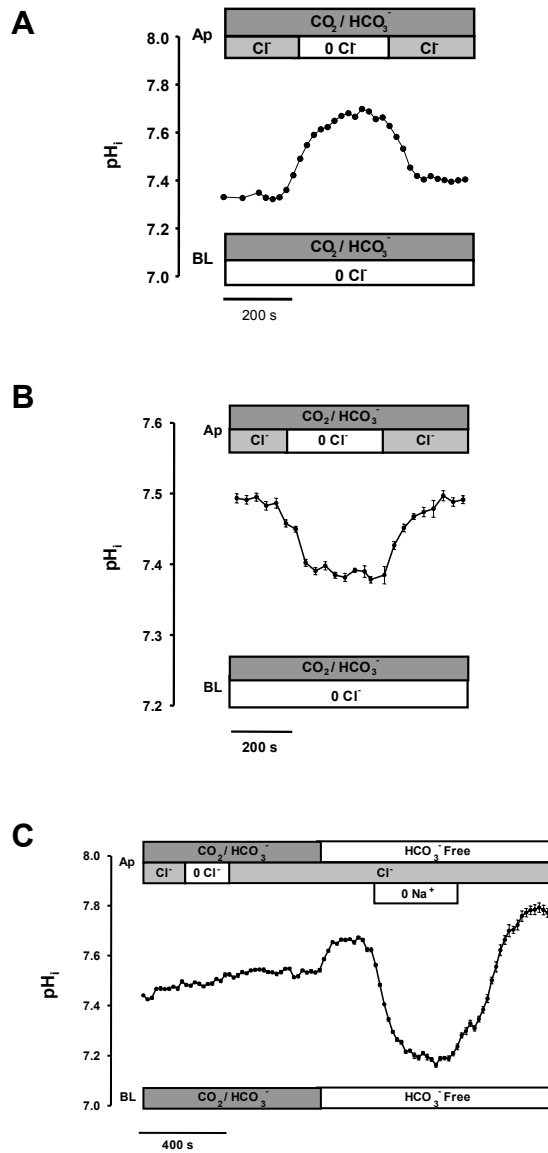


**Figure 5.8.** Changes in pH<sub>i</sub> during luminal Cl<sup>-</sup> removal and replacement in **A.** WT, **B.** DRA (-), and **C.** DRA (-)/CFTR (-) lower villous epithelia. The pH<sub>i</sub> was unchanged in DRA (-)/CFTR (-) epithelium during Cl<sup>-</sup> removal and replacement. To ensure viability of these preparations, apical Na<sup>+</sup>/H<sup>+</sup> activity was assessed by Na<sup>+</sup> removal and replacement in the absence of bath HCO<sub>3</sub><sup>-</sup>.

exchange activity was examined further in the lower villus by utilizing DRA (-)/CFTR (-) mice. Preliminary studies revealed that this paradoxical acidification is eliminated in the DRA (-)/CFTR (-) duodenum (Figure 5.7 and 5.8). Taken together, these findings indicate that 1) basal  $\text{HCO}_3^-$  secretion is primarily mediated by DRA (~80%) and PAT-1 (~20%)  $\text{Cl}^-/\text{HCO}_3^-$  exchange activity, 2) unlike the upper villous epithelium where PAT-1 activity predominates, DRA is the dominant  $\text{Cl}^-/\text{HCO}_3^-$  exchanger in the lower villous epithelium, 3) DRA exists in a complex interaction with CFTR in the lower villous epithelium, and 4) in the absence of DRA activity, removal of luminal  $\text{Cl}^-$  induces a paradoxical intracellular acidification by a process dependent on CFTR supporting the hypothesis that the  $\text{HCO}_3^-$  permeability of CFTR is increased in the absence of luminal  $\text{Cl}^-$ . Additional studies are needed to evaluate the nature of the interaction that exists between DRA and CFTR. Initial studies reveal that, similar to the upper villus, the lower villus of the CF mouse duodenum has an increased  $\text{pH}_i$  and significantly reduced rates of  $\text{Cl}^-/\text{HCO}_3^-$  exchange activity (Figure 5.9). Therefore, studies are planned to evaluate whether the interaction of DRA with CFTR in the lower villus is due to a facilitation of  $\text{Cl}^-/\text{HCO}_3^-$  exchange by CFTR or due to direct intermolecular interactions between the two proteins. Reagents blocking CFTR channel activity will test whether the activity of CFTR is required to support DRA  $\text{Cl}^-/\text{HCO}_3^-$  exchange. On the other hand, if the above studies indicate that the membrane presence of CFTR is required but not its  $\text{Cl}^-$  channel activity, then these results suggest an intermolecular interaction between CFTR and DRA.

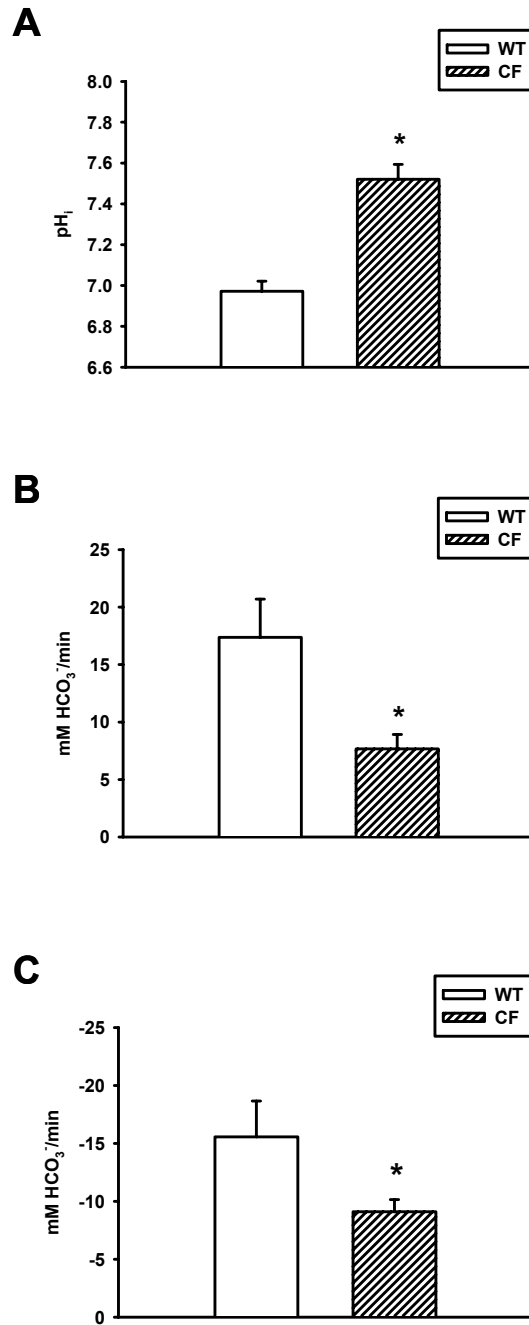


**Figure 5.9.** Summary of **A.** baseline  $pH_i$ , **B.**  $HCO_3^-$  influx, and **C.**  $HCO_3^-$  efflux rates in lower villous epithelial cells from WT (n = 5) and CF (n = 4) mice. \*Significantly different from WT.

## The Role of PAT-1 in Intestinal Peptide Absorption

### *Summary and Conclusions*

The upper villous epithelium of the duodenum is exposed to acid challenge not only from gastric effluent, but also from  $H^+$  influx via the  $H^+$  di-/tripeptide cotransporter PEPT1 (expressed predominantly in the upper villous epithelium) (28). Studies in the PAT-1 null duodenum indicate that PAT-1 is responsible for approximately 80% of villous apical  $Cl^-/HCO_3^-$  exchange activity (Chapter 3). In addition,  $pH_i$  measurements under conditions that isolate apical membrane acid-base transport in the PAT-1 (-) villous epithelium in the presence of  $CO_2/HCO_3^-$  have revealed a significantly reduced baseline  $pH_i$  as compared to WT suggesting that PAT-1 protects against epithelial cell acidification, ostensibly by running in  $Cl^-_{out}/HCO_3^-_{in}$  mode that is  $HCO_3^-$ -dependent (Chapter 3). Studies presented in Chapter 4 have indicated that PAT-1 is involved in  $pH_i$  regulation during dipeptide absorption. The activity of PAT-1 as a base importer ( $Cl^-_{out}/HCO_3^-_{in}$  exchange) would allow for transmembrane movement of membrane-impermeant  $HCO_3^-$  needed to combine with protons absorbed during transport of peptides through PEPT1 for the maintenance of  $pH_i$ . An initial study demonstrated an enhanced rate of  $Cl^-_{out}/HCO_3^-_{in}$  exchange via PAT-1 in the presence of the dipeptide Gly-Sar, providing support to this hypothesis (Chapter 4). Further studies revealed the involvement of carbonic anhydrase, specifically CAII, in peptide absorption and a reduction in the rate of  $Cl^-_{out}/HCO_3^-_{in}$  exchange in the presence of Gly-Sar to the level of the control during inhibition of carbonic anhydrase activity, endorsing the existence of a functional coupling between PAT-1 and carbonic anhydrase during PEPT1 transport. Taken together, these data indicate the existence of a  $HCO_3^-$  metabolon whereby PAT-1



and CAII mediate  $\text{HCO}_3^-$  uptake during  $\text{H}^+$ /peptide transport to minimize intracellular acidification and sustain peptide absorption.

### *Future Studies*

The preceding section and Chapter 4 have demonstrated the involvement of PAT-1 and CAII in peptide absorption. These studies have laid the groundwork for additional studies to expand our knowledge of the interaction between PAT-1 and CAII and the mode of activity of PAT-1 during peptide absorption.

To conclusively demonstrate whether PAT-1 functions in  $\text{Cl}^-_{\text{out}}/\text{HCO}_3^-_{\text{in}}$  exchange during dipeptide absorption, measurements of intracellular  $\text{Cl}^-$   $[\text{Cl}^-]_i$  during Gly-Sar absorption are planned with the use of the fluorescent dye 6-methoxy-*N*-ethyl-1,2-dihydroquinoline (diH-MEQ). A decrease in  $[\text{Cl}^-]_i$  during Gly-Sar exposure would provide definitive evidence that PAT-1 is acting as a  $\text{HCO}_3^-$  importer during peptide absorption via PEPT1. Currently, there is little data regarding use of  $[\text{Cl}^-]_i$  indicators in intact tissue. Therefore, extensive development of this technique will be required prior to experimentation to determine 1) the appropriate loading dose, 2) assessment of background fluorescence, photobleaching, and dye leakage, and 3) a calibration protocol for converting fluorescence to  $[\text{Cl}^-]_i$ . In addition, interpretation of intracellular  $\text{Cl}^-$  measurements during peptide absorption may be complicated by basolateral  $\text{Cl}^-$  uptake through the  $\text{Na}^+\text{K}^+2\text{Cl}^-$  cotransporter (NKCC1) and the  $\text{Cl}^-/\text{HCO}_3^-$  exchanger AE2. Therefore, it may be necessary to perform these studies under conditions that inhibit basolateral  $\text{Cl}^-$  uptake (i.e., bumetanide-treated or basolateral  $\text{Cl}^-$  free).

Initial studies in murine duodenal villous epithelia have demonstrated the presence of a functional interaction between PAT-1 and carbonic anhydrase (Chapter 4).

However additional studies are planned to determine whether a direct interaction between PAT-1 and CAII exists as well. Previous investigations in heterologous cell systems have co-localized PAT-1 and CAII to the plasma membrane, and a binding motif for CAII has been identified on the carboxy-terminus of the PAT-1 (4). In addition, phosphorylation by protein kinase C (PKC) of the adjacent residue on PAT-1 has been shown to decrease the interaction between PAT-1 and CAII (4). The ability of PAT-1 to directly bind with CAII will be evaluated in murine isolated duodenal villi by means of co-immunoprecipitation studies. In these studies, PAT-1 and CAII will be separately immunoprecipitated from the isolated villi and probed with CAII and PAT-1 antibodies, respectively, to determine whether a direct intermolecular association exists between PAT-1 and CAII.

Although our findings demonstrate the importance of PAT-1 in  $\text{pH}_i$  regulation during PEPT1 absorption, initial studies have demonstrated that inhibition of apical membrane  $\text{Cl}^-/\text{HCO}_3^-$  exchange with NFA results in a ~70% reduction in Gly-Sar uptake as indexed by  $I_{sc}$  current, which was surprising as NFA only inhibits ~60% of  $\text{Cl}^-/\text{HCO}_3^-$  exchange (Chapter 2 and 4). Therefore, additional studies are planned to directly examine Gly-Sar absorption by  $I_{sc}$  in PAT-1 (-) duodena as compared to WT. PEPT1 expression studies in isolated duodenal villi also are necessary to determine whether a decreased level of PEPT1 expression as measured by quantitative RT-PCR in isolated murine duodenal villi may be contributing to the impaired  $\text{pH}_i$  regulation in the PAT-1 (-) epithelium during peptide absorption. Further, the involvement of DRA in nutrient absorption has not been investigated. DRA demonstrates a significant contribution (30-40%) to apical  $\text{Cl}^-/\text{HCO}_3^-$  exchange in the upper duodenal villus and ~100% in the lower

duodenal villus of the mouse. Therefore, studies of DRA (-) mice assessing  $I_{sc}$  and  $pH_i$  regulation are warranted to investigate the contribution of DRA to PEPT1-mediated absorption.

## APPENDIX 1

### pH<sub>i</sub> MEASUREMENT IN INTACT INTESTINAL TISSUE

#### Setup of Perfusion Lines for Microfluorimetry Studies

1. To set up the perfusion lines, you need:

Six male 1/16 in. barbed luers

Two female 1/16 in. barbed luers

Two glass capillary tubes (15 cm in length; O.D. 1.5 mm; I.D. 1.17 mm)

Two pieces of silastic tubing (20 cm in length; I.D. 0.078 in.; O.D. 0.125 in.)

Two pieces of yellow/blue collared PVC tubing (18 in. in length; O.D. 1.52 mm)

Two blunt tip needles with luer hubs (20 gauge; ½ in. in length)

Two blunt tip needles with luer hubs (18 gauge; ½ in. in length)

Two pieces of PE160 tubing (95 cm in length; O.D. 1.57 mm; I.D. 1.14)

Four pieces of Tygon tubing (4 cm in length; O.D. 1/8 in.; I.D. 1/16 in.)

Two 3 mL syringes

2. Attach a glass capillary tube to a piece of silastic tubing. The capillary tube is placed directly in the warmed Ringer's solution to draw up the solution during the experimental protocol.

3. Attach a piece of the silastic tubing to a male barbed luer.

4. Attach the male barbed luer to a female barbed luer which is attached to a piece of yellow/blue collared PVC tubing in the end closest to the blue collar. Fit the PVC tubing to a Dynamax peristaltic pump by releasing the compression arm. This is accomplished by pressing the beveled trigger key toward the rollers. Then insert the blue collar into one of the left grooves on the collar bracket. Thread the tubing around the rollers so that the yellow collar fits into the groove on the opposite collar bracket. Then close the compression arm on the tubing and close the locking arm. Attach a male barbed luer to

the end of the PVC tubing closest to the yellow collar. The peristaltic pump should be set to a flow rate of 24.2 rpm.

5. Attach the male barbed luer from the PVC tubing to a 20 gauge blunt tip needle.

Remove the plunger from a 3 mL syringe. Remove the rubber stopper from the end of the plunger. Insert the blunt tip needle through the center of the rubber stopper. Position the rubber stopper into the barrel of the syringe so that it forms a seal.

6. Insert the tip of an 18 gauge blunt tip needle into a piece of PE160 tubing and attach this to the syringe tip. Introduce the PE160 tubing through the opening on the side of the microscope cage.

7. Attach a piece of Tygon tubing to the distal end of the in-line heater and insert the end of the PE160 tubing into the end of the Tygon tubing.

8. Attach a piece of Tygon tubing to the proximal end of the inline heater and attach a male barbed luer into the end. During the experiment, the male barbed luer will be attached to the horizontal Ussing chamber.

9. Repeat steps 2-8 to set up both the apical and basolateral perfusion lines.

10. The basolateral perfusion line will be the lower perfusion line in the peristaltic pump, and the apical perfusion line will be the upper line. PE160 tubing of the basolateral line should be labeled with green tape and should be run through the in-line heater that is labeled with green tape. The basolateral line will be attached into the bottom perfusion inlet of the Ussing chamber and the apical line will be attached to the top perfusion inlet of the Ussing chamber.

11. The perfusion lines should be changed once a week (or if switching drugs).

## Setting up for a BCECF Microfluorimetry Study

1. Warm Ringers solutions in a 40 °C water bath for at least 1 hour. In general, 250 ml of basolateral and 100 mL of apical solution are required per experiment. Gas  $\text{HCO}_3^-$ -buffered Ringer's (i.e., KBR and IBR) with 95%  $\text{O}_2$  /5%  $\text{CO}_2$ ; and  $\text{HCO}_3^-$ -free Ringers (i.e., TBR) with 100%  $\text{O}_2$  while warming.
2. Turn on the space heater underneath the microscope station and the warmer within the microscope cage, which should be set to 35 °C. Turn on solution in-line heater temperature probes to monitor the air temperature in the microscope cage. Close the sliding door on the microscope cage and allow the station to be heated for ~1 hour.
3. While everything is warming, add TTX (0.1  $\mu\text{M}$ ) and INDO (1.0  $\mu\text{M}$ ) and any other necessary drugs to the basolateral solution(s). Add INDO (1.0  $\mu\text{M}$ ) and any other necessary drugs to the apical solution(s).
4. Turn on the vacuum for the perfusion chamber. Check the beaker where fluid is collected to determine whether the beaker needs to be emptied prior to the experiment.
5. Turn on the xenon lamp. Turn on the silver filter wheel control box. Turn on the computer. Let the computer boot up completely. Turn on the camera.
6. Open axon imaging program. Go to Hardware--illumination settings. A window titled Ludl Filter Wheel should open. Turn the cube housing until the green tape is in front, which places the 535 nm emission filter into the field of view. Open the shutter (O: icon in the toolbar on the left of the screen). The Ludl Filter wheel window has a graphical representation of a filter wheel with the places for the filters numbered. The 440 nm wavelength is royal purple and should be positioned in optical port 1, and the 495 nm wavelength is teal and should be positioned in optical port 2. Check to make sure the

filters are in the appropriate location and position the filter wheel so that optical port 2 (495 nm filter) is placed in the field of view. Close the shutter and the Ludl Filter Wheel window.

7. Click on the third icon on the toolbar on the left side of the screen to set the computer to save all images (changes icon from red to green).

8. Change the file name on the acquisition. Go to Settings--Acquisition--the tab labeled General--and click Change. Name the file based upon the mouse's individual identification code and note the file name on the experimental record.

9. Put a 12x18 mm piece of bottom mesh (136 micron nylon mesh) on the chamber and secure over the pins. Replace the tubing on the bottom perfusion inlet (27 mm of PE160 tubing). If the tubing on the top perfusion inlet needs to be changed, use 17 mm of PE160 tubing. Both the top and bottom perfusion inlets use 18 gauge blunt tip needles. Cut a 20x60 mm piece of upper mesh (flexible nylon mesh with 1 mm openings).

10. Prime basolateral perfusion line. This is accomplished by placing the glass capillary tube of basolateral perfusion line into basolateral solution and turning on peristaltic pump to allow clockwise flow of fluid. Disconnect the syringe of the basolateral perfusion line from the PE160 tubing so that the syringe can be filled with ~1.5 mL of reserve fluid. Reattach the PE160 tubing and partially fill this tubing with fluid. Stop the peristaltic pump.

### **Starting a BCECF Microfluorimetry Experiment**

1. Set up an ice-cooled dissection bath using KBR with 1  $\mu$ M indomethacin (10  $\mu$ L from the concentrated stock in 100 ml of KBR). Sacrifice mouse. Remove duodenum via an

abdominal incision. Under the dissection microscope, open along the mesenteric border. Incubate in the dissection bath for 10 minutes.

2. While using a dissection microscope, pin tissue flat with the mucosal side down on a Sylgard-filled Petri dish. Score the tissue along the proximal end of the tissue with a #11 scalpel blade. Remove the serosa and muscularis externa along the longitudinal axis by blunt dissection using fine forceps.

3. For upper villous  $\text{pH}_i$  measurements, mount muscle-stripped intestinal preparations mucosal side up on a horizontal Ussing chamber with the pyloric end nearest the perfusion inlet (Figure A1.1). Put vacuum grease around the periphery of the chamber bottom so that it encircles the tissue. This can be accomplished by using a 10 mL syringe that has been filled with vacuum grease. Place top mesh over tissue. For lower villus measurements, a short piece of glass capillary tubing (1.2 mm O.D) is placed longitudinally beneath the mucosa on the supporting mesh. The mucosa is held against the tubing by two longitudinally oriented silk threads, thereby throwing the mucosa into relief. The overlying loose mesh is then sandwiched over the preparation to immobilize the tips of the villi (Figure A1.2).

4. Place top of chamber on, pull slightly on the upper mesh to trap the tips of a small percentage (< 1%) of villi under strands of the mesh (for upper villus preparations), and tighten flathead screws (1 mm in length) slowly.

5. Place chamber on the stage of the fluorescent microscope. Attach perfusion lines to perfusion inlets of chamber with the apical perfusion line attached to the top line of the chamber and the basolateral perfusion line attached to the bottom line of the chamber.



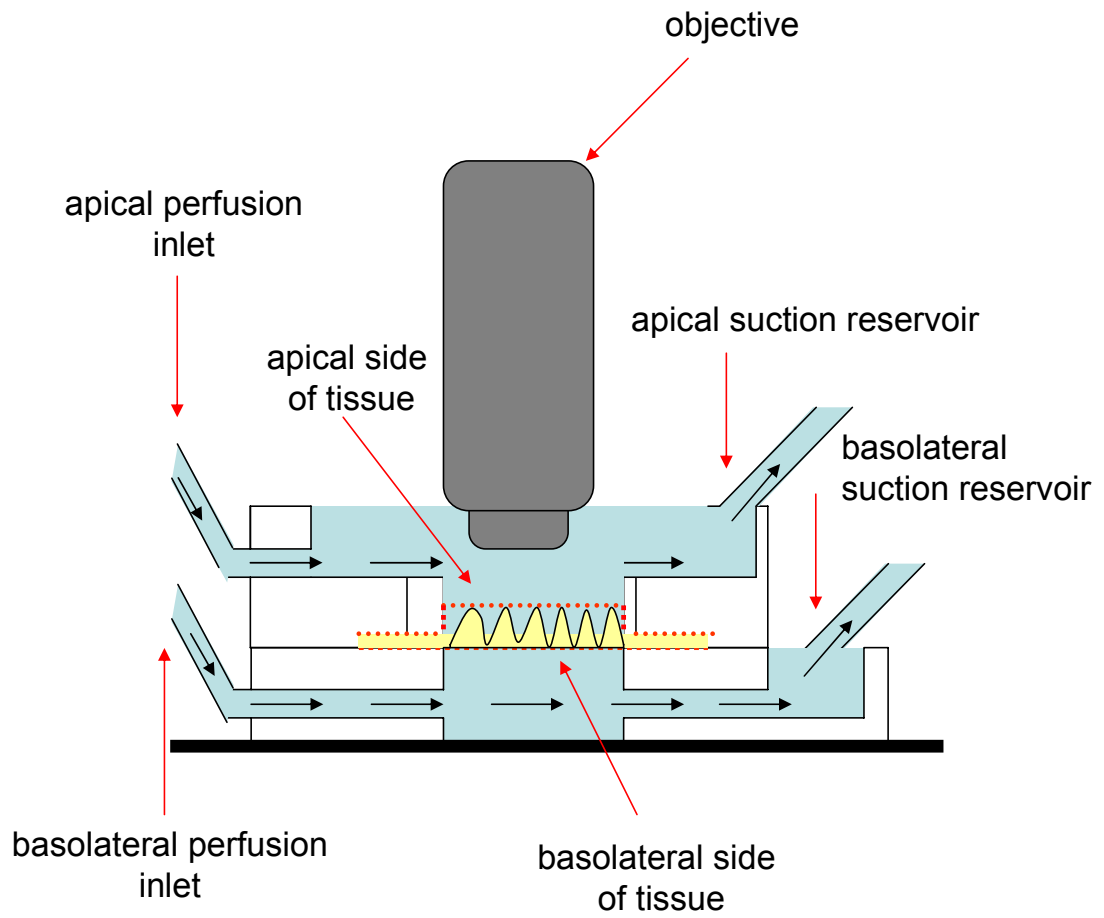


**Figure A1.1.** Schematic of horizontal Ussing chamber.

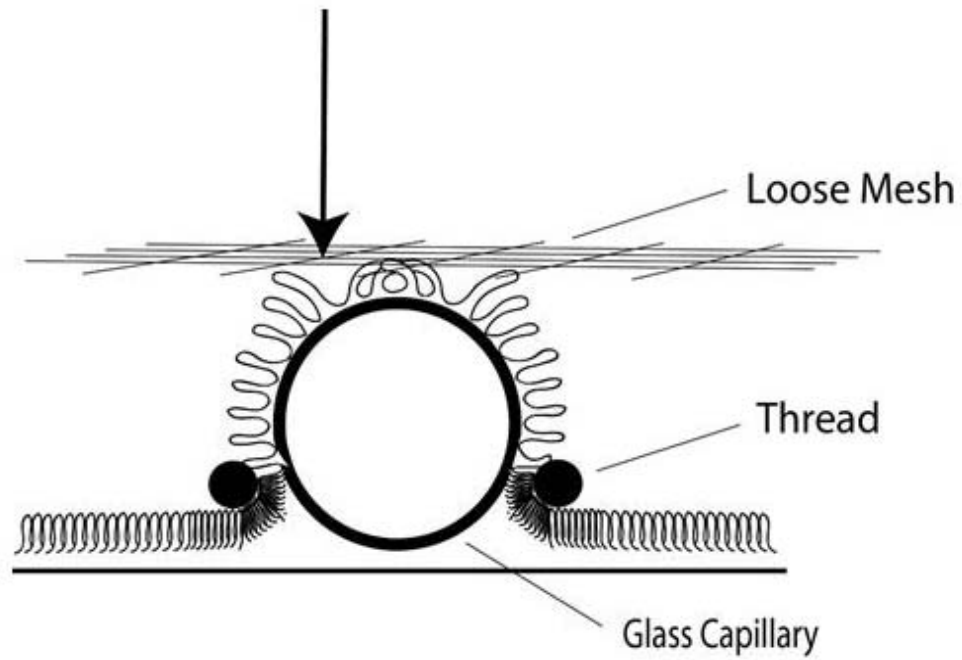


**Figure A1.2.** Schematic of duodenal preparation to visualize lower villous epithelium. A 2 cm length of 1.2 mm diameter glass capillary was placed on the serosal side of the mucosa which was secured to the capillary by two parallel threads 1 mm apart.

Attach chamber suction lines (16 gauge stainless steel suction tubes attached to 6 cm of silastic tubing that are fitted with 1/16 in. female barbed luers) to yellow vacuum tubing. Position the basolateral suction line in the basolateral suction reservoir of chamber (see Figure A1.1 and A1.3).

6. Start peristaltic pump. Because only the basolateral perfusion line is primed it will only perfuse this surface. Check to make sure there are no air bubbles in the basolateral opening of the chamber. If there are bubbles present, tilt the chamber at a 45° angle to the stage and strike it against the stage to force the bubbles from the chamber opening.

7. Place 1 mL of DL-dithiothreitol (DTT) solution (100 µM final concentration: 5 µl of a 20 mM stock is added to 1 mL of apical solution) on the apical surface of the tissue for 5 minutes to remove overlying mucus.

8. After the 5 minute DTT incubation, remove the DTT solution from the top of the tissue by vacuum.

9. While the tissue is incubating with DTT, make up the BCECF-AM dye solution. Each 50 µg tube of dye is rehydrated in 10 µl of Methyl sulfoxide (anhydrous). Add 2 µl of this stock to 1 ml of apical solution (16 µM final concentration) and vortex thoroughly to mix. Add the dye solution to the top of the tissue and allow it to incubate for ~10 minutes.

9. During BCECF incubation, place the chamber under the 40X water immersion objective. Place the solution in-line heater probes into the chamber. Turn on the bottom in-line heater. Place the cube housing in position "o" (open circle) so that there are no filters in the field of view. Pull out the filter sliders, turn on the microscope light source to an intensity of ~4.5, and push the camera stop in (See Figure A1.4).

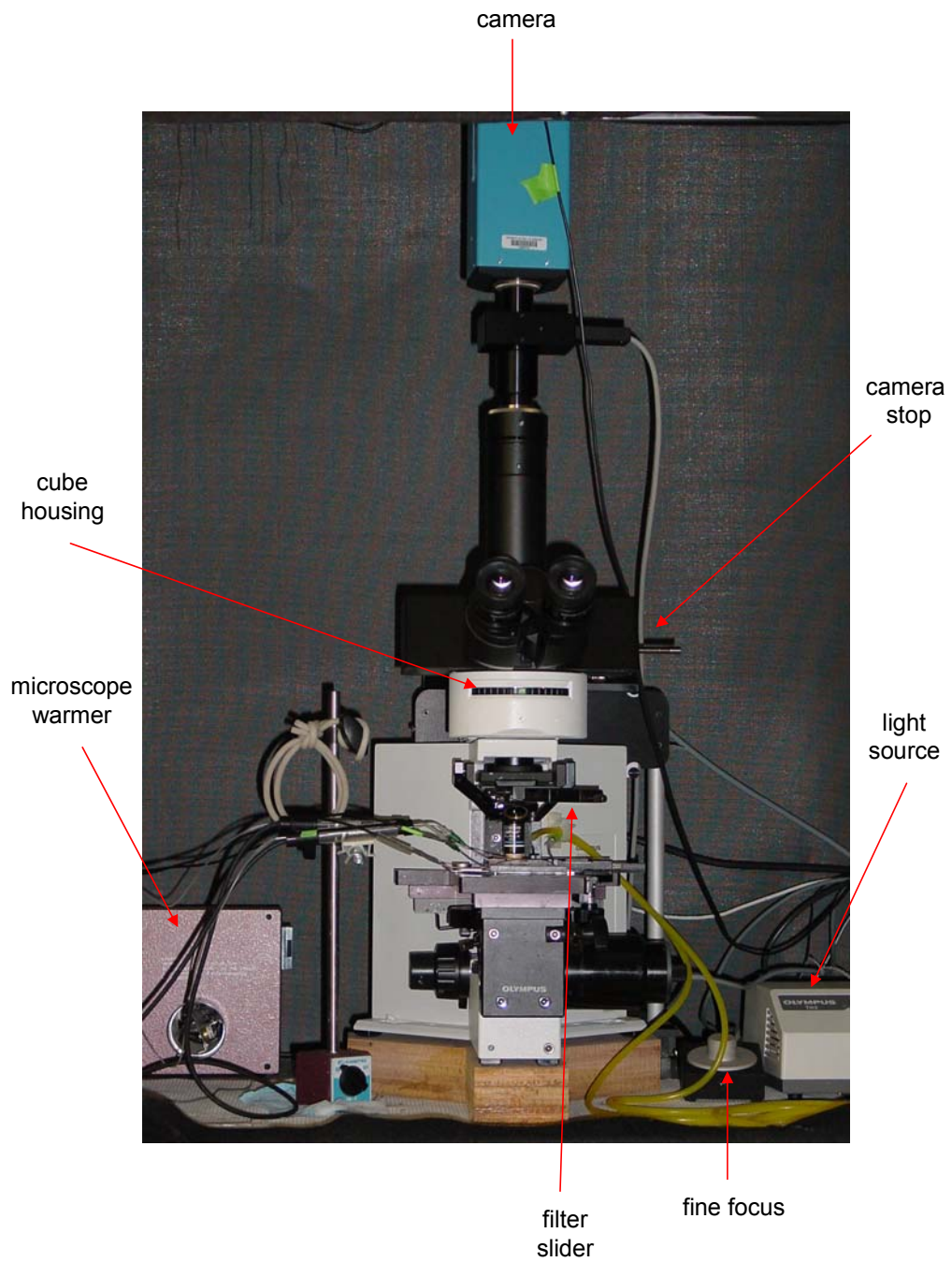


**Figure A1.3.** Experimental setup for measurement of  $pH_i$  in epithelial cells of intact duodenal villi.

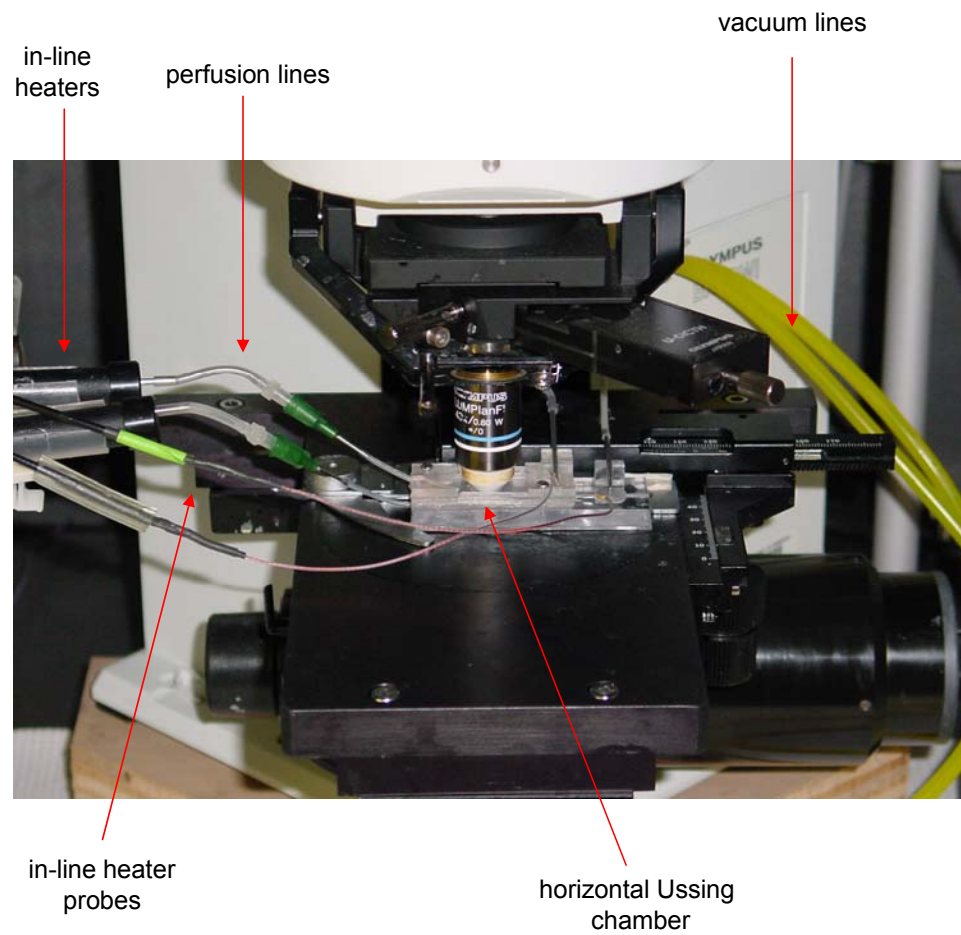


**Figure A1.4.** High power photograph of a setup for measurement of  $pH_i$  in epithelial cells of intact duodenal villi.

## **Image Acquisition and Analysis**

1. For  $\text{pH}_i$  measurements of the upper duodenal villus, focus on an area in the mid-region of a single, immobilized villus (~ 1 mm from the villous tip) (see Figure A1.5). For  $\text{pH}_i$  measurements of the lower villus, the criterion for lower villous epithelium is visualization of crypt openings within the same microscopic field.
2. Pull out the camera stop. Click the camera icon once on the axon imaging workbench. This should take a pseudo-colored picture (or a black and white depending on how the palette editor is set) of the villus. If the picture is all white, there is too much light. If the picture is all black (or purple to blue), there is too little light or the camera stop is not out. Adjust light or camera stop if necessary and retake the picture. When a satisfactory picture is acquired, select approximately 10 epithelial cells for ratiometric analysis using a 40X water immersion objective. Cover the bottom light with a black plastic strip. Turn the cube housing to the 535 nm emission filter (labeled with green on the cube), pull out the filter sliders if they are not already out and make sure the camera stop is out. Close the microscope cage to keep the tissue warmed. Let the BCECF-AM dye load for 10 minutes. The amount of loading should be checked every few minutes to make sure the tissue is loading appropriately. To assess dye loading, take fluorescent images for  $\lambda_1$  (495 nm excitation). Appropriate dye loading should be between 1000-2500 pixel values (which will appear on the screen as a color intensity ranging from light blue to green to yellow to orange). If the tissue does not load within 10 minutes, a second dose of dye solution should be applied to the apical surface of the tissue.
3. When the tissue is finished loading, place the apical perfusion line in the appropriate solution and prime the line. Place the top vacuum line in the apical vacuum reservoir.

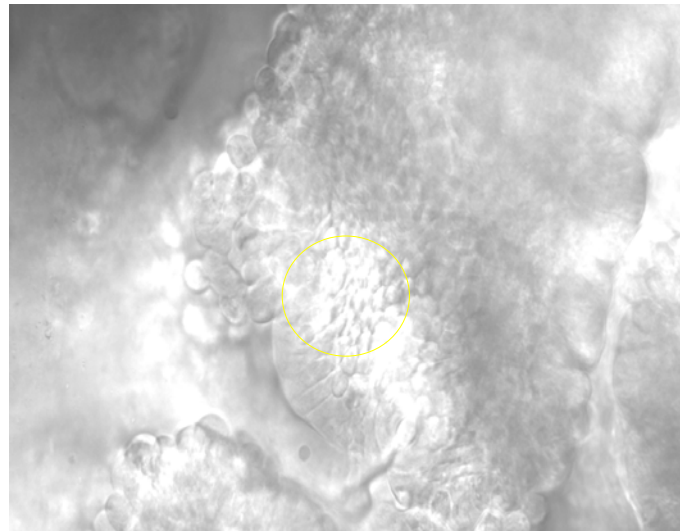


**Figure A1.5.** Locale in the mid-region of a single villus for the measurement of epithelial cell  $\text{pH}_i$ .

Turn on the top solution in-line heater. Check to make sure top vacuum has started. Check to make sure the apical surface of the chamber is being perfused and that the fluid level is not fluctuating during suction. Also, make sure the villus is still in focus, reposition if necessary, and reassess dye loading. Close the microscope cage.

4. Start the acquisition. Take 3 acquisitions in rapid succession and then place on a sample interval of 20 seconds with the use of the acquisition control pad. Fluorescence intensity (FI) of the selected area is recorded at the 535 nm emission with a Sensi-Cam digital camera and processed with Axon Imaging Workbench. Changes in intracellular pH ( $\text{pH}_i$ ) are measured by the dual excitation wavelength technique (440- and 495-nm). The intensity of emitted fluorescence at 495 nm stimulation is pH dependent, whereas that at 440 nm is not. The ratio is determined by dividing the intensity at 495 nm by that at 440 nm after subtracting the average emission of the background intensity (BGI) at each wavelength. The BGI is defined as the intensity of autofluorescence which was previously measured in villous epithelia from 6 mice in the absence of BCECF. The fluorescence ratio is calculated by the equation:

$$\text{Fluorescence ratio} = (\text{FI}_{495} - \text{BGI}_{495}) / (\text{FI}_{440} - \text{BGI}_{440})$$

Following the experiment, the resulting ratios are converted to  $\text{pH}_i$  according to the calculated ex vivo calibration curve (see Section A2).

5. After a stable ratio is attained (will take at least 3 minutes), rates of acidification or alkalization are calculated from the initial slope of  $\text{pH}_i$  changes during the first 80-100s after the experimental manipulation as  $\Delta\text{pH}_i/\text{s}$ , and the average  $\text{pH}_i$  during this period is calculated.



6. Convert  $\Delta\text{pH}_i/\text{s}$  to  $\Delta\text{pH}_i/\text{min}$ . Calculate net flux rates by multiplying the total buffering ( $\beta_{\text{total}}$ ) of the system at the average  $\text{pH}_i$  during anion exchange in  $\Delta\text{pH}_i/\text{min}$  (See Section A3).

**Cleaning up following Experiment:**

1. Between experiments, throw away all mesh and clean the chamber to remove vacuum grease. Rinse well with water. Clean objective with a Q-tip and Sparkle glass cleaner. Drain the perfusion lines. Check the fluid levels on all solutions prior to starting the next experiment.
2. Clean the scope station thoroughly at the end of the day (or if switching drugs). Rinse bubblers with water.
3. Weekly (or if switching drugs), throw away perfusion lines and clean in-line heaters by flushing with 20 ml of ethanol (70%) and 20 ml of DI water.
4. Once a week, soak the chamber in Alconox for 1 hour (or overnight). Do not expose the chamber to ethanol.

## APPENDIX 2

### CALIBRATION OF FLUORESCENT RATIO IN TERMS OF $\text{pH}_i$

#### Setting up for a $\text{pH}_i$ Calibration Experiment

1. Prepare 500 mL of High  $\text{K}^+$  pH buffers in 0.3 pH unit increments from 6.3 to 8.6. These solutions should not be gassed as they are prepared. TES-buffered Ringers (TBR) and unbuffered Krebs Ringer with TES (UK-TES) should be prepared for the initial perfusion of the tissue prior to the calibration experiment.
2. Make up a 4 mM stock of nigericin diluted in ethanol. Nigericin, which is an  $\text{H}^+/\text{K}^+$  antiporter, will cause rapid equilibration of the external and internal pH through an exchange of internal  $\text{K}^+$  for external  $\text{H}^+$ .
3. Put pH solutions in a 40°C water bath to warm in 100 ml bottles. Do not gas the pH buffer solutions. Put the TBR and UK-TES into the water bath to warm also. Gas TBR with 100%  $\text{O}_2$ .
4. Turn on the dry bath and replace the pH meter calibration solutions.
5. Set up for a BCECF microfluorimetry study (see Section A.1).
6. While everything is warming, add 7.5  $\mu\text{l}$  of the 4 mM nigericin stock to each 100 ml of pH buffer (30  $\mu\text{M}$  final concentration). Do not reuse solutions containing nigericin. TBR should contain TTX (0.1  $\mu\text{M}$ ) INDO (1.0  $\mu\text{M}$ ), and glucose (10 mM). The UK-TES needs INDO.
7. Calibrate the pH meter at 37°C.
8. Sacrifice mouse, mount tissue being calibrated mucosal side up (see Section A.1).

9. Start the perfusion with TBR (serosal). Put 1 mL of UK-TES on the mucosal side. Make up DTT in 1 ml of UK-TES (100  $\mu$ M final concentration). Remove the UK-TES from the top of the tissue by vacuum and replace with the DTT solution. Incubate the tissue for 5 minutes with DTT.
10. While the tissue is incubating with DTT, make up the BCECF-AM dye solution. Each 50  $\mu$ M tube of dye is rehydrated in 10  $\mu$ l of Methyl sulfoxide. Add 2  $\mu$ l of the BCECF-AM stock and 1  $\mu$ l of the 4 mM nigericin stock to 1 ml of the highest pH buffer.
11. After the 5 minute DTT incubation, apply the dye solution (note that nigericin will increase the efficiency of dye loading so the amount of loading should be checked after 5 minutes and every 2 minutes thereafter to make sure you don't overload your tissue).

#### **Calibration of 495/440 Ratio in Terms of pH<sub>i</sub>**

1. Place the chamber under the 40X water immersion objective. Place the solution in-line heater probes into the chamber. Turn on the bottom in-line heater. Place the cube housing in position "o" (open circle) so that there are no filters in the field of view. Pull out the filter sliders, turn on the microscope light source to an intensity of  $\sim$ 4.5, and push the camera stop in and follow the steps outlined in Section A1 under "Image Acquisition and Analysis."
2. When the tissue is finished loading, place both perfusion lines in the highest pH buffer solution. Start the top vacuum line. Turn on the solution in-line heaters. Put the pH electrode in the chamber in the top portion as close to the tissue as possible. Start the acquisition. Enter a comment indicating the pH the first buffer was titrated to. Write down the pH of the first buffer in the treatment column of the experiment sheet.

3. Allow the ratio to come to steady state while taking acquisitions every 60 seconds. When the 495/440 ratio reaches steady state, set the acquisition at 20 second intervals. enter a comment of "steady state," and take 5 readings. Record the pH of the solution in the chamber (from pH meter) in the solution pH column of the experiment sheet.
4. After 5 acquisitions transfer both perfusion lines to the next pH buffer according to the following protocols:

Protocol 1: pH 8.6 → pH 8.0 → pH 7.4 → pH 6.8 → pH 6.3

Protocol 2: pH 8.3 → pH 7.7 → pH 7.1 → pH 6.5

Enter a comment with the pH of the buffer. There should be a noticeable drop in the measured ratio since BCECF is essentially linearly related to pH between pH 6 and 8; however, at a pH above 8.0 there may be a minimal change in the measured ratio. Allow the 495/440 ratio to reach steady state. Set the acquisition at 20 second intervals enter a comment of "steady state" and take 5 readings. During this time, record the pH of the solution in the chamber (from the pH meter) in the solution pH column of the experiment sheet. Enter a comment indicating the pH the buffer was titrated to. Write down the pH of the buffer in the treatment column of the experiment sheet.

5. Repeat for each pH buffer (Figure A2.1).
6. Protocol 1 and 2 should both be repeated so that at least one set of data for each pH buffer are attained. The mean of the 495/440 ratio from the 10 selected areas over the steady state period for each pH buffer is defined as the ratio at the recorded steady state pH (measured by the pH meter). The calibration should result in a linear relationship between the pH and ratio (Figure A2.2) according to the following formula:

$$pH_i = (Fluor. ratio - y_o) / a$$

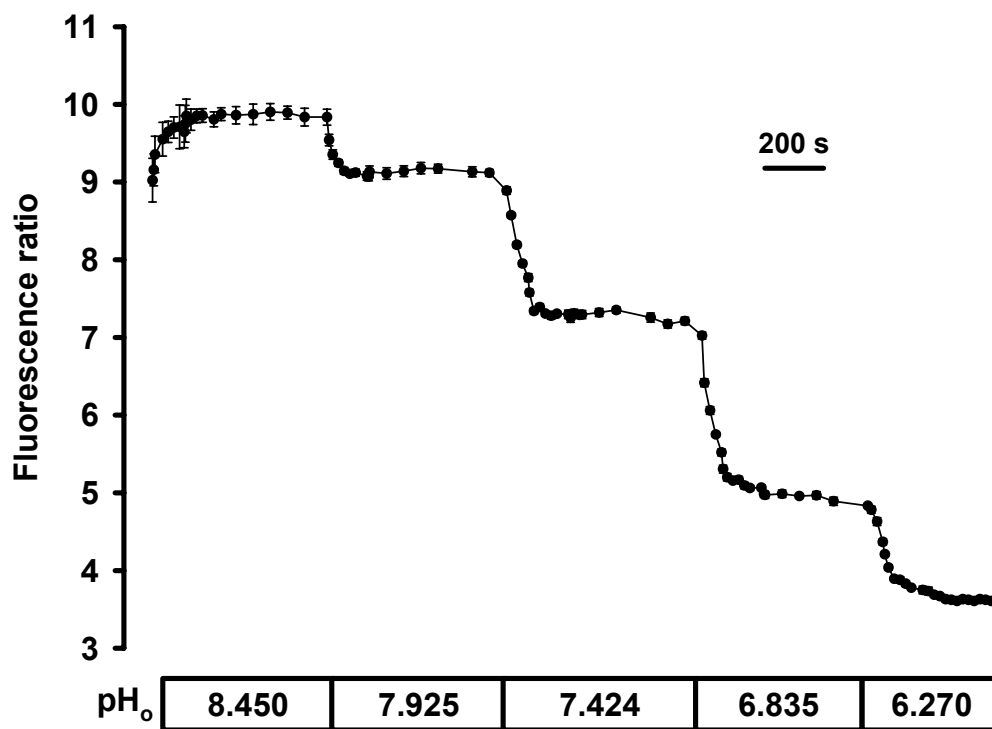


**Figure A2.1.** Time course of 495/440 fluorescence-excitation ratio during exposure to high K<sup>+</sup>-nigericin solutions of different pHs.

$$\text{pH}_i = (\text{Fluor ratio} + 19.87)/3.794$$

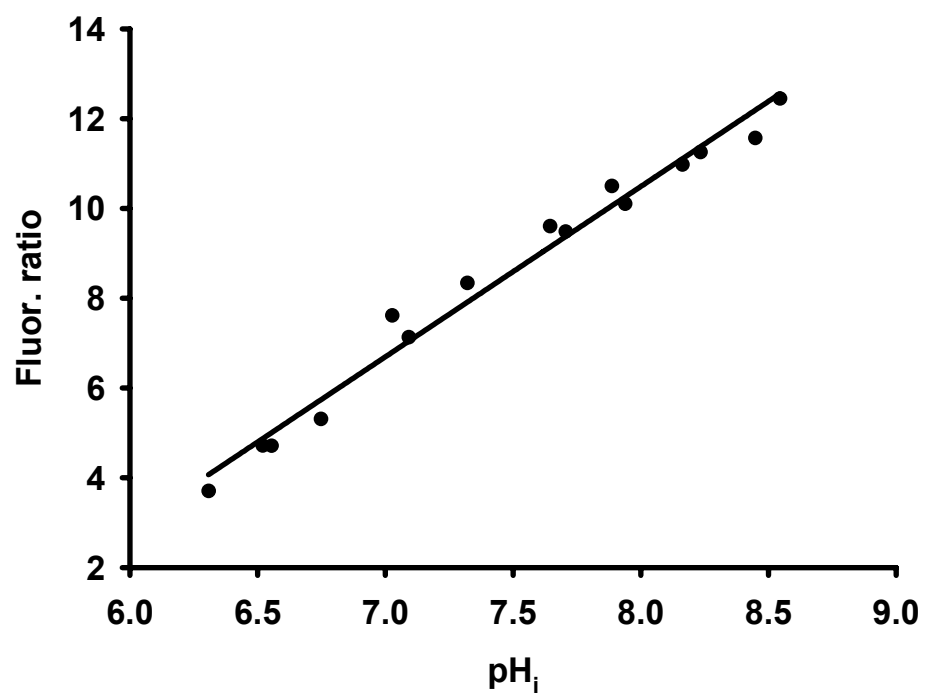


Figure A2.2. Dependence of normalized fluorescence-excitation ratio on pH<sub>i</sub>.

## APPENDIX 3

### DETERMINATION OF BUFFERING CAPACITY AND BASE FLUX

#### Setting up for an Intrinsic Buffering Capacity Experiment

1. Prepare 500 mL of  $\text{Na}^+$  and  $\text{HCO}_3^-$ -free Ringers containing varying concentrations of  $\text{NH}_4\text{Cl}$  (30, 20, 10, 5, and 1) to be used for luminal perfusion. In these solutions,  $\text{HCO}_3^-$  is replaced with TES,  $\text{Na}^+$  is replaced with  $\text{NMDG}^+$ , and the osmolarity of the  $\text{NH}_4\text{Cl}$  solutions is balanced with  $\text{NMDG}^+$ . Prepare 1 L of  $\text{Na}^+$  free TBR (0 mM  $\text{NH}_4\text{Cl}$ ). These solutions should be gassed with 100%  $\text{O}_2$  as they are prepared.
2. Put  $\text{NH}_4\text{Cl}$  Ringers in a 40°C water bath to warm in 100 ml bottles. Place  $\text{Na}^+$  free TBR in one 100 mL for luminal perfusion and one 250 mL bottle for serosal perfusion. Gas these buffer solutions with 100%  $\text{O}_2$ .
3. Turn on the dry bath and replace the pH meter calibration solutions.
4. Set up for a BCECF microfluorimetry study (see Section A1).
5. Serosal  $\text{Na}^+$  free TBR should contain TTX (0.1  $\mu\text{M}$ ) and INDO (1.0  $\mu\text{M}$ ). The luminal perfusates need INDO only.
6. Calibrate the pH meter at 37°C.
7. Sacrifice mouse, mount tissue being calibrated mucosal side up (see Section A.1).
6. Start the perfusion with  $\text{Na}^+$  free TBR (serosal). Put 1 mL of the  $\text{Na}^+$  Free TBR (luminal perfusate) on the luminal side. Make up DTT in 1 ml  $\text{Na}^+$  free TBR (100  $\mu\text{M}$

final concentration). Remove the Na<sup>+</sup> free TBR from the top of the tissue by vacuum and replace with the DTT solution. Incubate the tissue for 5 minutes with DTT.

7. While the tissue is incubating with DTT, make up the BCECF-AM dye solution. Each 50 μM tube of dye is rehydrated in 10 μl of Methyl sulfoxide. Add 2 μl of the BCECF-AM stock to 1 mL of Na<sup>+</sup> free TBR.

8. After the 5 minute DTT incubation, apply the dye solution to the luminal surface and load the tissue for 10 minutes.

### **Method for Measuring Intrinsic Buffering Capacity via NH<sub>4</sub>Cl Prepulse**

1. Place the chamber under the 40X water immersion objective. Place the solution in-line heater probes into the chamber. Turn on the bottom in-line heater. Place the cube housing in position "o" (open circle) so that there are no filters in the field of view. Pull out the filter sliders, turn on the microscope light source to an intensity of ~4.5, and push the camera stop in and follow the steps outlined in Section A1 under "Image Acquisition and Analysis."

2. When the tissue is finished loading, place the apical perfusion lines in the Na<sup>+</sup> free TBR. Start the top vacuum line. Turn on the solution in-line heaters. Put the pH electrode in the chamber in the top portion as close to the tissue as possible. Start the acquisition.

3. Allow the ratio to come to steady state while taking acquisitions every 60 seconds. When the 495/440 ratio reaches steady state, set the acquisition at 20 second intervals enter a comment of "steady state". During this time, record the pH of the solution in the chamber (from the pH meter) in the solution pH column of the experiment sheet.



4. After 5 acquisitions, transfer the apical perfusion line according to the following protocol:

Na<sup>+</sup> free TBR (0 mM NH<sub>4</sub>Cl) → 30 mM NH<sub>4</sub>Cl → 20 mM NH<sub>4</sub>Cl → 10 mM NH<sub>4</sub>Cl → 5 mM NH<sub>4</sub>Cl → 1 mM NH<sub>4</sub>Cl → 0 mM NH<sub>4</sub>Cl

Enter a comment indicating the concentration of NH<sub>4</sub>Cl. With 30 mM NH<sub>4</sub>Cl application, there should be a noticeable increase in the ratio as NH<sub>3</sub> enters the cell and combines with intracellular H<sup>+</sup> to form NH<sub>4</sub><sup>+</sup> and then a slight decrease in ratio can be recorded due to the entry (leakage) of NH<sub>4</sub><sup>+</sup>. Record the pH<sub>o</sub> at the alkaline peak of the trace. This point will be used to determine the magnitude of the pH<sub>i</sub> change. After the ratio hits a stable plateau, switch to the 20 mM NH<sub>4</sub>Cl buffer entering a comment to indicate the concentration of NH<sub>4</sub>Cl. There should be a noticeable drop in the measured ratio since intracellular NH<sub>4</sub><sup>+</sup> will dissociate into NH<sub>3</sub> which exits the cell. Record the pH<sub>o</sub> at the alkaline peak.

5. Repeat for each NH<sub>4</sub>Cl buffer.

6. Several experiments should be conducted in this manner in order to attain measurements of  $\beta_i$  for a wide range of pH<sub>i</sub>s.

### **General Principles and Calculations for Determining Intrinsic Buffering Capacity**

1. Intrinsic buffering capacity ( $\beta_i$ ) refers to the ability of intrinsic cellular components (biochemical and organellar) excluding CO<sub>2</sub>/HCO<sub>3</sub><sup>-</sup> to buffer changes in pH<sub>i</sub>.  $\beta_i$  can be calculated from the pH<sub>i</sub> changes produced by exposing the cell to a weak acid or base as shown in the following equation:

$$\beta_i = \frac{[\Delta base]}{\Delta pH_i} = - \frac{[\Delta acid]}{\Delta pH_i}$$

It is most accurately estimated in cells in which pH-regulatory mechanisms have been blocked. This can be achieved by calculating  $\beta_i$  in the absence of extracellular  $Na^+$  to block Na-dependent  $pH_i$  regulatory mechanisms (i.e., NHEs).

2. Using the ammonia prepulse method, one  $H^+$  is formed for every  $NH_4^+$  reduced to  $NH_3^-$ . Therefore,  $\beta_i$  can be calculated by the following equation:

$$\beta_i = \frac{\Delta[NH_4^+]_i}{\Delta pH_i}$$

3. Assuming  $[NH_3]_i = [NH_3]_o$ ,  $[NH_4^+]_i$  can be calculated using the following rearrangement of the Henderson-Hasselbalch equation:

$$[NH_4^+]_i = \frac{NH_4Cl_o \times 10^{(pK_a - pH_i)}}{1 + 10^{(pK_a - pH_o)}}$$

where  $pK_a$  is 8.9 at 37°C, and  $pH_i$  and  $pH_o$  are intracellular and extracellular pH measurements, respectively.

4. By varying the  $NH_4Cl$  concentration by a known amount (i.e., 30, 20, 10, 5, 1, and 0) and measuring  $pH_o$  (by pH meter) and  $pH_i$  (by BCECF) at the alkaline peak following changes in the concentration of  $NH_4Cl$ , the  $\Delta[NH_4^+]_i$  can be calculated.

5. By subtracting the  $pH_i$  measured during of the trace following the  $NH_4Cl$  concentration change from the  $pH_i$  preceding this change, the  $\beta_i$  is determined, which is considered to the buffering capacity at about the midpoint of the  $pH_i$  change. Values of  $\beta_i$  are determined at various  $pH_i$ s by varying the amounts of  $NH_4Cl$ .

6. The values of  $\beta_i$  calculated at the midpoint of the measured  $pH_i$  changes are fitted to a third-order polynomial according to the following formula:

$$f(x) = y^0 + ax + bx^2 + cx^3$$

where the values from this fitted curve are used as the values of  $\beta_i$  at various pH<sub>i</sub>s (Figure A3.1).

### Calculating HCO<sub>3</sub><sup>-</sup> Buffering Capacity, Total Buffering Capacity and Flux Rates

1. The contribution of CO<sub>2</sub>/HCO<sub>3</sub><sup>-</sup> to overall buffering in an open system can be substantial. Therefore, for studies performed in the presence of CO<sub>2</sub>/HCO<sub>3</sub><sup>-</sup>, it is necessary to determine HCO<sub>3</sub><sup>-</sup> buffering capacity ( $\beta_{HCO_3^-}$ ).
2. Assuming an open system with respect to CO<sub>2</sub>, which is highly permeable through the plasma membrane, and that its solubility and pK<sub>a</sub> value are the same at either side of the cell membrane, then:

$$\beta_{HCO_3^-} = 2.3[HCO_3^-]_i$$

3. [HCO<sub>3</sub><sup>-</sup>]<sub>i</sub> is calculated using the following rearrangement of the Henderson-Hasselbalch equation:

$$[HCO_3^-]_i = 10^{pH_i - pK_a} + \log[pCO_2 \times 0.03]$$

where pCO<sub>2</sub> is 38 mmHg (during gassing with 5% CO<sub>2</sub>), and pK<sub>a</sub> is 6.1 at 37°C.

4. The midpoint of the measured pH<sub>i</sub> changes from the  $\beta_i$  are used to determine [HCO<sub>3</sub><sup>-</sup>]<sub>i</sub> and  $\beta_{HCO_3^-}$  (Figure A3.1).
5. The total buffering capacity ( $\beta_{total}$ ) is then calculated from the following equation:

$$\beta_{total} = \beta_i + \beta_{HCO_3^-}$$

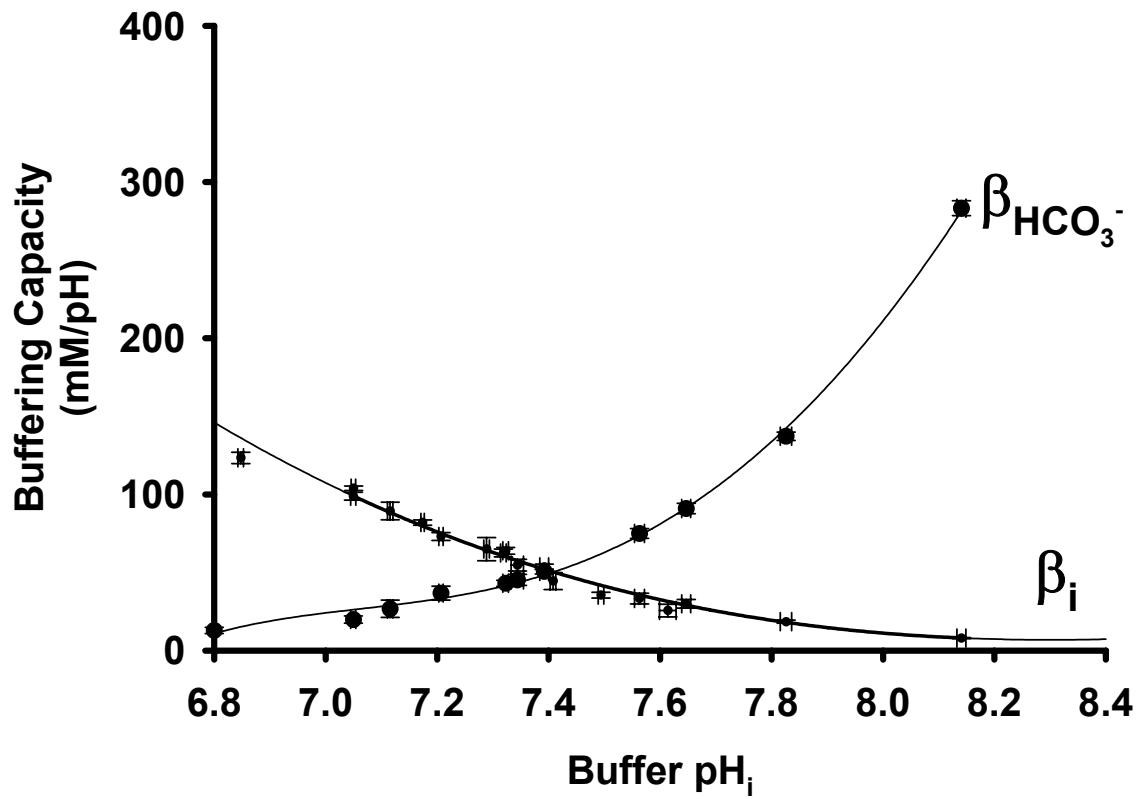


Figure A3.1. Plot of intrinsic buffering and  $\text{HCO}_3^-$  buffering capacity vs.  $\text{pH}_i$ .

where the values of  $\beta_{total}$  calculated at the midpoint of the measured  $\text{pH}_i$  changes are fitted to a inverse third-order polynomial, according to the formula:

$$f(x) = y^0 + \frac{a}{x} + \frac{b}{x^2} + \frac{c}{x^3}$$

The values from this fitted curve are used as the values of  $\beta_{total}$ , which are accordingly pH corrected.

6. The rates of  $\text{pH}_i$  change measured during experimental manipulation are converted to transmembrane net flux (J) using the equation  $J = \Delta\text{pH}/\Delta t \times \beta_{total}$ , and the  $\beta_{total}$  values used in the determination of net flux are calculated from the above equation using the average  $\text{pH}_i$  during the 90-s period of linear  $\Delta\text{pH}/\Delta t$  changes.

## BIBLIOGRAPHY

1. Electrophysiology of the cell membrane. In Boron WF and Boulpaep EL, ed. *Physiology of the Gastrointestinal Tract*. New York, Raven Press. 1987, *Medical Physiology*, edited by New York, Elsevier Science. 2002, p. 266-302.
2. CF Foundation Annual Patient Registry Data Report 2006. North American Cystic Fibrosis Foundation, Bethesda, MD.
3. Cystic Fibrosis Mutation Database Statistics 2006. The Hospital for Sick Children, Toronto, ON.
4. Alvarez BV, Vilas GL, and Casey JR. Metabolon disruption: a mechanism that regulates bicarbonate transport. *EMBO Journal* 24: 2499-2511, 2005.
5. Ameen NA, Alexis J, and Salas P. Cellular localization of the cystic fibrosis transmembrane conductance regulator in mouse intestinal tract. *Histochem Cell Biol* 114: 69-75, 2000.
6. Anderson MP, Gregory RJ, Thompson S, Souza DW, Paul S, Mulligan RC, Smith AE, and Welsh MJ. Demonstration that CFTR is a chloride channel by alteration of its anion selectivity. *Science* 253: 202-205, 1991.
7. Anderson MP and Welsh MJ. Calcium and cAMP activate different chloride channels in the apical membrane of normal and cystic fibrosis epithelia. *Proc Natl Acad Sci USA* 88: 6003-6007, 1991.
8. Bachmann O, Wuchner K, Rossmann H, Leipziger J, Osikowska B, Colledge WH, Ratcliff R, Evans MJ, Gregor M, and Seidler U. Expression and regulation of the Na<sup>+</sup>-K<sup>+</sup>-2Cl<sup>-</sup> cotransporter NKCC1 in the normal and CFTR-deficient murine colon. *J Physiol (Lond)* 549.2: 525-536, 2003.
9. Barone S, Amlal H, Xu J, Kujala M, Kere J, Petrovic S, Soleimani M. Differential regulation of basolateral Cl<sup>-</sup>/HCO<sub>3</sub><sup>-</sup> exchangers SLC26A7 and AE1 in kidney outer medullary collecting duct. *J Am Soc Nephrol*. 15: 2002-2011, 2004.
10. Berlioz F, Maoret JJ, Paris H, Laburthe M, Farinotti R, and Roze C.  $\alpha(2)$ -adrenergic receptors stimulate oligopeptide transport in a human intestinal cell line. *J Pharmacol Exp Ther* 294: 466-472, 2000.

11. Binder, H. J. and G. I. Sandle. Electrolyte absorption and secretion in the mammalian colon. In Johnson, LR, ed. *Physiology of the Gastrointestinal Tract*. New York, Raven Press. 1987, 1389-1418.
12. Boyarsky G, Ganz MB, Sterzel RB, and Boron WF. pH regulation in single glomerular mesangial cells I. Acid extrusion in absence and presence of  $\text{HCO}_3^-$ . *Am J Physiol Cell Physiol* 255: C844-C856, 1988.
13. Bukhave K and Rask-Madsen J. Saturation kinetics applied to in vitro effects of low prostaglandin E2 and F2 alpha concentrations on ion transport across human jejunal mucosa. *Gastroenterology* 78: 32-42, 1980.
14. Buyse M, Berlioz F, Guilmeau S, Tsocas A, Voisin T, Peranzi G, Merlin D, Laburthe M, Lewin MJ, Roze C, and Bado A. PepT1-mediated epithelial transport of dipeptides and cephalixin is enhanced by luminal leptin in small intestine. *J Clin Invest* 108: 1483-1494, 2001.
15. Buyse M, Tsocas A, Walker F, Merlin D, and Bado A. PEPT1-mediated fMLP transport induces intestinal inflammation in vivo. *Am J Physiol Cell Physiol* 283: C1795-C1800, 2002.
16. Byeon MK, Frankel A, Papas TS, Henderson KW, and Schweinfest CW. Human DRA functions as a sulfate transporter in Sf9 insect cells. *Prot Express Purif* 12: 67-74, 1999.
17. Chapman JM, Kim JH, Henderson KW, Spyropoulos DD, and Schweinfest CW. DRA, an intestinal anion transporter, suppresses cell growth and proliferation (Abstract). *Proc Am Assoc Cancer Res* 43: 990, 2003.
18. Chapman JM, Knoepp SM, Byeon MK, Henderson KW, and Schweinfest CW. The colon anion transporter, down-regulated in adenoma, induces growth suppression that is abrogated by E1A. *Cancer Res* 62: 5083-5088, 2002.
19. Chernova MN, Jiang L, Friedman DJ, Darman RB, Lohi H, Kere K, Vandorpe DH, and Alper SL. Functional comparison of mouse slc26a6 anion exchanger with human SLC26A6 polypeptide variants: differences in anion selectivity, regulation, and electrogenicity. *J Bio Chem* 280: 8564-8580, 2005.
20. Chernova M, Jiang NL, Shmukler BE, Schweinfest CW, Blanco P, Freedman SD, Stewart AK, and Alper SL. Acute regulation of the SLC26A3 congenital chloride diarrhoea anion exchanger (DRA) expressed in *Xenopus* oocytes. *J Physiol (Lond)* 549.1: 3-19, 2003.

21. Clarke LL, Gawenis LR, Bradford EM, Judd LM, Boyle KT, Simpson JE, Shull GE, Tanabe H, Ouellette AJ, Franklin CL, and Walker NM. Abnormal Paneth cell granule dissolution and compromised resistance to bacterial colonization in the intestine of CF mice. *Am J Physiol Gastrointest Liver Physiol* 286: G1050-G1058, 2004.
22. Clarke LL, Gawenis LR, Franklin CL, and Harline MC. Increased survival of CFTR knockout mice using an oral osmotic laxative. *Lab Animal Sci* 46: 612-618, 1996.
23. Clarke LL, Grubb BR, Yankaskas JR, Cotton CU, McKenzie A, and Boucher RC. Relationship of a non-CFTR mediated chloride conductance to organ-level disease in *cftr* (-/-) mice. *Proc Natl Acad Sci USA* 91: 479-483, 1994.
24. Clarke LL and Harline MC. CFTR is required for cAMP inhibition of intestinal Na<sup>+</sup> absorption in a cystic fibrosis mouse model. *Am J Physiol Gastrointest Liver Physiol* 270: G259-G267, 1996.
25. Clarke LL and Harline MC. Dual role of CFTR in cAMP-stimulated HCO<sub>3</sub><sup>-</sup> secretion across murine duodenum. *Am J Physiol Gastrointest Liver Physiol* 274: G718-G726, 1998.
26. Clarke LL, Stien X, and Walker NM. Intestinal bicarbonate secretion in cystic fibrosis mice. *JOP* 2, *Suppl* 4: 263-267, 2001.
27. Collins FS. Cystic fibrosis: molecular biology and therapeutic implications. *Science* 256: 774-779, 1992.
28. Daniel H. Molecular and integrative physiology of intestinal peptide transport. *Annu Rev Physiol* 66: 361-384, 2004.
29. Delaney SJ, Alton EFWF, Smith SN, Lunn DP, Farley R, Lovelock PK, Thomson SW, Hume DA, Lamb D, Porteous DJ, Dorin JR, and Wainwright BJ. Cystic fibrosis mice carrying the missense mutation G551D replicate human genotype/phenotype correlations. *Embo J* 15: 955-963, 1996.
30. DeRoos ADG, Schultz BD, Venglarik CJ, Singh AK, Frizzel RA, and Bridges RJ. Glybenclamide blockade of CFTR (Abstract). *Pediatr.Pulmonol.* (Suppl. 9), 213. 1993.
31. Donowitz M and Welsh MJ. Regulation of mammalian small intestinal electrolyte secretion. In Johnson, LR, ed. *Physiology of the Gastrointestinal Tract*. New York, Raven Press. 1987, 351-1388.



32. Du L, Xi L, Chu S, Kere J, and Montrose MH. Chloride/hydroxyl and nitrate/hydroxyl exchange by DRA/CLD protein (Abstract). *FASEB J.* 17, A467. 2003.
33. Dunk CR, Brown CDA, and Turnberg LA. Stimulation of Cl/HCO<sub>3</sub> exchange in rat duodenal brush border membrane vesicles by cAMP. *Pfluegers Arch* 414: 701-705, 1989.
34. Elgavish A. High intracellular pH in CFPAC: a pancreas cell line from a patient with cystic fibrosis is lowered by retrovirus-mediated CFTR gene transfer. *Biochem Biophys Res Commun* 180: 342-348, 1991.
35. Elgavish A and Meezan E. Altered sulfate transport via anion exchange in CFPAC is corrected by retrovirus-mediated CFTR gene transfer. *Am J Physiol Cell Physiol* 263: C176-C186, 1992.
36. Flemstrom G. Gastric and duodenal mucosal bicarbonate secretion. In Johnson, LR, ed. *Physiology of the Gastrointestinal Tract*. New York, Raven Press. 1987, 1011-1030.
37. French PJ, van Doorninck JH, Peters RH, Verbeek E, Ameen NA, Marino CR, De Jonge HR, Bijman J, and Scholte BJ. A delta F508 mutation in mouse cystic fibrosis transmembrane conductance regulator results in a temperature-sensitive processing defect in vivo. *J Clin Invest* 98: 1304-1312, 1996.
38. Ganapathy V, Ganapathy ME, and Leibach FH. Intestinal transport of peptides and amino acids. In Barrett, KE and M Donowitz, eds. *Gastrointestinal Transport Molecular Physiology*. San Diego, Academic Press. 2001, 379-412.
39. Gawenis LR, Franklin CL, Simpson JE, Palmer BA, Walker NM, Wiggins TM, and Clarke LL. cAMP inhibition of murine intestinal Na<sup>+</sup>/H<sup>+</sup> exchange requires CFTR-mediated cell shrinkage of villus epithelium. *Gastroenterology* 125: 1148-1163, 2003.
40. Gawenis LR, Stien X, Shull GE, Schultheis PJ, Woo AL, Walker NM, and Clarke LL. Intestinal NaCl transport in NHE2 and NHE3 knockout mice. *Am J Physiol Gastrointest Liver Physiol* 282: G776-G784, 2002.
41. Gray MA, Plant S, and Argent BE. cAMP-regulated whole cell chloride currents in pancreatic duct cells. *Am J Physiol Cell Physiol* 264: C591-C602, 1993.
42. Greeley T, Shumaker H, Wang Z, Schweinfest CW, and Soleimani M. Downregulated in adenoma and putative anion transporter are regulated by CFTR in cultured pancreatic duct cells. *Am J Physiol Gastrointest Liver Physiol* 281: G1301-G1308, 2001.

43. Guba M, Kuhn M, Forssmann WG, Classen M, Gregor M, and Seidler U. Guanylin strongly stimulates rat duodenal  $\text{HCO}_3^-$  secretion: Proposed mechanism and comparison with other secretagogues. *Gastroenterology* 111: 1558-1568, 1996.
44. Hirokawa M, Takeuchi T, Chu S, Akiba Y, Wu V, Guth PH, Engel E, Montrose MH, and Kaunitz JD. Cystic fibrosis gene mutation reduces epithelial cell acidification and injury in acid-perfused mouse duodenum. *Gastroenterology* 127: 1162-1173, 2004.
45. Hogan, D. L., Crombie, D. L., Isenberg, J. I., Svendsen, P., Schaffalitzky de Muckadell, O. B., and Ainsworth, M. A. Acid-stimulated duodenal bicarbonate secretion involves a CFTR-mediated transport pathway in mice. *Gastroenterology* 113, 533-541. 1997.
46. Hogan DL, Crombie DL, Isenberg JI, Svendsen P, Schaffalitzky de Muckadell OB, and Ainsworth MA. CFTR mediates cAMP- and  $\text{Ca}^{2+}$ -activated duodenal epithelial  $\text{HCO}_3^-$  secretion. *Am J Physiol Gastrointest Liver Physiol* 272: G872-G878, 1997.
47. Illek B, Tam AWK, Fischer H, and Machen TE. Anion selectivity of apical membrane conductance of Calu 3 human airway epithelium. *Pfluegers Arch* 437: 812-822, 1999.
48. Jacob P, Rossmann H, Lamprecht G, Kretz A, Neff C, Lin-Wu E, Gregor M, Groneberg DA, Kere J, and Seidler U. Down-regulated in adenoma mediates apical  $\text{Cl}^-/\text{HCO}_3^-$  exchange in rabbit, rat, and human duodenum. *Gastroenterology* 122: 709-724, 2002.
49. Jiang Z, Grichtchenko II, Boron WF, and Aronson PS. Specificity of anion exchange mediated by mouse Slc26a6. *J Biol Chem* 277: 33963-33967, 2002.
50. Kennedy DJ, Leibach FH, Ganapathy V, and Thwaites DT. Optimal absorptive transport of the dipeptide glycylsarcosine is dependent on functional  $\text{Na}^+/\text{H}^+$  exchange activity. *Pflugers Arch* 445: 139-146, 2002.
51. Kere J, Lohi H, and Hoglund P. Genetic Disorders of Membrane Transport III. Congenital chloride diarrhea. *Am J Physiol Gastrointest Liver Physiol* 276: G7-G13, 1999.
52. Kerem, B., J. Rommens, JA. Buchanan, D. Markiewicz, TK. Cox, A. Chakravarti, M. Buchwald, and L. Tsui. Identification of the cystic fibrosis gene: genetic analysis. *Science* 245: 1073-1080, 1989.

53. Knauf F, Yang CL, Thomson RB, Mentone SA, Giebisch G, and Aronson PS. Identification of a chloride-formate exchanger expressed on the brush border membrane of renal proximal tubule cells. *Proc Natl Acad Sci USA* 98: 9425-9430, 2001.
54. Ko SBH, Luo X, Hager H, Rojek A, Choi JY, Licht C, Suzuki M, Muallem S, Nielsen S, and Ishibashi K. AE4 is a DIDS-sensitive  $\text{Cl}^-/\text{HCO}_3^-$  exchanger in the basolateral membrane of the renal CCD and the SMG duct. *Am J Physiol Cell Physiol* 283: C1206-C1218, 2002.
55. Ko SBH, Shcheynikov N, Choi JY, Luo X, Oshibashi K, Thomas PJ, Kim JY, Kim KH, Lee MG, Naruse S, and Muallem S. A molecular mechanism for aberrant CFTR-dependent  $\text{HCO}_3^-$  transport in cystic fibrosis. *Embo J* 21: 5662-5672, 2002.
56. Ko SBH, Zeng W, Dorwart MR, Luo X, Kim KH, Millen L, Goto H, Naruse S, Soyombo A, Thomas PJ, and Muallem S. Gating of CFTR by the STAS domain of SLC26 transporters. *Nature Cell Biol* 6: 343-350, 2004.
57. Kottra G, Stamford A, and Daniel H. PEPT1 as a paradigm for membrane carriers that mediate electrogenic bidirectional transport of anionic, cationic and neutral substrates. *J Biol Chem* 277: 32683-32691, 2002.
58. Lamprecht G, Baisch S, Schoenleber E, and Gregor M. Transport properties of the human intestinal anion exchanger DRA (down-regulated in adenoma) in transfected HEK293 cells. *Pfluegers Arch* 449: 479-490, 2005.
59. Lamprecht G, Heil A, Baisch S, Lin-Wu E, Yun CC, Kalbacher H, Gregor M, and Seidler U. The down regulated in adenoma (dra) gene product binds to the second PDZ domain of the NHE3 kinase A regulatory protein (E3KARP), potentially linking intestinal  $\text{Cl}^-/\text{HCO}_3^-$  exchange to  $\text{Na}^+/\text{H}^+$  exchange. *Biochemistry* 41: 12336-12342, 2002.
60. Lee MG, Choi JY, Luo X, Strickland E, Thomas PJ, and Muallem S. Cystic fibrosis transmembrane conductance regulator regulates luminal  $\text{Cl}^-/\text{HCO}_3^-$  exchange in mouse submandibular and pancreatic ducts. *J Biol Chem* 274: 14670-14677, 1999.
61. Lee MG, Wigley WC, Zeng W, Noel LE, Marino CR, Thomas PJ, and Muallem S. Regulation of  $\text{Cl}^-/\text{HCO}_3^-$  exchange by cystic fibrosis transmembrane conductance regulator expressed in NIH 3T3 and HEK 293 cells. *J Biol Chem* 274: 3414-3421, 1999.

62. Linsdell P, Tabcharani JA, Rommens JM, Hou YX, Chang XB, Tsui LC, Riordan JR, and Hanrahan JW. Permeability of wild-type and mutant cystic fibrosis transmembrane conductance regulator chloride channels to polyatomic anions. *J Gen Physiol* 110: 355-364, 1997.
63. Lohi H, Lamprecht G, Markovich D, Heil A, Kujala M, Seidler U, and Kere J. Isoforms of SLC26A6 mediate anion transport and have functional PDZ interaction domains. *Am J Physiol Cell Physiol* 284: C769-C779, 2003.
64. Luo X, Choi JY, Ko SBH, Pushkin A, Kurtz A, Ahn W, Lee MG, and Muallem S.  $\text{HCO}_3^-$  salvage mechanisms in the submandibular gland acinar and duct cells. *J Biol Chem* 276: 9808-9816, 2001.
65. Mackenzie B, Loo DD, Fei Y, Liu WJ, Ganapathy V, Leibach FH, and Wright EM. Mechanisms of the human intestinal  $\text{H}^+$ -coupled oligopeptide transporter hPEPT1. *J Biol Chem* 271: 5430-5437, 1996.
66. Madara JL and Trier JS. Functional morphology of the mucosa of the small intestine. In Johnson, LR, ed. *Physiology of the Gastrointestinal Tract*. New York, Raven. 1987, 1209-1249.
67. McEwan, GTA, Daniel H, Fett C, Burgess MN, and Lucas ML. The effect of Escherichia coli STa enterotoxin and other secretagogues on mucosal surface pH of rat small intestine in vivo. *Proc R Soc Lond B Biol Sci* 234: 219-237, 1988.
68. McMurtrie HL, Cleary HJ, Alvarez BV, Loisel FB, Sterling D, Morgan PE, Johnson DE, and Casey JR. The bicarbonate transport metabolon. *J Enzyme Inhib Med Chem* 19: 231-236, 2004.
69. Melvin JE, Park K, Richardson L, Schultheis P, and Shull GE. Mouse down-regulated in adenoma (DRA) is an intestinal  $\text{Cl}^-/\text{HCO}_3^-$  exchanger and is up-regulated in colon of mice lacking the NHE3  $\text{Na}^+/\text{H}^+$  exchanger. *J Biol Chem* 274: 22855-22861, 1999.
70. Merlin D., Steel A, Gewirtz AT, Si-Tahar M, Hediger MA, and Madara JL. hPepT1-mediated epithelial transport of bacteria-derived chemotactic peptides enhances neutrophil-epithelial interactions. *J.Clin.Invest* 102: 2011-2018, 1998.
71. Moseley RH, Hoglund P, Wu GD, Silberg DG, Haila S, de la Chapelle A, Holmberg C, and Kere J. Downregulated in adenoma gene encodes a chloride transporter defective in congenital chloride diarrhea. *Am J Physiol Gastrointest Liver Physiol* 276: G185-G192, 1999.
72. Mount DB and Romero MF. The SLC26 gene family of multifunctional anion exchangers. *Pfluegers Arch* 447: 710-721, 2004.

73. Musch MW, Arvans DL, Field M, Wu GD, and Chang EB. DRA is apical intestinal anion exchanger functionally coupled to NHE2 and NHE3 to mediate electroneutral NaCl absorption (Abstract). *Gastroenterology* 124, A40. 2003.
74. Naruhashi K, Sai Y, Tamai I, Suzuki N, and Tsuji A. PepT1 mRNA expression is induced by starvation and its level correlates with absorptive transport of cefadroxil longitudinally in the rat intestine. *Pharm Res* 19: 1423, 2002.
75. Novak I and Greger R. Properties of the luminal membrane of isolated perfused rat pancreatic ducts. *Pfluegers Arch* 411: 546-553, 1988.
76. O'Loughlin EV, Hunt DM, Bostrom TE, Hunter D, Gaskin KJ, Gyory A, and Cockayne DJH. X-ray microanalysis of cell elements in normal and cystic fibrosis jejunum: evidence for chloride secretion in villi. *Gastroenterology* 110: 411-418, 1996.
77. Ohrui T, Skach W, Thompson M, Matsumoto-Pon J, Calayag C, and Widdicombe JH. Radiotracer studies of cystic fibrosis transmembrane conductance regulator. *Am J Physiol Cell Physiol* 266: C1586-C1593, 1994.
78. Parkkila S and Parkkila AK. Carbonic anhydrase in the alimentary tract. Roles of the different isozymes and salivary factors in the maintenance of optimal conditions in the gastrointestinal canal. *Scand J Gastroenterol* 31: 305-317, 2005.
79. Petrovic S, Wang Z, Ma L, Seidler U, Forte JG, Shull GE, and Soleimani M. Colocalization of the apical Cl<sup>-</sup>/HCO<sub>3</sub><sup>-</sup> exchanger PAT1 and gastric H-K-ATPase in stomach parietal cells. *Am J Physiol* 283: G1207-G1216, 2002.
80. Poulsen JH, Fischer H, Illek B, and Machen TE. Bicarbonate conductance and pH regulatory capability of cystic fibrosis transmembrane conductance regulator. *Proc Natl Acad Sci USA* 91: 5340-5344, 1994.
81. Powell, DW. Intestinal Water and Electrolyte Transport. In Johnson, LR, ed. *Physiology of the Gastrointestinal Tract*. New York, Raven Press. 1987, 1267-1306.
82. Praetorius, J, Friis UG, Ainsworth MA, De Muckadell OBS, and Johansen T. The cystic fibrosis transmembrane conductance regulator is not a base transporter in isolated duodenal epithelial cells. *Acta Physiol Scand* 174: 327-336, 2002.
83. Pratha V, Hogan DL, Martensson B, and Isenberg JI. Cystic fibrosis patients (CF) have impaired duodenal mucosal transport. *Gastroenterology* 114: G1655, 1998.

84. Pratha VS, Hogan DL, Martensson BA, Bernard J, Zhou R, and Isenberg JI. Identification of transport abnormalities in duodenal mucosa and duodenal enterocytes from patients with cystic fibrosis. *Gastroenterology* 118: 1051-1060, 2000.
85. Reddy MM and Quinton PM. Control of dynamic CFTR selectivity by glutamate and ATP in epithelial cells. *Nature* 423: 756-760, 2003.
86. Riordan JR, Rommens JM, Kerem B, Alon N, Rozmahel R, Grzelczak Z, Zielenski J, Lok S, Plavsic N, and Chou JL. Identification of the cystic fibrosis gene: cloning and characterization of complementary DNA. *Science* 245: 1066-1073, 1989.
87. Seidler U, Blumenstein I, Kretz A, Viellard-Baron D, Rossmann H, Colledge WH, Evans M, Ratcliff R, and Gregor M. A functional CFTR protein is required for mouse intestinal cAMP-, cGMP- and Ca<sup>2+</sup>-dependent HCO<sub>3</sub><sup>-</sup> secretion. *J Physiol (Lond)* 505: 411-423, 1997.
88. Sellin JH. Intestinal electrolyte absorption and secretion. In Sleisenger MH and Fordtran JS, eds. *Gastrointestinal Disease*. Philadelphia, W.B. Saunders. 1998, 954-976.
89. Shcheynikov N, Kim KH, Kim K, Dorwart MW, Ko SBH, Goto H, Naruse S, Thomas PJ, and Muallem S. Dynamic control of cystic fibrosis transmembrane conductance regulator Cl<sup>-</sup>/HCO<sub>3</sub><sup>-</sup> selectivity by external Cl<sup>-</sup>. *J Biol Chem* 279: 21857-21865, 2004.
90. Sheldon RJ, Malarchik ME, Fox DA, Burks TF, and Porreca F. Pharmacological characterization of neural mechanisms regulating mucosal ion transport in mouse jejunum. *J Pharmacol Exp Therap* 249: 572-582, 1988.
91. Short, DB, Trotter KW, Reczek D, Kreda SM, Bretscher A, Boucher RC, Stutts MJ, and Milgram SL. An apical PDZ protein anchors the cystic fibrosis transmembrane conductance regulator to the cytoskeleton. *J Biol Chem* 273: 19797-19801, 1998.
92. Silberg DG, Wang W, Moseley RH, and Traber PG. The *Down Regulated in Adenoma (dra)* gene encodes an intestine-specific membrane sulfate transport protein. *J Biol Chem* 270: 11897-11902, 1999.
93. Simpson JE, Gawenis LR, Walker NM, Boyle KT, and Clarke LL. Chloride conductance of CFTR facilitates Cl<sup>-</sup>/HCO<sub>3</sub><sup>-</sup> exchange in the villous epithelium of intact murine duodenum. *Am J Physiol Gastrointest Liver Physiol* 288: 1241-1251, 2005.

94. Simpson JE, Walker NM, and Clarke LL. Recovery from proton di-/tripeptide transport-mediated intracellular acidification in the duodenal villous epithelium of Na<sup>+</sup>/H<sup>+</sup> exchanger isoform 3 (NHE3) knockout mice (Abstract). *FASEB J* A146, 2005.
95. Sly WS and Hu PY. Human carbonic anhydrases and carbonic anhydrase deficiencies. *Annu Rev Biochem* 64: 375-401, 1995.
96. Smith JJ and Welsh MJ. cAMP stimulates bicarbonate secretion across normal, but not cystic fibrosis airway epithelia. *J Clin Invest* 89: 1148-1153, 1992.
97. Snouwaert JN, Brigman KK, Latour AM, Malouf NN, Boucher RC, Smithies O, and Koller BH. An animal model for cystic fibrosis made by gene targeting. *Science* 257: 1083-1088, 1992.
98. Spicer SS, Lewis SE, Tashian RE, and Shulte BA. Mice carrying a CAR-2 null allele lack carbonic anhydrase II immunohistochemically and show vascular calcification. *Am J Pathol* 134: 947-954, 1989.
99. Spiegel S, Phillipper M, Rossmann H, Riederer B, Gregor M, and Seidler U. Independence of apical Cl<sup>-</sup>/HCO<sub>3</sub><sup>-</sup> exchange and anion conductance in duodenal HCO<sub>3</sub><sup>-</sup> secretion. *Am J Physiol Gastrointest Liver Physiol* 285: G887-G897, 2003.
100. Sterling D, Alvarez BV, and Casey JR. The extracellular component of a transport metabolon. Extracellular loop 4 of the human AE1 Cl<sup>-</sup>/HCO<sub>3</sub><sup>-</sup> exchanger binds carbonic anhydrase IV. *J Biol Chem* 277: 25239-25246, 2002.
101. Sterling D, Brown NJ, Supuran CT, and Casey JR. The functional and physical relationship between DRA bicarbonate transporter and carbonic anhydrase II. *Am J Physiol Cell Physiol* 283: C1522-C1529, 2002.
102. Sterling D, Reithmeier RAF, and Casey JR. A transport metabolon. Functional interaction of carbonic anhydrase II and chloride/bicarbonate exchangers. *J Biol Chem* 276: 47886-47894, 2001.
103. Stewart AK, Boyd CAR, and Vaughan-Jones RD. A novel role for carbonic anhydrase: cytoplasmic pH gradient dissipation in mouse small intestinal enterocytes. *J Physiol (Lond)* 516: 209-217, 1999.
104. Strong TV, Boehm K, and Collins FS. Localization of cystic fibrosis transmembrane conductance regulator mRNA in the human gastrointestinal tract by *in situ* hybridization. *J Clin Invest* 93: 347-354, 1994.

105. Tabcharani JA, Rommens JM, Hou YX, Chang XB, Tsui LC, Riordan JR, and Hanrahan JW. Multi-ion pore behavior in the CFTR chloride channel. *Nature* 366: 79-82, 1993.
106. Thamocharan M, Bawani SZ, Zhou X, and Adibi SA. Functional and molecular expression of intestinal oligopeptide transporter (Pept-1) after a brief fast. *Metabolism* 48: 681-684, 1999.
107. Thamocharan M, Bawani SZ, Zhou X, and Adibi SA. Hormonal regulation of oligopeptide transporter pept-1 in a human intestinal cell line. *Am J Physiol Cell Physiol* 276: C821-C826, 1999.
108. Thomas JA, Buchsbaum RN, Zimniak A, and Racker E. Intracellular pH measurements in ehrlich ascites tumor cells utilizing spectroscopic probes generated *in situ*. *Biochemistry* 18: 2210-2218, 1979.
109. Thomson RB, Wang T, Thomson BR, Tarrats L, Girardi A, Mentome S, Soleimani M, Kocher O, Aronson PS. Role of PDZK1 in membrane expression of renal brush border ion exchangers. *Proc Natl Acad Sci USA* 102: 13331-13336, 2005.
110. Thwaites DT, Brown DA, Hirst BH, and Simmons NL. H<sup>+</sup>-coupled dipeptide (glycylsarcosine) transport across apical and basal borders of human intestinal Caco-2 cell monolayers displays distinctive characteristics. *Biochim Biophys Acta* 1151: 237-245, 1993.
111. Thwaites DT, Brown DA, Hirst BH, and Simmons NL. Transepithelial glycylsarcosine transport in intestinal Caco-2 cells mediated by expression of H<sup>+</sup>-coupled carriers at both apical and basal membranes. *J Biol Chem* 268: 7640-7642, 1993.
112. Thwaites DT, Ford D, Glanville M, and Simmons NL. H<sup>+</sup>/solute-induced intracellular acidification leads to selective activation of apical Na<sup>+</sup>/H<sup>+</sup> exchange in human intestinal epithelial cells. *J Clin Invest* 104: 629-635, 2005.
113. Thwaites DT, Kennedy DJ, Raldua D, Anderson CMH, Mendoza ME, Bladen CL, and Simmons NL. H<sup>+</sup>/dipeptide absorption across the human intestinal epithelium is controlled indirectly via a functional Na<sup>+</sup>/H<sup>+</sup> exchanger. *Gastroenterology* 122: 1322-1333, 2002.
114. Tuo B, Riederer B, Wang Z, Colledge WF, Soleimani M, and Seidler U. Involvement of the anion exchanger Slc26a6 in PGE<sub>2</sub>- but not forskolin-stimulated murine duodenal HCO<sub>3</sub><sup>-</sup> secretion. *Gastroenterology* 130: 349-58, 2006.



115. van Heeckeren AM, Schluchter LM, Drumm ML, and Davis PB. Role of Cfr genotype in the response to chronic *Pseudomonas aeruginosa* lung infection in mice. *Am J Physiol Lung Cell Mol Physiol* 287: L944-52, 2004.
116. Vavricka SR, Musch MW, Chang JE, Nakagawa Y, Phanvijhitsiri K, T. Waypa TS, Merlin D, Schneewind O, and Chang EB. hPepT1 transports muramyl dipeptide, activating NF-KB and stimulating IL-8 secretion in human colonic Caco2/bbe cells. *Gastroenterology* 127: 1401-1409, 2004.
117. Walker D., Thwaites DT, Simmons NL, Gilbert HJ, and Hirst BH. Substrate upregulation of the human small intestinal peptide transporter, hPepT1. *J Physiol* 507: 697-706, 1998.
118. Walker NM, Flagella M, Gawenis LR, Shull GE, and Clarke LL. An alternate pathway of cAMP-stimulated Cl<sup>-</sup> secretion across the NKCC1-null murine duodenum. *Gastroenterology* 123: 531-541, 2002.
119. Wang, Z, Wang T, Petrovic S, Tuo B, Riederer B, Barone S, Lorenz JN, Seidler U, Aronson PS, and Soleimani M. Renal and intestine transport defects in Slc26a6-null mice. *Am J Physiol Cell Physiol* 288: C957-C965, 2005.
120. Wang, ZH, Petrovic S, Mann E, and Soleimani M. Identification of an apical Cl<sup>-</sup>/HCO<sub>3</sub><sup>-</sup> exchanger in the small intestine. *Am J Physiol Gastrointest Liver Physiol* 282: G573-G579, 2002.
121. Weintraub WH and Machen TE. pH regulation in hepatoma cells: roles for Na-H exchange, Cl-HCO<sub>3</sub> exchange, and Na-HCO<sub>3</sub> cotransport. *Am J Physiol Gastrointest Liver Physiol* 257: G317-G327, 1989.
122. Welsh MJ, Tsui LC, Boat TF, and Beaudet AL. Cystic Fibrosis. In Scriver CR, Beaudet AL, Sly WS, Valle D, and Fredrickson DS, eds. *Metabolic and Molecular Basis of Inherited Disease*. New York, McGraw Hill. 1995, 3799-3863.
123. Willumsen NJ and Boucher RC. Intracellular pH and its relationship to regulation of ion transport in normal and cystic fibrosis human nasal epithelia. *J Physiol (Lond)* 455: 247-269, 1992.
124. Xie Q, Welch R, Mercado A, Romero MF, and Mount DB. Molecular characterization of the murine Slc26a6 anion exchanger: functional comparison with Slc26a1. *Am J Physiol Renal Physiol* 283: F826-F838, 2002.
125. Xu J, Barone S, Petrovic S, Wang Z, Seidler U, Riederer B, Ramaswamy K, Dudeja PK, Shull GE, and Soleimani M. Identification of an apical Cl<sup>-</sup>/HCO<sub>3</sub><sup>-</sup> exchanger in gastric surface mucous and duodenal villus cells. *Am J Physiol Gastrointest Liver Physiol* 285: G1225-G1234, 2003.

126. Zeiher BG, Eichwald E, Zabner J, Smith AP, Puga PB, McCray PB, Capecchi MR, Welsh MJ, and Thomas KR. A mouse model for the  $\Delta F508$  allele of cystic fibrosis. *J Clin Invest* 96: 2051-2064, 1995.

## VITA

Janet Elizabeth Simpson was born July 5, 1976, in Arlington Heights, Illinois. After attending public schools in Clinton, Mississippi, she received a B.S. in Biological Sciences from Mississippi State University in 1998. She continued her education at Mississippi State University and was awarded the Doctor of Veterinary Medicine Degree in 2001. She then attended the University of Missouri-Columbia where she completed a residency in Comparative Medicine in 2004 and is scheduled to complete a Ph.D. in Biomedical Sciences in August 2006.